CHARACTERIZATION OF [^{11}C]METHYL-LOSARTAN AS A NOVEL RADIOTRACER FOR PET IMAGING OF THE AT_1 RECEPTOR

MASTER'S OF SCIENCE THESIS

By

Rawad Antoun

This thesis is submitted as a partial fulfillment of the

M.Sc. program in Cellular and Molecular Medicine.

Submitted 22 September 2010

University of Ottawa, Faculty of Medicine,

Department of Cellular and Molecular Medicine

ABSTRACT

The Angiotensin II Type 1 (AT_1) receptor is the main receptor responsible for the effects of the renin-angiotensin system, and its expression pattern is altered in several diseases. [^{11}C]Methyl-Losartan has been developed based on the clinically used AT_1 receptor antagonist Losartan. The aim of this work is to characterize the pharmacokinetics, repeatability and reliability of measurements, binding specificity and selectivity of [^{11}C]Methyl-Losartan in rats using *in vivo* small animal positron emission tomography (PET) imaging, *ex vivo* biodistribution and *in vitro* autoradiography methods. Also, we aim to measure the presence of metabolites in the kidney and plasma using high-performance liquid chromatography. We have demonstrated *in vivo* that [^{11}C]Methyl-Losartan is taken up in the AT_1 receptor-rich kidneys and that it is displaceable by selective AT_1 receptor antagonists. Using *ex vivo* biodistribution, we have confirmed these results and demonstrated that [^{11}C]Methyl-Losartan binds selectively to the AT_1 receptor over the AT_2, Mas and β-adrenergic receptors. *In vitro* autoradiography results confirmed these renal binding selectivity studies. [^{11}C]Methyl-Losartan was also shown to have one and two C-11 labeled metabolites in the plasma and kidneys, respectively. In conclusion, [^{11}C]Methyl-Losartan is a promising agent for studying the AT_1 receptor in rat models with normal and altered AT_1 receptor expression using small animal PET imaging.

TABLE OF CONTENTS

LIST OF TABLES

LIST OF FIGURES

LIST OF ABBREVIATIONS

%ID/g	Percent of injected dose per gram of tissue
ACE	Angiotensin converting enzyme
Ang 1-7	Angiotensin 1-7
Ang I	Angiotensin I
Ang II	Angiotensin II
ANOVA	Analysis of variance
AT_1	Angiotensin II Type 1
AT_2	Angiotensin II Type 2
DAG	Diacyl glycerol
DV	Distribution volume
EDTA	Ethylenediaminetetraacetic acid
FOV	Field of view
HF	Heart failure
HPLC	High performance liquid chromatography
I.v.	Intra-venous
I.p.	Intra-peritoneal
IP_3	Inositol triphosphate
JAK	Janus kinase
MAPK	Mitogen-activated protein kinase
MI	Myocardial infarction
NADH	Nicotinamide-adenine dinucleotide
NADPH	Nicotinamide-adenine dinucleotide phosphate
PET	Positron emission tomography
PKC	Protein kinase C
PLC	Phospholipase C
RAS	Renin-angiotensin system
ROI	Region of interest
SAR	Structure-activity relationship
SD	Standard deviation
SPECT	Single photon emission computed tomography

ACKNOWLEDGEMENTS

I would like to thank my supervisor Dr. Jean N. DaSilva, and my co-supervisor Dr. Rob S.B. Beanlands for their guidance, mentorship and support throughout this work. I would also like to thank the members of my advisory committee, Dr. Robert A. deKemp and Dr. Kevin Burns, for their input into the project design and evaluation of my progress. I would like to thank Stephanie Thorn, Miran Kenk and James Thackeray, senior members of our PET bio-testing lab, for the management and their leadership in all aspects of this work. I would like to thank all present and past members of our PET bio-testing lab for their help in data collection; this includes Adam Thomas, Kumiko Mackasey, Marika Kolajova, Natasha Arksey, Matt Lenardis, Paige Buttenaar and Sheryn Kirkpatrick. I would like to thank the PET radiochemistry lab for the formulation and synthesis of tracer required for all the experiments performed: Dr. Tayebeh Hadizad, Jeffrey Collins, Samantha Mason, Paul Coletta, Julian Walcott, and Elena Dobrota. Thank you to the Jennifer Renaud and Dr. Mireille Lortie for their input into image analysis and kinetic modeling. I would like to thank Myra Kordos and Julia Lockwood for the handling of animals and image acquisition for all PET scans. I would like to thank the entire Animal Care and Veterinary Services team for the daily handling and caring of all animals used in this work. Thanks to Robert W. Davies for his input into the statistical analyses. I would like to thank the granting agencies which provided funding for my stipend and for the work performed: Canadian Institutes of Health Research (MOP-80203), Heart and Stroke Foundation of Ontario (PRG6242) and Imaging Network Ontario – Ontario Preclinical Imaging Consortium (MRI ORF #RE03-51).

SPECIAL THANKS

I dedicate a special thank you to my parents and my brothers who have always been compassionate and encouraging in all my endeavours. I could not have completed this work without their unconditional support. This thesis is dedicated to them, Joseph, Thérèse, Ghadi and Alen. Thank you!

1 INTRODUCTION

1.1 THE RENIN-ANGIOTENSIN SYSTEM

The renin-angiotensin system (RAS) is a crucial hormonal system involved in the regulation of blood pressure. The RAS modulates water and sodium dynamics by promoting salt and water reabsorption in the renal tubules and thus increasing circulating volume. In the cardiovascular system, it acts to increase heart rate and force of contractility, as well as vasoconstriction. RAS signaling also increases sympathetic activity in the brain and promotes drinking behavior. Its effects on the adrenal glands and pituitary gland stimulate the secretion of aldosterone and vasopressin, respectively (de Gasparo et al. 2000; Paul et al. 2006).

1.1.1 ANGIOTENSIN II SYNTHESIS AND METABOLISM

Angiotensin II (Ang II) is regarded as the main effector peptide in the RAS. Synthesis of Ang II occurs in response to a physiological stimulus such as a decrease in blood pressure, which activates the release of renin from the kidneys. Renin is an enzyme that converts the polypeptide angiotensinogen, which is released from the liver, into the decapeptide angiotensin I (Ang I) by cleaving off the first 10 amino acids from the parent peptide. Ang I is then further cleaved into the octapeptide Ang II by the angiotensin converting enzyme (ACE), which is located at the surface of the pulmonary and renal epithelium (Figure 1) (de Gasparo et al. 2000). Although ACE is regarded as the main enzyme responsible for the conversion of Ang I to Ang II, there are ACE-independent pathways responsible for this hydrolysis. Most notably, chymase (which is a serine protease) can act similarly to ACE and cleave Ang I to form Ang II (Urata et al. 1996).

Circulating Ang II is quickly degraded in the system and several angiotensin derived metabolites have been identified (de Gasparo et al. 2000). The first of which is angiotensin 1-7

(Ang 1-7), which is produced by the cleavage of the Pro^{7}-Phe^{8} bond of Ang II by a prolyl carboxypeptidase, or cleavage of Ang I by the endopeptidases neprilysin, metallo endopeptidase or prolyl endopeptidase (Ferrario and Iyer 1998; Tan et al. 1993). It is suggested that Ang 1-7 binds to a non-AT_1 non-AT_2 receptor and elicits anti-hypertensive responses (Ferrario and Iyer 1998). Ang II can also be cleaved at the Asp^{1}-Arg^{2} site by aminopeptidase A to form angiotensin 2-8, named angiotensin III. Moreover, the angiotensin 3-8 fragment, named angiotensin IV, has been identified, and is formed by cleaving Arg^{2} from angiotensin III by aminopeptidase B. The relative importance of these last two peptides relative to Ang II is still debated as their functions and effects are poorly understood (Wright et al. 1995).

1.1.2 ANGIOTENSIN II STRUCTURE

Structure-activity relationship (SAR) studies have shown that the Tyr^{4}, His^{6}, Phe^{8} amino acid resides and the C-terminal of the Ang II peptide are critical to its biological activity (Figure 2). Based on nuclear magnetic resonance spectroscopy and molecular modeling studies, Ang II is proposed to adopt a compact hairpin model stabilized by hydrogen bonding. The Val^{3}, Ile^{5} and Pro^{7} amino acid residues are proposed to be responsible for the conformational structure and folding of the peptide and thus are likely responsible for the proper orientation of the three amino acids forming the Ang II pharmacophore (Tyr^{4}, His^{6}, Phe^{8}). It is interesting to note that the tetrazole-biphenyl structure present in several AT_1 receptor antagonists resembles the structure formed by the three side chains of Tyr^{4}, His^{6} and Phe^{8} (Tzakos et al. 2004).

As well, it is suggested that the Asp^{1} residue is not important for Ang II receptor agonism and that replacing Asp^{1} with Sar^{1} actually enhances agonism and reduces degradation. This exchange, in combination with the replacement of Phe^{8} (which is known to be important for the biological activity of Ang II) with Ile^{8}, form the basis for the synthetic Sar^{1},Ile^{8}-Ang II peptide. This peptide in turn forms the basis for [^{125}I]Sar^{1},Ile^{8}-Ang II: a very important radioligand with

antagonistic properties that is now widely used to study angiotensin receptors (Tzakos et al. 2004).

1.1.3 RECEPTORS

There are two main subtypes of pharmacologically distinct Ang II receptors (Type 1 and 2) that have been characterized. Ang II mediates most of its effects via the Angiotensin II Type 1 (AT_1) receptor, and this receptor-ligand axis is responsible for most of the effects associated to the RAS. The AT_1 and the Ang II Type 2 (AT_2) receptors are both seven transmembrane G-protein coupled receptors (GPCR) and share 34% amino acid sequence identity. The actions of the AT_1 receptor will be discussed in detail further; however it is important to note that activation of the AT_2 receptor has been shown to have opposing effects to the AT_1 receptor. It has been suggested that the AT_2 receptor may act as a regulatory mechanism to prevent over-activation of the RAS. Other receptors in the system have also been identified. Notably, a binding site for angiotensin IV has recently been recognized and termed AT_4. Its function is still poorly understood despite being located in several organs, including the brain, heart, adrenal glands and kidneys, although at low densities compared to the AT_1 and AT_2 receptors (de Gasparo et al. 2000). As well, the Mas receptor has also recently been identified and its expression has been established in the kidney. The Mas receptor is a GPCR suggested to play a role in water balance and regulation of blood pressure, and is responsible for the anti-hypertensive effects of Ang 1-7 (Dilauro and Burns 2009; Santos et al. 2003).

1.2 THE ANGIOTENSIN II TYPE 1 RECEPTOR

Despite the presence of other receptors in the RAS, such as the AT_2, AT_4 and Mas receptors, the AT_1 receptor is regarded as the main effector of this system. Here we describe

further the properties of the AT_1 receptor by looking at its protein structure, signaling and regulation, distribution in the system, and its actions on the system.

1.2.1 STRUCTURE

The human, rat and mouse AT_1 receptor is comprised of 359 amino acids and has a molecular mass of approximately 41 kDa. Hydropathy analysis suggests the presence of seven transmembrane domains which fold into α-helices to form the membrane spanning secondary structure of the protein typical of GPCRs. Rats, as well as other rodents, have two isoforms of the AT_1 receptor: AT_{1A} and AT_{1B}, which are coded by two separate genes located on chromosomes 17 and 2 respectively. Despite their disparity in tissue distribution, expression and regulation, these two isoforms share 95% amino acid sequence homology and are not differentiable in regards their binding and activation properties (de Gasparo et al. 2000). The human AT_1 receptor gene is located on chromosome 3q, and based on cDNA analysis shares 95% amino acid sequence identity with the rat (and bovine) receptors (Bergsma et al. 1992; Curnow et al. 1992; Furuta et al. 1992).

1.2.2 SIGNALING AND REGULATION

The AT_1 receptor is classified under the GPCR superfamily of receptors and is suggested to bind to multiple G proteins. Its main signaling cascade occurs via interaction and activation of the G_q pathway (de Gasparo et al. 2000). Upon agonist binding and activation, there is a change in receptor conformation accompanied by an exchange of guanine diphosphate for guanine triphosphate by the G protein α subunit ($G_{\alpha q}$). $G_{\alpha q}$ then mediates its response by activating phospholipase C (PLC). PLC cleaves phosphatidylinositol biphosphate into two intracellular messengers: inositol triphosphate (IP_3) and diacyl glycerol (DAG), which subsequently act to increase intracellular Ca^{2+} levels and activate protein kinase C (PKC), respectively (Figure 3) (Karnik et al. 2003; Neves et al. 2002; Wagenaar et al. 2002). The AT_1 receptor has also been

reported to couple to other signaling pathways including, but not limited to: the tyrosine kinase activation pathway, adenylate cyclase inhibition pathway (through $G_{\alpha i}$), JAK/STAT pathway, MAPK pathways, and NADH/NADPH oxidases pathways (de Gasparo et al. 2000; Kaschina and Unger 2003; Wagenaar et al. 2002; Yang et al. 1997).

The AT_1 receptor is subject to cellular regulatory mechanism such as desensitization, internalization, resensitization, up- and down-regulation, however the exact mechanisms of action in all cells is not yet fully understood. Similarly to other GPCRs, agonist activation by endogenous Ang II can lead to endocytosis and recycling of the proteins, resulting in a down-regulation of AT_1 receptors (Mento et al. 1998). Chronic stimulation of the AT_1 receptor with Ang II may also lead to down-regulation of its gene expression. Alternatively, inhibition of Ang II formation by ACE inhibitors, and thus impaired stimulation of the AT_1 receptor and its signaling cascade up-regulate receptor expression (Mento et al. 1998). Many pathological conditions and associated stimuli can regulate the expression of the AT_1 receptor at the transcriptional and translational level. These effects will be discussed in section 1.3 (Altered AT_1 Receptor Expression).

1.2.3 DISTRIBUTION

The AT_1 receptors are mainly expressed in the adrenal glands, kidneys, vasculature, brain and heart, which comprise the main organs responsible for the pressor effects of Ang II (Chang and Lotti 1991; Paul et al. 2006). Chang and Lotti reported the relative distribution of AT_1 receptors in monkeys, rabbits and rats using [^{125}I]Sar^1,Ile^8-Ang II binding assays. The highest binding density was observed in the adrenal cortex, followed by the kidney cortex, aorta, brain and finally heart (Table 1) (Chang and Lotti 1991). However, Llorens-Cortes and colleagues performed mRNA studies on rats and suggested that the AT_1 receptor mRNA levels are higher in the liver and the kidneys compared to the adrenal gland (Llorens-Cortes et al. 1994). This would

indicate either a differential regulation at the transcriptional and translational level, or inter-study variability in regards to absolute AT_1 receptor quantification.

Although Chang and Lotti propose that density is very low in the heart of rats, monkeys and rabbits, cardiac AT_1 receptor presence should not be underestimated. Autoradiography studies demonstrate binding of [^{125}I]Sar^1,Ile^8-Ang II in the atrial and ventricular myocardium, the vascular smooth muscle cells of the aorta, the pulmonary arteries, the superior vena cava, and innervation sites such as the atrioventricular node and the atrioventricular bundle in Sprague-Dawley rats (Allen et al. 1990; Allen et al. 2000).

In the kidney, AT_1 receptors are localized in the cortex (i.e. the glomeruli, tubules) and in the outer medulla (i.e. the vasa recta, tubules). This distribution is highly conserved amongst species, including rodents, primates and humans (Allen et al. 1999; Allen et al. 2000; de Gasparo et al. 2000; Goldfarb et al. 1994).

In the adrenal gland, autoradiography studies reveal the presence of both AT_1 and AT_2 receptor subtypes in the cortex and medulla. However, differences exist in regards to their relative distribution in these areas. In rodents, monkeys and humans, the AT_1 receptors are mostly contained, in the zona glomerulosa of the adrenal cortex and their expression is higher than that of the AT_2 receptor. In contrast, AT_1 receptors are not present in the zona fasciculata and zona reticularis, and low levels are detected in the medulla, which mostly contains AT_2 receptors (Allen et al. 1999; Allen et al. 2000).

In the brain, presence of the AT_1 receptor has been identified using [^{125}I]Sar^1,Ile^8-Ang II binding in regions outside and inside the blood-brain barrier. Outside the blood brain barrier, the AT_1 receptor is mainly expressed in the circumventricular organs such as subfornical organ (SFO), organum vasculosum of the lamina terminalis (OVLT), median eminence (ME), anterior pituitary, and the area postrema of the hindbrain. Inside the blood-brain barriers, the organs

which express the AT_1 receptor include the median preoptic nucleus, hypothalamic paraventricular nucleus (PVN), anteroventral preoptic (AVPV), suprachiasmatic (SCN), and periventricular nuclei, and discrete regions of the lateral and dorsomedial hypothalamus (Allen et al. 1999; Allen et al. 2000).

In the liver, the presence of AT_1 receptors is also well established. Murphy and colleagues have reported the presence of AT_1 receptor mRNA in rats (Murphy et al. 1991). Yu and colleagues have also reported the presence of AT_1 receptor protein in the liver using western blot analysis. The AT_1/GAPDH expression ratio in the liver was approximately 6 to 7 fold lower than in whole kidney samples in this study (Yu et al. 2010).

In sum, the AT_1 receptor is highly expressed in the kidneys, the adrenal glands (zona glomerulosa) and the liver, and to a lesser extent in the heart, the vasculature and the brain. These organs comprise the main focus of our research regarding the AT_1 receptor.

1.2.4 ACTIONS

The known distribution of the AT_1 receptor in the system is closely linked to the sites where Ang II elicits its actions, i.e. the heart, vasculature, kidneys, brain, adrenal glands, and liver. Direct exposure of vascular smooth muscle cells to circulating Ang II results in vascular constriction by activation of the AT_1 receptors. Experiments show that Ang II is capable of inducing a contractile response in explanted New Zealand White rabbit aortas, and that this response can be attenuated with specific and selective AT_1 receptor antagonists (Cappelli et al. 2008). This vasoconstriction is mediated by the AT_1 receptor's signalling cascade which acts via phophorylation of target proteins by PKC, and release of Ca^{2+} into the cell via IP_3 signaling (Kaschina and Unger 2003).

In the kidneys, the AT_1 receptor can modulate glomerular filtration rate by its differential effect on the afferent and efferent arterioles in the glomeruli. AT_1 activation in the

nephrons can also leads to increases in sodium and water retention by modulating the permeability of the renal tubules. In the brain, the stimulation of the AT_1 receptors inside and outside the blood brain barrier was also shown to increase sympathetic activity, alter drinking behavior and salt intake, and cause release of vasopressin from the posterior pituitary gland. Vasopressin is a hormone that acts to increase overall vascular resistance and can mediate its effects by acting on renal tubules to promote passive water reabsorption. In the adrenal gland, the AT_1 receptor causes the synthesis and secretion of aldosterone from the zona glomerulosa cells of the adrenal cortex. Aldosterone mainly acts by increasing sodium reabsorption in the renal tubules. The release of vasopressin and aldosterone in response to AT_1 receptor activation acts in synergy with circulating Ang II to increase fluid volume and systemic blood pressure (de Gasparo et al. 2000; Kaschina and Unger 2003; Paul et al. 2006). In sum, the overall action of AT_1 receptor activation is to increase blood pressure via cardiovascular, neuronal and hormonal systems.

1.2.5 INTRACELLULAR AT_1 RECEPTORS

Until recently, the AT_1 receptor and the RAS have been considered to act exclusively at the systemic level or in local organ-specific sub-systems. However, growing evidence would suggest the presence and expression of AT_1 receptors and other components of the RAS inside certain cell types which act independently of the systemic RAS.

Haller and colleagues showed evidence for the presence of intracellular Ang II receptors in vascular smooth muscle cells. Microinjections of Ang II caused an increase in $[CA^{2+}]_i$, and this response was abolished by the co-injection of the AT_1 specific antagonist CV-11974 (Candesartan). This response was observed as a result of intracellular and not extracellular exposure to these compounds, and surface expression of the AT_1 receptor had no effect of the observations (Haller et al. 1996). Moreover, Baker and colleagues overexpressed the Ang II

peptide intracellularly *in vitro* using neonatal rat ventricular myocytes and *in vivo* via an adenoviral vector, and demonstrated a marked hypertrophy of the cells and the entire heart respectively. This effect was not blocked by circulating Losartan (AT_1 receptor blocker), which suggests an intracellular mechanism for this response (Baker et al. 2004). Several functional intracellular components of the RAS, including renin, Ang II and the AT_1 receptor, have been identified. Nonetheless, the full implication of intracellular AT_1 receptors, and their possible interactions with intracellular and extracellular targets is not yet understood (De Mello 2006; Fyhrquist and Saijonmaa 2008; Re and Cook 2006).

1.3 ALTERED AT_1 RECEPTOR EXPRESSION

It is well established that the RAS and the AT_1 receptor play an important role in the regulation of blood pressure. Many physiological and pathological stimuli alter the expression of the AT_1 receptor, suggesting that it is involved in the pathogenesis and/or progression of diseases. The following section looks at physiopathologies which can affect the expression of the AT_1 receptor and is meant to highlight chosen studies which demonstrate some of these changes.

1.3.1 SODIUM

Sodium in a well recognized modulator of blood pressure and thus it is not surprising that it can affect the regulation of the RAS. A growing body of evidence suggests that sodium levels influence the expression of the AT_1 receptor in several tissues, however the exact nature of this effect is conflicting based on the published data.

Douglas and colleagues have demonstrated that after six weeks of low sodium diet, plasma renin activity, plasma aldosterone and blood Ang II concentrations were markedly increased in rats. This was accompanied by an increase in Ang II binding sites in the adrenal

cortex. On the other hand, sodium loading caused the opposite effect, by decreasing plasma renin, plasma aldosterone, blood Ang II, and Ang II binding sites in the adrenal gland (Douglas and Catt 1976). In the kidney, Du and colleagues have shown that the mRNA levels of the AT_1 and AT_{1A} receptors were increased two-fold compared to controls after 14 days of low-sodium diet in Wistar rats (Du et al. 1995). Subsequent work from the same group suggests these changes in AT_1 mRNA are accompanied by parallel changes in receptor expression in the kidneys as assessed by [^{125}I]Sar^1,Ile^8-Ang II binding assays (Wang et al. 1997a).

Contrary to these findings, Szabo and colleagues have presented data to suggest that AT_1 receptors are down-regulated by dietary sodium restriction and up-regulated by sodium loading in beagle dogs. This was measured by *in vivo* PET imaging and *in vitro* autoradiography of the kidneys. The use of a low-sodium diet followed by high-sodium diet regimen (and vice versa) in the same animals might explain the difference in observed results. The authors also acknowledge the confounding outcomes of these studies and suggest that there may be inter-species differences in regards to the regulation of AT_1 receptors in response to dietary sodium changes (Szabo et al. 2001).

Work from Nishiyama and colleagues on Dahl salt-resistant rats demonstrates that high sodium diet causes a down-regulation of the AT_1 receptor in the renal cortex, whereas these levels are unaffected by low sodium diet, or in salt-sensitive rats with high or low sodium diet (Nishiyama et al. 2004). Interestingly, in the heart, no changes in AT_1 receptor densities were observed in either Dahl salt-sensitive or salt-resistant with either high sodium or low sodium diet (Sumida et al. 1998). Wang and colleagues also reported data to suggest that AT_1 receptor density in the brain increases in response to high sodium diet at 4 weeks in both Dahl salt-sensitive and salt-resistant rats, but that this response is observed earlier at 1 and 2 weeks in salt-sensitive rats (Wang et al. 2003).

In sum, these results demonstrate that sodium intake affects the expression of the AT_1 receptor. However, more work is needed in order to elucidate some of the regulatory mechanisms in place which can modulate these changes.

1.3.2 ESSENTIAL HYPERTENSION

Essential, or primary, hypertension is the most common form of hypertension affecting approximately 95% of all patients with chronically elevated blood pressure (Carretero and Oparil 2000). The etiology of essential hypertension is unknown and thus, it is difficult to recreate this pathology experimentally in animal models and usually requires pharmacological treatment or surgery to alter the physiological state. However, the opposite of hypertension can be demonstrated using genetic studies performed on mice. These studies show that knocking out the AT_{1A} receptor gene leads to a significant reduction in resting blood pressure, and a marked un-responsiveness to circulating Ang II, suggesting that the AT_1 receptor is a key component in blood pressure regulation (Ito et al. 1995).

Clinically, blockade of the AT_1 receptor using specific antagonists such as Losartan or inhibition of Ang II synthesis using ACE inhibitors, are used in the treatment of hypertension and have benefits beyond lowering of blood pressure, such as reducing cardiovascular morbidity and mortality in patients with hypertension, diabetes and left-ventricular hypertrophy (Birkenhager and de Leeuw 1999; Dahlof et al. 2002; Hanif et al. 2010). In 1994, Bonnardeaux and colleagues identified the presence of a polymorphism in the AT_1 receptor gene (A1166C) in patients with essential hypertension, but could not associate it to a functional variant in the coding region of the protein (Bonnardeaux et al. 1994). However, experimental studies expressing this polymorphism in rats suggested an increased responsiveness to Ang II, indicating that the AT_1 receptor might play a role in essential hypertension (van Geel et al. 1998).

1.3.3 DIABETES

Diabetes is a disease characterized by an imbalance in glycemia. Type 1 diabetes arises when the beta cells of the pancreas are unable to produce insulin, and type 2 diabetes is characterized by an un-responsiveness of the insulin receptor which leads to exacerbation of the beta cells. Streptozotocin (STZ) is drug that targets and kills the insulin-forming beta cells of the pancreas. Use of STZ on animals has provided a well established model of diabetes which recapitulates some of the symptoms and effects of this disease.

Complications arising from diabetes have been associated with changes in AT_1 receptor expression levels. It has been shown that there is an upregulation of AT_1 receptor mRNA in the myocardium of diabetic rats 14 days after STZ treatment (Sechi et al. 1994). Brown and colleagues have shown that in this model the AT_1 mRNA changes may be a reflection of time- and tissue-dependent alterations of AT_1 receptors. Using STZ treated rats, the authors have shown an increase in AT_1 receptor density at 4 and 12 weeks; which peaked at 4 weeks in the left ventricle, and at 12 weeks in the liver and adrenals. However in the kidney, a decrease was observed and was lowest at 12 weeks (Brown et al. 1997).

Clinical evidence suggests that diabetic nephropathy and glomerulonephritis may also affect AT_1 receptor levels (glomerulonephritis is a renal condition characterized by inflammation of the glomeruli and associated with renal failure). Wagner and colleagues used reverse transcription polymerase chain reaction analyses on whole biopsy and isolated renal glomeruli samples, and found that AT_1 receptor mRNA was lower in patients with diabetic nephropathy and glomerulonephritis when compared to control samples (Wagner et al. 1999). These changes in the kidney were accompanied by increases in atrial myocardial AT_1 mRNA and protein expression as was shown in type 2 diabetic patients undergoing bypass surgery (Reuter et al. 2006). Treatments with ACE inhibitors and AT_1 receptor blockers have demonstrated

protective effects from the development of nephropathy and prevented the deterioration of renal function in patients with type 2 diabetes mellitus (Brenner et al. 2001; Lewis et al. 1993; Lewis et al. 2001; Ravid et al. 1996). This evidence implicates the RAS and the AT_1 receptor in the development and pathology of diabetes, reinforcing the need for further insight into this relationship.

1.3.4 NEPHROPATHY

Nephropathy has also been shown to affect the expression of the AT_1 receptor. In a swine model of renovascular hypertension, the most common form of secondary hypertension, renal artery stenosis caused the over-expression of AT_1 receptors in the kidneys as was demonstrated by *in vivo* using PET imaging and correlated *in vitro* autoradiography studies (Xia et al. 2008). Llorens-Cortes and colleagues demonstrated that in a 2-kidney-1-clip model (complete left renal artery ligation and occlusion), the AT_{1B} mRNA level was reduced in the adrenal gland (Llorens-Cortes et al. 1994). In male Wistar rat models of reduced renal mass hypertension (5/6 nephrectomy), AT_1 receptor transcripts, as measured by Northern blot analysis, were shown to be upregulated approximately eight-fold in the aorta and three-fold in the heart compared to sham operated counterparts at 12 days post-surgery, with an associated elevation in systolic blood pressure (Wang et al. 1997b). Vaziri and colleagues demonstrated that these changes were accompanied by a two- to three-fold increase in AT_1 receptors in the remnant kidney at 8 weeks post-surgery as measured by Western blotting (Vaziri et al. 2007). In the most severe case where a bilateral nephrectomy was performed on rats, a down-regulation of AT_1 receptor mRNA in the adrenal gland and brain stem as early as 24 hours after surgery was observed (Iwai and Inagami 1992). These studies all look at different tissues, however this still suggests that renal diseases affecting either blood flow or function of the kidney can alter the expression of AT_1 receptors in several organs.

1.3.5 MYOCARDIAL INFARCTION AND HEART FAILURE

Perhaps the strongest body of evidence to suggest that there are pathology-related AT_1 receptor alterations is demonstrated by the myriad of studies showing changes in the expression of AT_1 receptors and/or other components of the RAS following myocardial infarction (MI).

Using radioligand binding assays, Reiss and colleagues have demonstrated an up-regulation in AT_1 receptor mRNA and density in the myocardium as early as 2-3 days following MI in rats. This was accompanied by ventricular failure and cardiac hypertrophy (Reiss et al. 1993). These observations were paralleled by studies in the same MI model showing that one week following coronary artery ligation, there is still a marked increase in AT_1 receptor density in the myocardium, and an associated ventricular failure (Meggs et al. 1993). Tan and colleagues measured AT_1 receptor densities at 4 and 8 weeks post-MI in male Wistar rats and observed an increase in AT_1 receptor density in the brain. In the heart, up-regulation was seen in all regions of the ventricles with the highest increase being noted in the infarct area. However, the opposite was noticed in the kidneys where a down-regulation was observed (Tan et al. 2004). Mento and colleagues looked specifically at the kidneys, and using receptor binding assays were able to demonstrate structure specific changes in AT_1 receptor expression. In fact, at 4 to 6 weeks post-MI, there was up-regulation of AT_1 receptors in the renal glomeruli and a down-regulation in the renal vasculature (Mento et al. 1998).

Changes in AT_1 receptor and RAS activity also play an important role in the progression of ventricular hypertrophy, cardiac remodeling and heart failure (HF) after MI, and evidence suggests that interference with RAS pathways reduces cardiac remodeling associated with MI. Loss of function in the affected areas of the myocardium after MI is partly compensated for by increases in a number of hormones, including Ang II. Clinical evidence shows that the level of

circulating Ang II progressively increases in the first three days following MI (McAlpine et al. 1988). Cohn stipulates that although initially this is an adaptive response, chronically this phenomenon will contribute to detrimental cardiac remodeling (Cohn 2000).

Schieffer and colleagues demonstrated that a six week treatment with either ACE inhibitor Enalapril or AT_1 receptor blocker Losartan, starting at seven days post-MI in rats, caused a significant reduction in cardiac hypertrophy, vascular resistance, interstitial fibrosis and an increase in myocardial capillary density (Schieffer et al. 1994). As well, AT_{1A} receptor knock-out mice showed improved survival and less cardiac remodeling at four weeks post-MI (Harada et al. 1999). Van Kats and colleagues have also demonstrated that the use of ACE inhibitor Captopril and AT_1 receptor blocker Eprosartan in pigs after MI was able to reduce right and left ventricular hypertrophy and cardiac remodeling. This study highlights the important contribution of Ang II and the AT_1 receptor in cardiac remodeling in an animal model which is more representative of the human condition (van Kats et al. 2000). It is important to note that remodeling is a multifactorial process that can be characterized by inflammation, fibrosis, ventricular wall thinning, and chamber dilation in the heart (Dorn 2009; McAlpine et al. 1988). It is clear that the AT_1 receptor plays a role in mediating these changes, although it is important to consider that not all of the effects observed are solely attributable to the AT_1 receptor and more work is needed to fully understand its role.

Chronically, the negative effects attributed to MI and cardiac remodeling are often associated with HF (Dorn 2009; McAlpine et al. 1988). Contrary to the previous studies reporting increased AT_1 expression post-MI in animal models, end-stage HF has been associated with decreases in AT_1 receptor mRNA levels in the human myocardium (Haywood et al. 1997; Regitz-Zagrosek et al. 1997). These changes were paralleled by decreases in the AT_1 receptor density in samples of patients with HF (Asano et al. 1997). This discrepancy might reflect a time-

dependent change associated with the development of HF after MI, with the interplay between physiological cardiac insufficiency and neurohormonal alterations changing through the progression of the disease. A better understanding of these regulatory changes is still needed. Cumulatively, this evidence does however implicate a role for the AT_1 receptor in the pathogenesis of MI and HF.

1.4 NUCLEAR IMAGING

1.4.1 POSITRON EMISSION TOMOGRAPHY

Positron emission tomography (PET) is a nuclear imaging modality used for non-invasive *in vivo* imaging in humans and in animals. The basic principles behind PET involve the detection of a radioactive atom, such as carbon-11 (^{11}C), using a specialized scintillation crystal detection system in the PET camera. Carbon-11 is a radioactive isotope of carbon, which decays to boron-11 via positron emission. When this occurs, a proton from the nucleus gets converted to a neutron, and releases a positron (e^+), which is the antimatter counterpart of the electron (e^-). Upon meeting an electron, the annihilation of both sub-atomic particles occurs and releases two gamma photons (γ) moving in opposite direction at approximately 180^o from each other. These photons are then detected by scintillator crystals paired to photomultiplier tubes positioned in a cylindrical arrangement, and the simultaneous detection of two photons in coincidence is recorded (Figure 4). By acquiring coincidence data over a large period of time, reconstruction of the isotope distribution is possible, and allows localization of the radioactive source.

The advantage of PET over other imaging modalities such as X-ray and computed tomography, which mostly give anatomical information, is that PET allows molecular imaging of sub-cellular targets. If the radioactive element, e.g. carbon-11, is incorporated into a pharmacological compound, the localization of radioactivity can be attributed to the distribution and/or retention of that compound due to binding to specific cellular targets such as cell-surface

receptors. Another advantage of PET over other molecular imaging modalities is that it allows the use of isotopes, such as carbon-11, nitrogen-13, oxygen-15 and fluorine-18, that do not alter the organic nature and properties of endogenous molecules or pharmacological compounds such as drugs (Wahl 2002).

1.4.2 SINGLE PHOTON EMISSION COMPUTED TOMOGRAPHY

Single photon emission computed tomography (SPECT) is a nuclear imaging modality that allows molecular imaging similarly to PET. However, SPECT makes use of isotopes which undergo gamma decay, e.g. technetium-99m, iodine-123 and indium-111, and single photon detection with a SPECT camera. Many differences in the image acquisition technology exist as well (Germano and Berman 2006), although they will not be discussed in this thesis.

1.4.3 QUANTIFICATION AND KINETIC MODELING

PET image data can be quantified in numerous ways and several methods have been developed to analyze the behavior of radiotracers in animals and humans. In 1990, using [N-^{11}C-methyl]-(–)-Cocaine PET studies in humans, Logan described a graphical method of quantifying the ratio of radiotracer in tissue relative to plasma at equilibrium for reversibly binding ligands, and its application in one-tissue-compartment and two-tissue-compartment models. In essence, $\int_0^T C_{PET}(t)dt/C_{PET}(T)$ (min) is plotted against $\int_0^T C_P(t)dt/C_{PET}(T)$ (min·cm^3/ml), where $C_p(t)$ is the concentration of tracer in plasma and $C_{PET}(t)$ is the concentration of tracer in the tissue, and a straight line is fitted to the linear part of the data. If the ligand binds reversibly, the plot will become linear after an initial transitional phase. The slope of this line will correspond to the distribution volume (DV) in ml/cm^3 of this tracer in the predefined region.

From a physiological point of view, the DV of a given tracer is an indicator of that tracer's concentration in a given tissue. If the tracer binds to a specific target, its concentration

can be an indicator of binding potential to a given molecular target. Thus, the DV can be used as an indirect indicator of protein expression and/or binding potential for reversibly binding ligands, i.e. a higher protein expression or binding affinity will result in a higher DV value. The DV can also be modulated by the plasma input function; which is an indicator of tracer concentration in the plasma available for tissue uptake. If the plasmatic tracer concentration is increased, the DV will decrease as a result. Thus, the DV is defined as the concentration of radiotracer in tissue over plasma at equilibrium (steady-state) and provides a quantifiable parameter for repeated measurements and assessment of repeatability and reliability (Logan et al. 1990).

1.4.4 REPEATABILITY, RELIABILITY AND REPRODUCIBILITY

To address this last point, Bland and Altman have developed a method to assess the repeatability[1] and/or reliability[2] of measurements. Bland and Altman suggest that generating a linear regression and using the correlation coefficient to measure agreement may be inappropriate and lead to false interpretations that assume good repeatability and reliability. Take a simple scenario for example: a group of ten rats each receive two scans to measure myocardial blood flow. Results show that for each rat, scan #2 results are approximately 40% lower that scan #1 results, when in reality myocardial blood flow did not change between the two scans. If a plot of scan #2 vs. scan #1 was to be generated, there is a high likelihood that the data would follow a linear relationship, and that the correlation coefficient would be high. Therefore, the authors suggest that looking at the difference between the two values is more indicative of this test's ability to measure myocardial blood flow reliably. To this end, the Bland-

[1] Repeatability is defined as the variation in measurements when the same data is analysed repeatedly by the same person with the same instrument under the same conditions, i.e. verifying the accuracy of the analysis methods.

[2] Reliability is defined as the variation in measurements when only one variable is altered, i.e. comparing baseline scans performed on the same subject at two different time points, e.g. test re-test.

Altman analysis consists of calculating the difference between measurement #1 and measurement #2 (e.g. scan #2 - scan #1), and expressing this difference as a function of the mean between measurement #1 and #2 (e.g. [scan #1 + scan #2]/2) for each subject (or sample) in a given study. The mean difference and its standard deviation (SD) can then be calculated. The 95% confidence interval can be approximated by its upper bound, represented by the mean + 1.96 SD, and its lower bound, represented by the mean - 1.96 SD. The variability can be measured by dividing the previously calculated SD of the mean difference by the mean of the measurement in question (e.g. “SD of the mean difference”/“mean myocardial blood flow”). A variability of 20% or less and a mean difference that is zero or close to zero are desirable as they indicate that the results of repeated measurements are repeatable and reliable (Bland and Altman 1986).

Reproducibility is defined as the ability to reproduce a given experiment and its results independently of the first experiment, i.e. confirming the results of published work. Ideally, this component of the work would be performed by another institution and was therefore not explored as part of this thesis.

1.4.5 RECEPTOR OCCUPANCY LIMITATION

Another consideration to take into account regarding PET imaging quantification is receptor occupancy. Hume and colleagues suggest that the concentration of bound ligand does not always follow a linear relationship with free ligand concentration in the system. Using the saturation kinetics of PET radioligands, they suggest that for appropriate quantification using kinetic models in small animal PET imaging, receptor occupancy must be 1% for high affinity tracers. For intermediate and low affinity tracers, the amount of injectable mass and allowable free ligand concentration in the system can increase accordingly. However, the authors acknowledge that this limitation is very difficult to achieve as it requires very high specific

activity and that a receptor occupancy of 5% may still be acceptable (Hume et al. 1998; Hume and Myers 2002).

1.5 AT_1 RECEPTOR RADIOLIGANDS

To date, and to our knowledge, eight radioligands for the AT_1 receptor have been synthesized and evaluated for *in vivo* nuclear imaging.

1.5.1 [^{123}I][SAR^1,ILE^8]ANG II AND [^{125}I][SAR^1,ILE^8]ANG II

The first attempt at imaging the AT_1 receptor *in vivo* was performed in 1994 and utilized two analogs of the Ang II peptide: [^{123}I][Sar^1,Ile^8]Ang II and [^{125}I][Sar^1,Ile^8]Ang II, and a γ-camera to acquire planar images. Preliminary biodistribution studies in male Sprague-Dawley rats showed specific binding in the liver, kidneys and adrenal glands, but also non-specific binding (~50% in adrenal) when blocking with the AT_1 receptor antagonist L-158,809. Imaging in rats and Rhesus monkeys was performed and uptake was observed in the liver and kidneys following i.v. administration of [^{123}I][Sar^1,Ile^8]Ang II. However, image quality was very poor, kidneys were not well defined and only partial blocking was observed with L-158,809 (Gibson et al. 1994).

1.5.2 [^{11}C]MK-996 AND [^{11}C]L-159,884

The first PET ligand targeted at the AT_1 receptor was [^{11}C]MK-996 (Figure 5A) and was reported to be useful for imaging AT_1 receptors in canine kidneys using PET (Mathews et al. 1995). However, due to the difficult synthesis of [^{11}C]MK-996, an analog of this compound, [^{11}C]L-159,884 (Figure 5B), was developed by the same group (Hamill et al. 1996). Biodistribution studies using CD-1 mice reported that [^{11}C]L-159,884 was taken up in the heart, lungs, liver and kidneys, and that blocking the AT_1 receptor with various antagonists caused a significant reduction in tracer uptake in the heart, lungs and kidneys but not in the liver (Kim et al. 1996). Later studies in beagle dogs demonstrated uptake of [^{11}C]L-159-884 in the liver and

kidney cortex, and that the AT_1 receptor antagonist MK-996 could displace this tracer form the kidney (Szabo et al. 1998). This tracer was also able to detect changes in AT_1 receptor expression in response to alterations in dietary sodium intake (Szabo et al. 2001). Additionally, [^{11}C]L-159,884 was reported to bind to AT_1 receptors in the adrenal glands (not previously reported) and kidneys of adult female beagles (Owonikoko et al. 2004). This tracer also detected changes in receptor density in these organs, however rapid metabolism in humans was reported and [^{11}C]L-159,884 was therefore considered unsuitable for human PET imaging (Mathews et al. 2004; Owonikoko et al. 2004). The most recent studies on this radioligand show that [^{11}C]L-159,884 was used to image the AT_1 receptor in baboons with uptake in the renal cortex, however not to the same extent as the succeeding tracer: [^{11}C]KR31173 (Zober et al. 2006).

1.5.3 [^{11}C]KR31173

The latest tracer from the same group at Johns Hopkins University, [^{11}C]KR31173 (Figure 5C), was evaluate using biodistribution in CD-1 mice. After i.v. injection of [^{11}C]KR31173, highest uptake was observed in the adrenal glands, kidneys, liver, lungs and heart. Blocking the AT_1 receptors with MK-996, KR31173 or SK-1080 significantly reduced uptake in the adrenal glands, kidneys, lungs and heart (Mathews et al. 2004; Zober et al. 2006). Imaging was also performed on mice, beagle dogs and baboon and displayed specific uptake in the kidneys of all three species (Zober et al. 2006). Further studies performed on pigs showed renal uptake of [^{11}C]KR31173. When these animals were subjected to a renal artery stenosis in the right kidney and subsequent renovascular hypertension, tracer retention was increased in that kidney and associated with an increased AT_1 receptor expression as measured by autoradiography (Xia et al. 2008).

1.5.4 TC-99M LOSARTAN

Tc-99m Losartan (Figure 6) is the only SPECT radioligand currently being used *in vivo* for imaging the AT_1 receptor in animals. Authors propose that Tc-99m Losartan has a higher affinity to the AT_1 receptor than the parent compound Losartan, 60 pmol/L vs. 10 nmol/L, respectively, and a better biodistribution profile due to the introduction of peptide characteristics into the Losartan pharmacophore, but lack to present this data. Male Swiss Webster mice were subjected to a permanent ligation MI and studied at 3 weeks post-MI. Tc-99m Losartan displayed an increased uptake in infarct area when compared to controls as was assessed by *ex vivo* and *in vivo* SPECT imaging (Verjans et al. 2008). When comparing this compound to Losartan, it is important to note that despite the addition of a large lipophilic group at the 5' position on the imidazole ring (hydroxyl position), Tc-99m Losartan still maintained its affinity for the AT_1 receptor.

1.5.5 [^{11}C]METHYL-CANDESARTAN AND [^{11}C]TH4

Finally, our group at the University of Ottawa Heart Institute (Ottawa, Canada) has developed analogs of the clinically used AT_1 receptor blocker (ARB) Candesartan: [^{11}C]Methyl-Candesartan and its desethyl derivative [^{11}C]TH4 as two potential AT_1 radioligands (Figure 7A and B). Biodistribution studies on these compounds suggest that [^{11}C]Methyl-Candesartan has potential for *in vivo* imaging as it was shown to be specific and selective for the AT_1 receptor over the AT_2, Mas, β-adrenergic and α_2-adrenergic receptors (Hadizad et al. 2009a). Our studies have also demonstrated that [^{11}C]Methyl-Candesartan is taken up in kidneys and displays good image quality making it suitable for AT_1 receptor density quantification *in vivo* using small animal PET imaging (Hadizad 2010, submitted to press).

To date, many studies looking AT_1 receptor imaging have been performed on animals; however no reports on human imaging have been published. Work is thus still underway to develop the ideal AT_1 receptor radioligand suitable for clinical imaging of AT_1 receptors.

1.6 [^{11}C]METHYL-LOSARTAN AS A RADIOLIGAND FOR THE AT_1 RECEPTOR

Based on the structure of the clinically used AT_1 receptor antagonist Losartan (Figure 8A), our lab has developed a novel radiotracer, [^{11}C]Methyl-Losartan (Figure 8B), that has the potential to bind specifically to the AT_1 receptor and allow its imaging with PET. Clinically, Losartan is currently used as an anti-hypertensive drug for the treatment of essential hypertension and in the management of HF, type 2 diabetes, and nephropathy (Brenner et al. 2001; Dahlof et al. 2002; Pitt et al. 2000; Pitt et al. 1997; Ramasubbu et al. 2007). The effects of Losartan are also attributed to EXP-3174 (Figure 9) which is the main metabolism product of Losartan. EXP-3174 also possesses AT_1 receptor antagonistic properties and has 10 times the affinity of its parent compound for the AT_1 receptor (Krovat and Langer 2003).

Based on SAR studies, Losartan (DuP 753) and Methyl-Losartan have similar potencies in inhibiting specific binding of [^{3}H]Ang II (IC_{50}=0.019 µM and IC_{50}=0.032 µM, respectively) as tested on male Sprague-Dawley rat adrenal cortical microsomes (Carini et al. 1991). As was seen previously in section 1.5.4 (Tc-99m Losartan), the addition of a large group at the 5' position of the imidazole ring did not hinder binding and even improved affinity for the AT_1 receptor, and thus corroborates the SAR findings reported by Carini and colleagues (Verjans et al. 2008).

Moreover, peptide SAR studies identified the Tyr^4, His^6 and Phe^8 amino acids as important for Ang II binding and activation (Tzakos et al. 2004). Three dimensional structure analysis suggests that the arrangement of the three side-chains of these amino acids resembles that of the tetrazole-biphenyl ring conformation in Losartan (Matsoukas et al. 1994; Nikiforovich

et al. 1994; Nikiforovich and Marshall 1993; Pierson and Freer 1992). [^{11}C]Methyl-Losartan shares this characteristic structural feature present in many AT_1 receptor blockers, also known as “sartans”, e.g. Losartan, Valsartan, Irbesartan and Candesartan (de Gasparo et al. 2000; Kaschina and Unger 2003).

1.7 TABLES AND FIGURES

Table 1 – Relative distribution of AT_1 receptors in rat, rabbit and monkeys according to Chang and colleagues. Data is adapted from *in vitro* binding assays performed using [^{125}I]Sar^{1},Ile^{8}-Angiotensin II (Chang and Lotti 1991).

	Tissue	Counts (CPM/mg tissue)	Ratio to heart
Rat	Adrenal cortex	23466	1460
	Kidney cortex	6284	391
	Aorta	122	7.61
	Brain	317	19.8
	Heart	16	1
Rabbit	Adrenal cortex	46582	1454
	Kidney cortex	1501	46.9
	Aorta	124	3.87
	Brain	114	3.54
	Heart	32	1
Monkey	Adrenal cortex	3848	316
	Kidney cortex	449	36.8
	Aorta	146	12
	Brain	63	5.19
	Heart	12	1

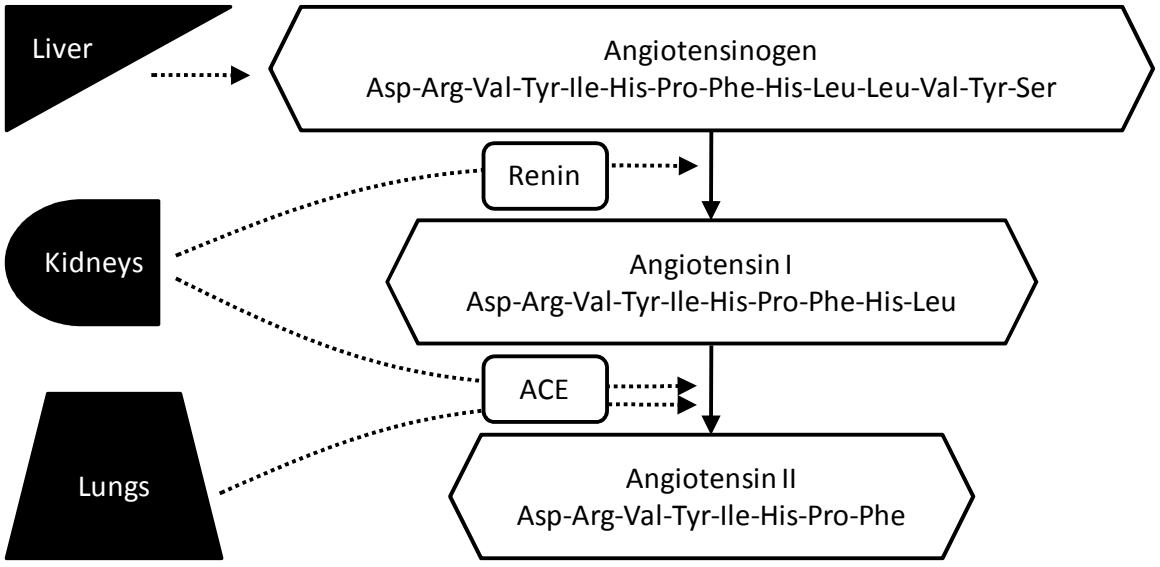

Figure 1 – Angiotensin II synthesis pathway. ACE: Angiotensin converting enzyme.

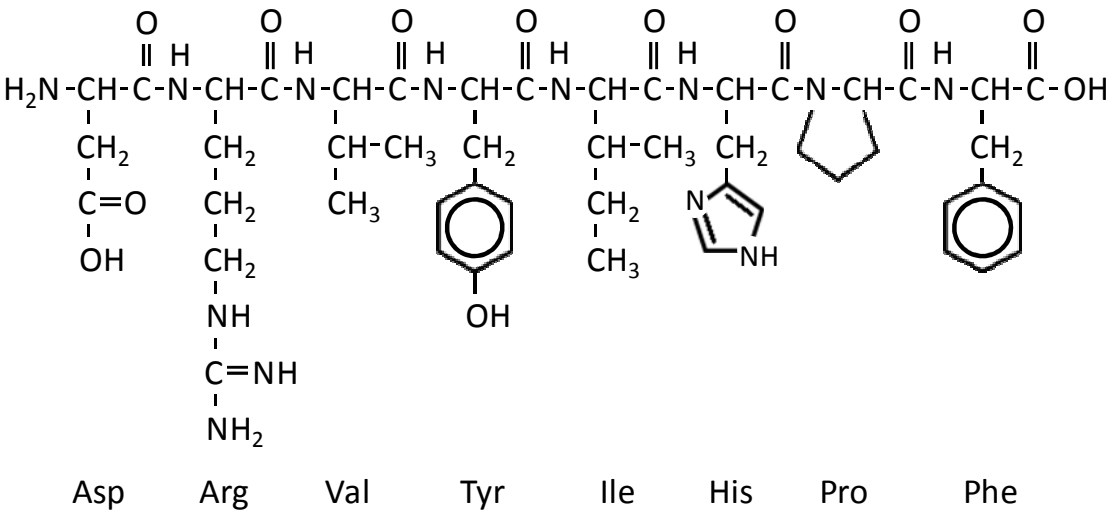

Figure 2 – Angiotensin II octapeptide structure.

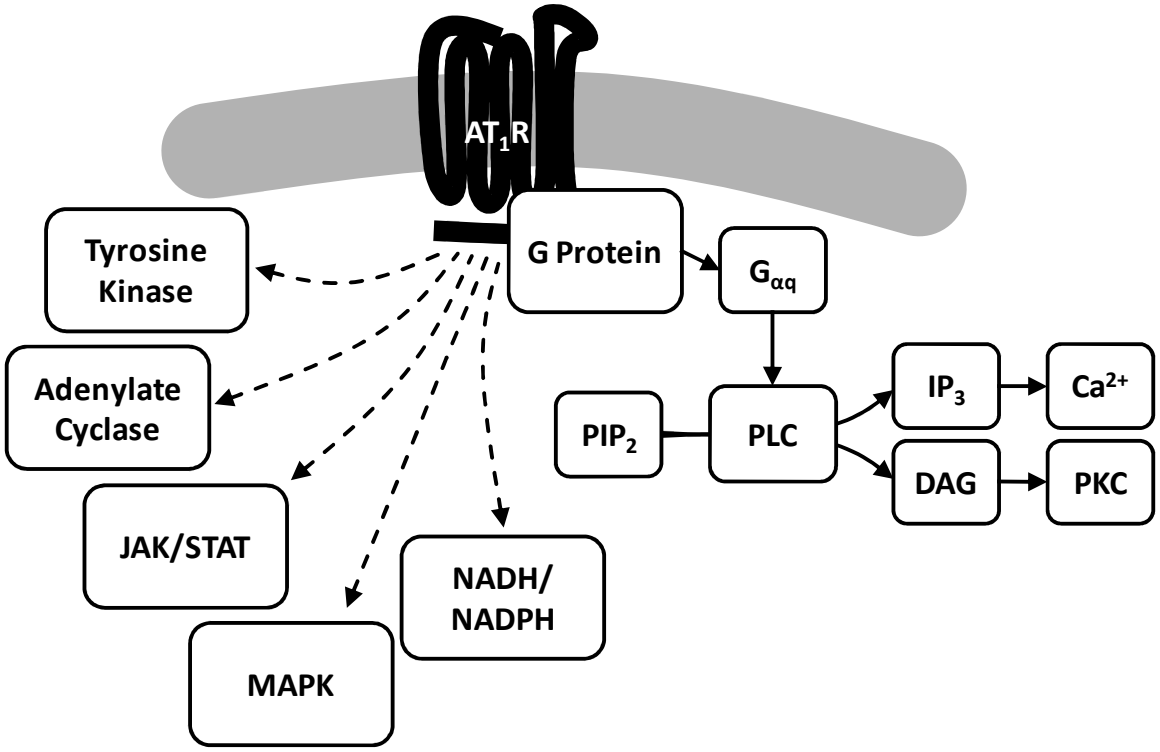

Figure 3 – AT_1 receptor signal transduction pathways. $G_{\alpha q}$: G protein α subunit, PIP_2: phosphatidylinositol biphosphate, PLC: phospholipase C, IP_3: inositol triphosphate, DAG: diacyl glycerol, PKC: protein kinase C.

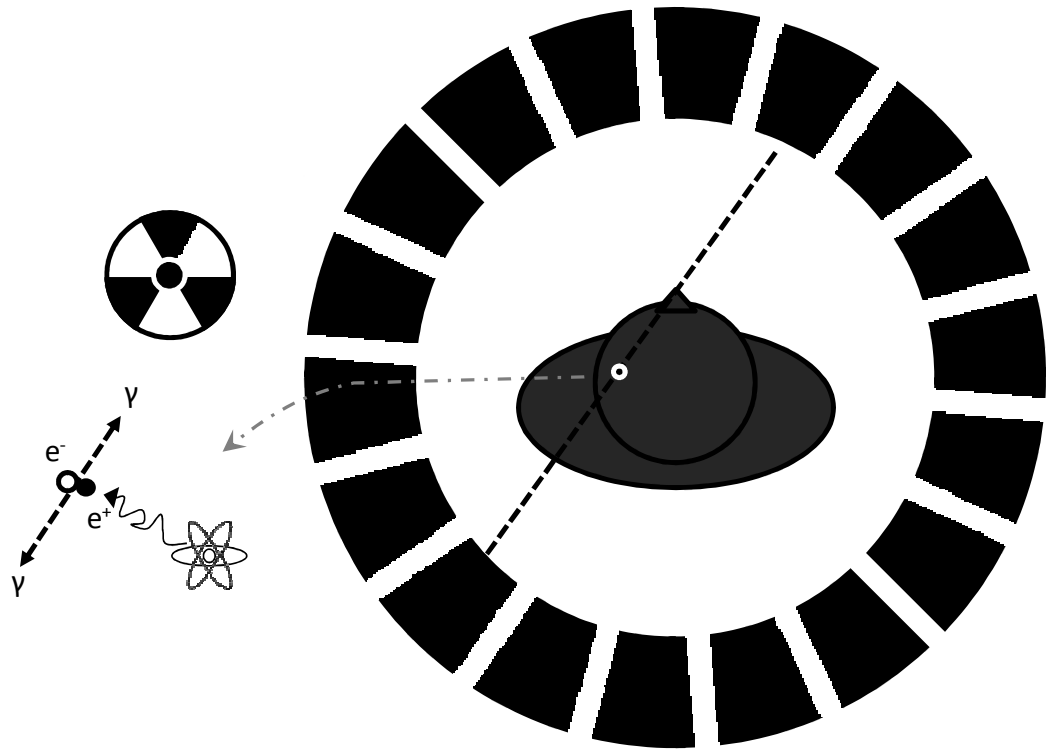

Figure 4 – Representation of a PET scanner and radioactive positron decay. e^-: electron, e^+: positron, γ: gamma photons.

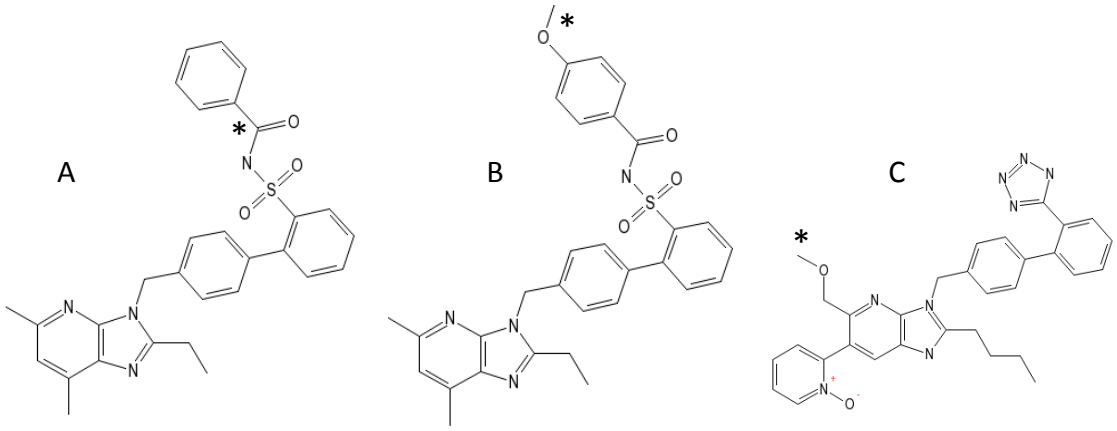

Figure 5 – Chemical structure of Johns Hopkins radiotracers. (A) [^{11}C]MK-996 (Mathews et al. 1995), (B) [^{11}C]L-159,884 (Hamill et al. 1996) and (C) [^{11}C]KR31173 (Mathews et al. 2004). C-11 radioactive atom position indicated by asterisk.

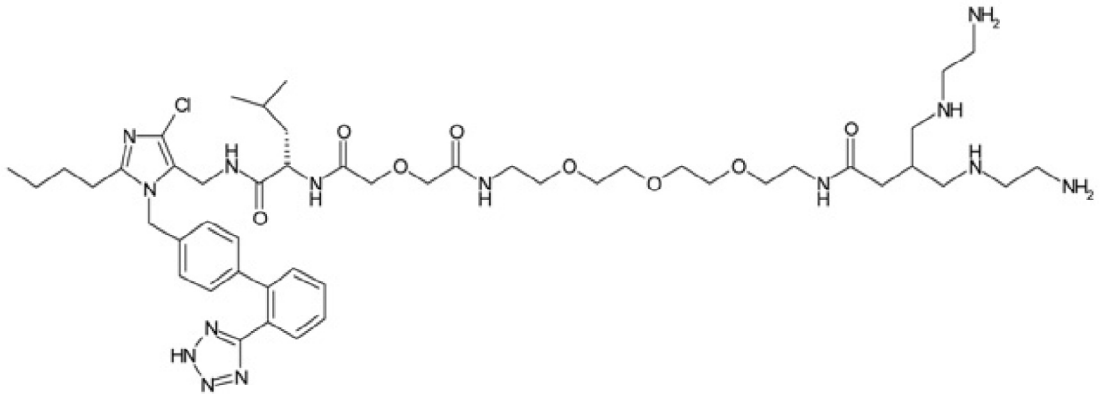

Figure 6 – Chemical structure of Tc-99m Losartan (Verjans et al. 2008).

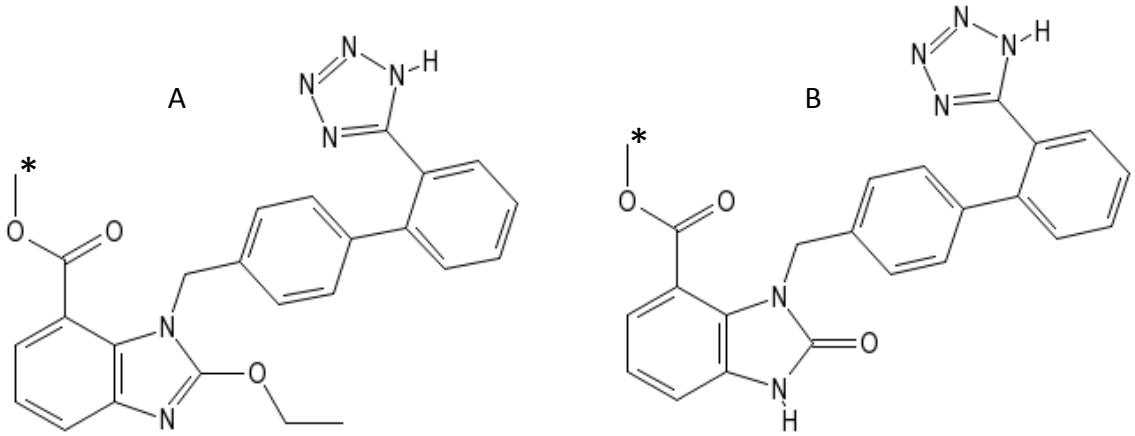

Figure 7 – Chemical structure of (A) [^{11}C]Methyl-Candesartan and (B) [^{11}C]TH4 (Hadizad et al. 2009a). C-11 radioactive atom position indicated by asterisk.

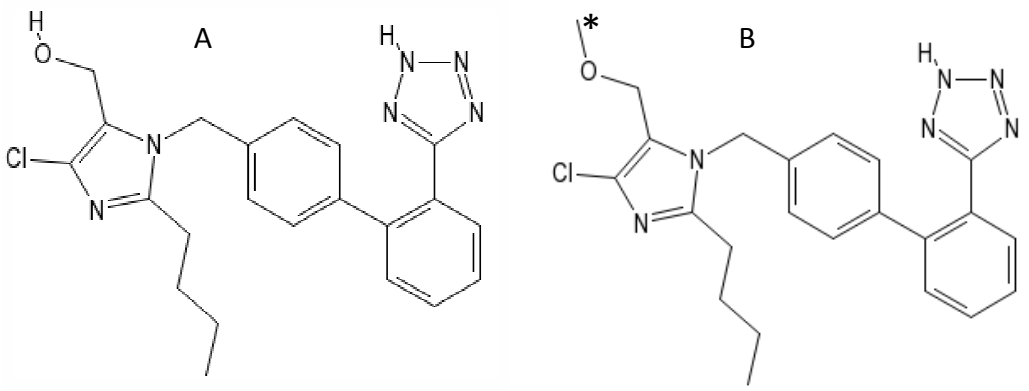

Figure 8 – Chemical structure of (A) Losartan and (B) [^{11}C]Methyl-Losartan (Hadizad et al. 2009b). C-11 radioactive atom position indicated by asterisk.

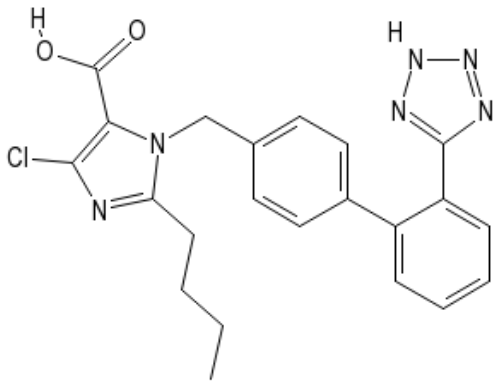

Figure 9 – Chemical structure of EXP-3174.

2 HYPOTHESES

- [^{11}C]Methyl-Losartan will exhibit high tissue to blood contrast, specific retention in AT_1 receptor rich regions, and allow repeatable and reliable AT_1 receptor imaging and quantification with small animal PET.
- [^{11}C]Methyl-Losartan will bind specifically and selectively to the AT_1 receptor *in vivo*, *ex vivo* and *in vitro*.
- The presence, if any, of labeled metabolites in the plasma and kidneys will not prevent AT_1 receptor density measurements.

3 OBJECTIVES

- Characterize the pharmacokinetics, time course and binding specificity of [^{11}C]Methyl-Losartan in rats using *in vivo* microPET imaging.
- Determine binding specificity and selectivity of [^{11}C]Methyl-Losartan for the AT_1 receptor over the AT_2, Mas and β-adrenergic receptors in rats using *ex vivo* biodistribution and *in vitro* autoradiography methods.
- Evaluate the presence and specific binding of radiolabeled metabolites in the plasma and kidney using high performance liquid chromatography.

4 MATERIALS AND METHODS

4.1 GENERAL PROCEDURES

4.1.1 ANIMALS

All animal procedures were performed in accordance with the guidelines of the University of Ottawa Animal Care Committee and the Canadian Council on Animal Care for the Use and Care of Laboratory Animals. For all animal experiments, normal male Sprague-Dawley rats were purchased from Charles River Laboratories. Rat were housed in pairs, fed standard chow and water *ad libitum* and kept on a 12 hour light-dark cycle. Rats were allowed a minimum of 5 days of acclimatization upon arrival before any experiments were performed.

4.1.2 DRUGS

Losartan was purchased from Merck & Co. Inc., Candesartan and EXP-3174 were purchased from Toronto Research Chemicals Inc., and PD-123,319, A-779 and Propranolol were purchased from Sigma-Aldrich Co.

4.1.3 RADIOCHEMICAL SYNTHESIS

[^{11}C]Methyl-Losartan (2-Butyl-4-chloro-5-([^{11}C]methoxymethyl)-1-[[2′-tetrazole-5-yl]biphenyl-4-yl]methyl]imidazole) was synthesized in a three-step process. Starting with the parent compound Losartan, the tetrazole ring was protected with a trityl group in the first step. In the second step, the hydrogen from the hydroxyl was replaced with an ^{11}C-methyl group. And in the third step, the protective was removed by hydrolysis under acidic conditions (Figure 10) (Hadizad et al. 2009b). The radiochemical purity was >99%, the chemical purity >95% and the radiochemical yield 30-60% at end of synthesis. The specific activity range was 20-3600 mCi/μmol and yield was between 1 and 85 mCi.

[^{11}C]Methyl-EXP3174 (2-Butyl-4-chloro-5-([^{11}C]methyl ester)-1-[2′-(1H-tetrazol-5-yl)1,1′-biphenyl-methyl]imidazole) (Figure 11) was synthesized in a similar three-step process. Starting with EXP-3174, the tetrazole ring was protected with a trityl group in the first step. In the second step, the hydrogen from the carboxylic acid was replaced with an ^{11}C-methyl group. And in the third step, the protective was removed by hydrolysis under acidic conditions (Figure 12) (Hadizad et al. 2010). The specific activity range was 800-2500 mCi/µmol and yield was between 5 and 25 mCi.

4.1.4 STATISTICAL ANALYSIS

Unless otherwise specified, statistical analysis was performed using one-way analysis of variance (ANOVA) and a Bonferroni post-hoc analysis was used to compare all groups to control. A P value of <0.05 was considered significant for all tests.

4.2 MICROPET IMAGING

4.2.1 CONTROL SCANS

MicroPET imaging was performed to evaluate time course, tissue uptake and pharmacokinetics of [^{11}C]Methyl-Losartan (n=21 scans). Animals (weighing 200-450 g) were anaesthetized and kept unconscious throughout scan using a nose cone with isoflurane (1-2%). Rats were placed on microPET scanner bed in supine position and body temperature was maintained at 37^{o}C. Rats were positioned in the PET camera to include the heart and both kidneys in the field of view (FOV). Body temperature, heart rate and respiratory rate were monitored throughout the scans. Rats were injected with 0.5-2.2 mCi (18.5-81.4 MBq) of [^{11}C]Methyl-Losartan in an injection volumes of less than 1 ml (to reduce any systemic volume effects) via a 26 gauge catheter (Hospira VeniSystems) into the lateral tail vein. The specific activity ranged from 100 to 2500 mCi/µmol (3.7-92.5 GBq/µmol), the injected mass was

between 0.2-28.0 µg and injected dose between 0.6-47 µg/kg. A dynamic 60 min C-11 emission scan (Inveon, Siemens) was acquired and a 10 min transmission scan with Co-57 was performed either immediately preceding or following the emission scan.

Unless otherwise specified, all microPET data was reconstructed into a dynamic histogram with twelve 10 sec frames, three 1 min frames and eleven 5 min frames for a 60 minute scan using OSEM3D/Map (β=1) reconstruction algorithm. Corrections were applied for scatter to compensate for photon deflection, and attenuation to compensate for loss of photons due by tissue density. Time activity curves (TACs) were generated for the left atrial cavity, kidneys, liver and background by drawing regions of interest (ROIs) using the Siemens software (Siemens Inveon Research Workplace) according to a standard operating procedure outlined in section 8 (Appendix).

Regional tracer kinetics were quantified using the Logan graphical method to estimate DVs for the right and left kidney cortices (Logan et al. 1990). The left atrial cavity served as arterial blood input for this analysis. For the scope of this thesis, no corrections were made for plasma to blood activity ratio or for metabolites, and DV values are therefore considered uncorrected.

4.2.1.1 [^{11}C]Methyl-EXP3174

It is well established that Losartan is mainly metabolized by the liver into its active analog EXP-3174; which displays approximately 10 times the affinity to the AT_1 receptor (Krovat and Langer 2003). As a sub-experiment, microPET imaging was performed using [^{11}C]Methyl-EXP3174 and followed the protocol described above in the previous section (n=2 scans). Rats were injected with 0.2-2.1 mCi (7.4-77.7 MBq) of [^{11}C]Methyl-EXP3174, the specific activity ranged from 800 to 2500 mCi/µmol (29.6-92.5 GBq/µmol), the injected mass was between 0.4-1.7 µg and injected dose between 1.2-4.6 µg/kg. Results were analyzed in the same way. Only

control scans were done with [^{11}C]Methyl-EXP3174 and none of the subsequently described experiments were performed with this tracer. The objective of this study was a preliminary evaluation of the potential of [^{11}C]Methyl-EXP3174 as a novel AT_1 receptor radioligand.

4.2.2 TEST RE-TEST

To optimize the scanning protocol and verify reliability of results, 7 rats were scanned a second time in a different session and using a new [^{11}C]Methyl-Losartan tracer formulation. This second control scan was performed as described in section 4.2.1 (Control Scans), and took place within a few weeks of the first scan. Results from both scans were compared to each other; a 95% confidence interval was generated for the mean difference between both scans and used to determine whether or not this difference is significantly different from zero. A Bland-Altman analysis (Bland and Altman 1986) was also performed to assess the agreement and reliability of the entire procedure.

4.2.3 INJECTED DOSE EFFECT

To monitor the effect of changing the dose on the generated DVs, specific activity, injected activity, injected mass, rat weight and injected dose were recorded or calculated for all control scans (n=21 scans). Generated Logan DVs were then plotted against these values and evaluated for any trend using a linear regression analysis. Briefly, the correlation coefficient (R^2) was tested against a null hypothesis of R^2=0 using the formula $t = R \times \sqrt{n - 2/1 - R^2}$ to generate a *t* value, which was then determined significant or not based on a cumulative *T* distribution. As confirmation of this test, the slope of the data was also considered significantly different from zero if the 95% confidence interval for the slope did not overlap with zero. If the correlation coefficient and the slope were significantly different from zero, then the DV values

were said to follow a trend dependant on the given independent variable (specific activity, injected activity, injected mass, rat weight and injected dose).

4.2.4 BINDING SPECIFICITY

To assess binding specificity rats were imaged as described in section 4.2.1 (Control Scans) with a co-injection of selective AT_1 receptor antagonists Losartan (20 mg/kg i.v. co-injection) (n=4 scans) or Candesartan (5 mg/kg i.v. co-injection) (n=4 scans) (Hadizad et al. 2009a). A statistical test was performed using a two-tailed paired t-test to compare the DV values of blocking scans to their respective baseline scans.

4.2.5 DISPLACEMENT STUDIES

For this sub-study, rats were scanned as described in section 4.2.1 (Control Scans). At 10 minutes post-injection, one rat was injected with a blocking dose of the selective AT_1 receptor antagonist Losartan (20 mg/kg i.v. bolus). Another rat received the same Losartan (bolus) treatment but at 17 min. We expect to observe a decrease in tissue activity at time of Losartan injection reflecting displacement of the radiotracer from the AT_1 receptor binding sites by the antagonist. This will serve as a qualitative confirmation for binding specificity.

The following reconstruction frames were used for these scans:

- 10 min post-injection: twelve 10 sec frames, thirteen 1 min frames and nine 5 min frames.
- 17 min post-injection: twelve 10 sec frames, three 1 min frames, two 5 min frames, ten 1 min frames and seven 5 min frames.

4.2.6 IMAGE ANALYSIS: DRAWING REGIONS OF INTEREST

To this date, a standardized method of analyzing kidney scans had not been established by our group. Unlike cardiac scans which can be processed semi-automatically using the in-

house developed software FlowQuant (Klein et al. 2010), renal scans are not handled by an automated process. In order to properly analyze scan data, a standardized method had to be established to draw regions of interest and determine DVs for the kidneys using the Siemens Inveon camera software provided by the manufacturer. As per that objective, a standard operating procedure was established and is outlined fully in section 8 (Appendix). Although results are not included in this thesis, factors that were analyzed and compared to establish SOP include, but are not limited to:

- Kidney sections to use, i.e. upper apex vs. mid section vs. lower apex
- Lower and upper intensity threshold of image and ROIs
- Time frames, i.e. early frames vs. late frames
- Time frames for Logan DV calculation, i.e. 10-40 min, 10-60 min, 20-40 min vs. 20-60 min.

This protocol was established using [^{11}C]Methyl-Losartan scans, but the methods can be extrapolated to [^{11}C]Methyl-EXP3174, [^{11}C]Methyl-Candesartan and [^{11}C]TH4 scans, which are all novel AT_1 receptor radioligands developed by our group.

4.2.7 INTRA-USER AND INTER-USER VARIABILITY

To verify that data analysis methods render repeatable results, all baseline scans were analyzed by the same user twice (Rawad E. Antoun) and a third time by an unbiased, blinded user following the same analysis instructions (Kumiko C. Mackasey, M.Sc. candidate) (n=13 scans). To simplify the results, only the DV for the left kidney was generated. To assess intra-user variability, results from the same user were plotted against each other and a best fit curve was generated to measure linearity of results and correlation coefficient. The slope of the dataset was compared to an ideal correlation (slope of 1) and considered significantly different from 1 if the 95% confidence interval for this slope did not overlap with 1. The mean difference

between both analyses was also evaluated by generating a 95% confidence interval for this difference and determining whether or not this difference is significantly different from zero. As well, a Bland-Altman analysis was performed to compare the repeatability of the results (Bland and Altman 1986). Inter-user variability was also assessed by performing the same analyses using the results from the two different users.

4.2.8 BLOOD AND PLASMA SAMPLING

An important consideration when calculating tissue DVs is accounting for tracer concentration in plasma relative to whole blood (Logan 1990). Typically, when a blood input function is not readily available and/or usable from image data, intra-venous (i.v.) blood sampling is used to determine the time-activity of tracer in the plasma (Logan 1990). In our studies, blood activity data is available from the images analyses (ROIs drawn around the left atrial cavity). However, this gives us no information about the relative proportion of [^{11}C]Methyl-Losartan in the plasma compartment relative to whole blood. Thus, we performed blood and plasma sampling to obtain an adjusted plasma time activity curve (n=5 rats).

Animals received the analgesic buprenorphine (0.048 mg/kg sub-cutaneous) at least one hour prior to procedure. Rats were anaesthetized and kept unconscious throughout the procedure using a nose cone with isoflurane (1-2%). Rats were placed in supine position and a midline incision was made from the sternum to the jaw using a no. 15 scalpel blade. The carotid artery was then exposed using blunt dissection to separate the sternohyoid muscles and the vagus nerve from the artery. The artery was punctured using a 23 gauge syringe needle and a canula (PE50 tubing) was placed through the opening towards the heart and fastened with 4.0 silk sutures. The other end of the catheter was connected to a 3-way stop-cock, one opening served for blood collection, whereas the other opening was connected to a heparinized saline-filled syringe. The catheter was flushed with saline between each sample collection. Rats were

injected with 0.5-2.5 mCi (18.5-92.5 MBq) of [^{11}C]Methyl-Losartan via a 26 gauge catheter into the lateral tail vein. Blood samples were collected at 30 sec, 1, 5, 10, 20, 30, 45 and 60 min into ehtylenediaminetetraacetic acid (EDTA) coated tubes (Microvette CB 300, Sarstedt).

Whole blood samples were then transferred to pre-weighed gamma counter tubes (VWR), counted for radioactivity in a gamma counter (Packard, Cobra II), and weighed. Samples were then centrifuged at 3000 g (4000 rpm) for 5 min (Jouan) to separate plasma from whole blood. Plasma supernatant samples were then transferred to another set of pre-weighed gamma counter tubes (VWR), counted for radioactivity in a gamma counter (Packard, Cobra II), and weighed. Decay-corrected counts were normalized to samples weights, and results are expressed as plasma to whole blood ratio over time. For these calculations, plasma was considered to represent 55% of whole blood.

4.3 BIODISTRIBUTION

4.3.1 CONTROL AND COMPETITION

Biodistribution methods were adapted from work previously published by our group (Greene et al. 2009; Hadizad et al. 2009a; Kenk et al. 2007; Kenk et al. 2010; Lourenco et al. 2006; Thackeray et al. 2007) and were performed to evaluate relative tissue uptake and binding specificity and selectivity of [^{11}C]Methyl-Losartan for AT_1 over AT_2, Mas, and β-adrenergic receptors. Conscious animals were placed in rat holders and injected via the lateral tail vein with 0.3-1.6 mCi (11.1-59.2 MBq) (specific activity 100-700 mCi/µmol, mass 0.2-4.5 µg) of [^{11}C]Methyl-Losartan in a volume of less than 1 ml using 28½ G insulin syringes (B-D). Controls received tracer alone (n=10 rats), whereas other groups received a co-injection or pre-treatment of selective antagonists of the AT_1 (Losartan 20 mg/kg i.v. or Candesartan 5 mg/kg i.v., co-injection (n=4 rats per group)), AT_2 (PD-123,319 5 mg/kg i.v., 5 min prior (n=8 rats)), Mas (A-779 100 µg/kg i.v., 5 min prior (n=12 rats)), and β-adrenergic (Propranolol 20 mg/kg intra-peritoneal,

15 min prior (n=8 rats)) receptors to assess binding specificity and selectivity (Bayorh et al. 2002; Hadizad et al. 2009a; Naruse et al. 2002; O'Donnell 1993; Ozdemir et al. 2009; Sun et al. 2007). All drugs were dissolved in saline (0.9%) and pH was adjusted within 6 to 8 by adding sodium bicarbonate (8.4%). Based on the time course from initial control microPET scans, rats were sacrificed by decapitation at 10 minutes post-injection; the time point displaying maximal tissue to blood contrast in the kidneys. Trunk blood was collected in heparinized tubes (BD Vacutainer) at sacrifice. The following tissues of interest were dissected out into pre-weighed gamma counter tubes (VWR): right atrium, left atrium, right ventricle, left ventricle, septum, aorta, kidney cortex, kidney outer medulla, kidney inner medulla, adrenal gland, hypothalamus, cerebellum, brain stem, rest of brain, lung sample, liver sample and skeletal muscle sample (quadriceps). The same tracer dose was also injected in a 100 mL volume of saline (0.9%) which served as a standard. Empty tubes were also used as background. All tubes were then counted for radioactivity in a gamma counter (Packard, Cobra II) and weighed. Decay corrected counts were calculated as a percent of the injected dose per gram of tissue (%ID/g), and normalized to blood to be expressed as a ratio to blood.

To note, the Propranolol group is presented but was excluded from statistical analysis for reasons which will be detailed further in the discussion section 6.2.3 (Statistical Test).

4.3.2 INJECTED DOSE EFFECT

To monitor the effect of changing the dose on the tissue uptake and ratio to blood, the injected activity, injected mass and injected dose were recorded or calculated for all control rats (n=10 rats). Ratio to blood for kidney cortex and outer medulla were then plotted against these values and evaluated for any trend using a linear regression analysis. As described previously in section 4.2.3 (Injected Dose Effect), the correlation coefficient (R^2) was tested against a null hypothesis of R^2=0 using the formula $t = R \times \sqrt{n - 2/1 - R^2}$ to generate a t value, which was

then determined significant or not based on a cumulative *T* distribution. As confirmation of this test, the slope of the data was also considered significantly different from zero if the 95% confidence interval for the slope did not overlap with zero. If the correlation coefficient and the slope were significantly different from zero, then the ratio to blood values were said to follow a trend dependant on the given independent variable (injected activity, injected mass and injected dose).

4.4 AUTORADIOGRAPHY

Autoradiography was performed to confirm *in vivo* microPET and *ex vivo* biodistribution specificity and selectivity studies. A method previously published by our group (Kenk et al. 2007) was adapted for use with [^{11}C]Methyl-Losartan. Naïve rats were sacrificed by decapitation and kidneys quickly removed, immersed in Optimal Cutting Temperature Compound (Tissue-Tek), frozen on dry ice and stored at -80^{o}C until sectioning. Kidneys were sectioned in the axial axis into 20 µm-thick slices at -18^{o}C with a cryostat (Leica CM3050 S). Three sections per slide were thaw mounted on glass slides (VWR) and stored at -80^{o}C until the day of the experiment.

On the day of the experiment, slides were pre-washed in incubation buffer (150 mM NaCl, 10 mM sodium phosphate dibasic, 5 mM EDTA, pH 7.4) for 15 min and then incubated in the presence of 5 nM [^{11}C]Methyl-Losartan for 45 min at room temperature. To assess the binding specificity and selectivity of [^{11}C]Methyl-Losartan, incubation buffer contained a 10 µM concentration of specific antagonists of the AT_1 (Losartan or Candesartan), AT_2 (PD-123,319), Mas (A-799), and β-adrenergic (Propranolol) receptors. Each incubation condition contained 3 slides from 3 different rats for a total of 9 sections per incubation condition. After incubation, slides were washed twice (2 min at 4^{o}C) in tracer-free, drug-free incubation buffer, once (2 min at 4^{o}C) in deionized water and gently air dried. Sections were then exposed to phosphor imaging plates (Kodak) for 2 hours in complete darkness. Standards with known concentrations

of [^{11}C]Methyl-Losartan were blotted on silica gel coated aluminum backing thin layer chromatography plates (Whatman) and exposed alongside slides. This was done to ensure that detected radioactivity was within the linear range of detection and quantification of the phosphor imaging system. Phosphor plates were then read at a 50 µM resolution (BioRad Molecular Imager FX) and quantified (AlphaEaseFC, Alpha Innotech).

For quantification, a rectangular shaped region was drawn in the kidney cortex and total counts were recorded for that area. The same area of each section, and the same rectangular shape size was used to quantify all sections for one given dataset. To note, damage to certain sections occurred during transfers and drying, resulting in 5 to 7 quantifiable sections for any given group of data. Due to the very high variability in the results, the experiment was repeated several times and results from all experiments were combined by normalizing each data point to the mean control value for that day. Each data point was then expressed as fold of control (n=30 control, n=20 PD-123,319, n=21 A-779, n=22 Propranolol, n=30 Losartan, n=35 Candesartan kidney sections).

4.5 METABOLITE ANALYSIS

To determine the presence of C-11-labeled metabolites that could adversely affect both microPET imaging and kinetic modeling, metabolite analyses were performed to determine the proportion of detected radioactivity accounted for by the unchanged [^{11}C]Methyl-Losartan in the plasma and kidneys. Rats were injected with 7-17 mCi (259-629 MBq) of [^{11}C]Methyl-Losartan i.v. via the lateral tail vein. Based on the time course from the initial microPET scans, rats were sacrificed by decapitation at 10 minutes post-injection (n=4 rats). Another group of rats received the same injection but were sacrificed 45 minutes post-injection (n=4 rats) to determine the change in relative proportions of unchanged tracer to labeled metabolite(s), with the latest time point expected to exhibit the highest presence of metabolite(s). Finally, a third

and fourth group of rats received a co-injection of Losartan (20 mg/kg i.v., n=3 rats) or Candesartan (5 mg/kg i.v., n=3 rats) and sacrificed at 10 min to assess any change in tracer to metabolite(s) ratio due to specific binding of the metabolite(s) to the AT_1 receptor. These four groups are referred to as Normal at 10 min, Normal at 45 min, Blocked Losartan at 10 min and Blocked Candesartan at 10 min, respectively.

At sacrifice, kidneys and trunk blood were collected and kept on ice until use. Kidneys were homogenized in 80:20 etathanol:water and centrifuged at 60,000 g (22,000 rpm) for 15 min (Beckman L8-70M Ultracentrifuge). The supernatant was collected, evaporated and re-dissolved in 2-4 ml of 1/99 CH_3CN/water (v/v) containing 0.4 g/ml urea. The solution was filtered through 0.22 µm Cathivex-GS (Millipore, Ireland) syringe filters and injected onto the high performance liquid chromatography (HPLC) system. Plasma samples were prepared by blood centrifugation (3000 g (4000 rpm) for 5 min) followed by dissolution of 1 g/ml urea into the plasma. The solution was then filtered through 0.22 µm Cathivex-GS (Millipore, Ireland) syringe filters and injected onto the HPLC system. Urea was added to disrupt protein interactions, typically plasma protein, and allow binding of the compounds to the capture column (Hilton et al. 2000).

The HPLC column-switch method developed by Hilton and colleagues (Figure 13) was adapted for use with [^{11}C]Methyl-Losartan (Hilton et al. 2000). Following sample injection, [^{11}C]Methyl-Losartan and its metabolites are trapped by the capture column (hand-packed with polymeric reverse phase sorbent; Oasis HLB; Waters Corp.), then flow is reversed and the trapped components were flushed onto the analytical column (Luna C18, Phenomenex). The solvents used for the HPLC were optimized for [^{11}C]Methyl-Losartan and consist of 1/99 acetonitrile/water (v/v) as solvent 1 and 40/60 acetonitrile/ammonium formate (v/v) as solvent 2. The eluted compounds were analyzed by two detectors: a UV absorbance detector (Waters

486) and an HPLC coincidence radiation detector (Bioscan), both linked to a chromatography data integration system (PeakSimple). Data was decay corrected and chromatograms were analyzed by measuring the area under the curve and expressing this value as a percentage of total activity for that sample.

In all experiments, non-radioactive kidneys (n=9 samples) and blood (n=8 samples) were extracted from normal rats and subsequently spiked with [^{11}C]Methyl-Losartan, then processed as described above to assess any potential effect of processing on tracer and to evaluate the efficiency of the HPLC capture column. These samples are referred to as control for metabolism studies. As well, a standard sample of authentic [^{11}C]Methyl-Losartan was also injected for each experiment to evaluate the efficiency of the HPLC capture column and confirm the column retention time on that day (n=13 samples). Thirdly, a non-radioactive kidney was processed as described above and injected to establish a baseline UV trace for all other kidney samples (n=1 sample). Finally, in an attempt to elucidate the identity of a potential metabolite, a sample of authentic Methyl-EXP3174 was also injected onto the HPLC column to assess its retention time (n=1 sample).

4.6 FIGURES

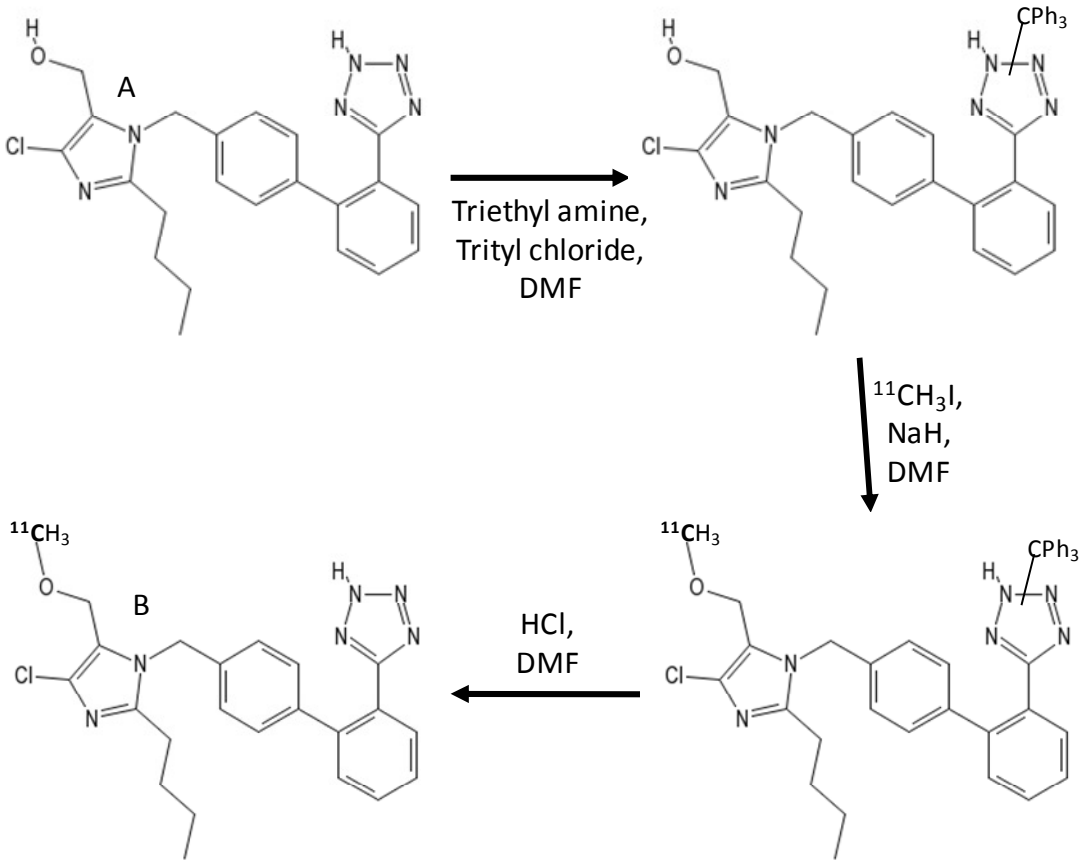

Figure 10 – Synthesis scheme of [^{11}C]Methyl-Losartan (B) starting from the parent compound Losartan (A) (Hadizad et al. 2009b).

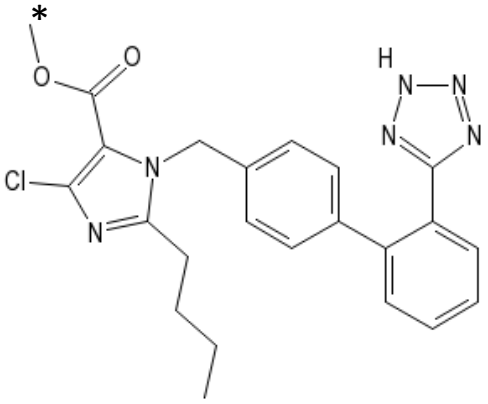

Figure 11 – Chemical structure of [^{11}C]Methyl-EXP3174 (Hadizad et al. 2010). C-11 radioactive atom position indicated by asterisk.

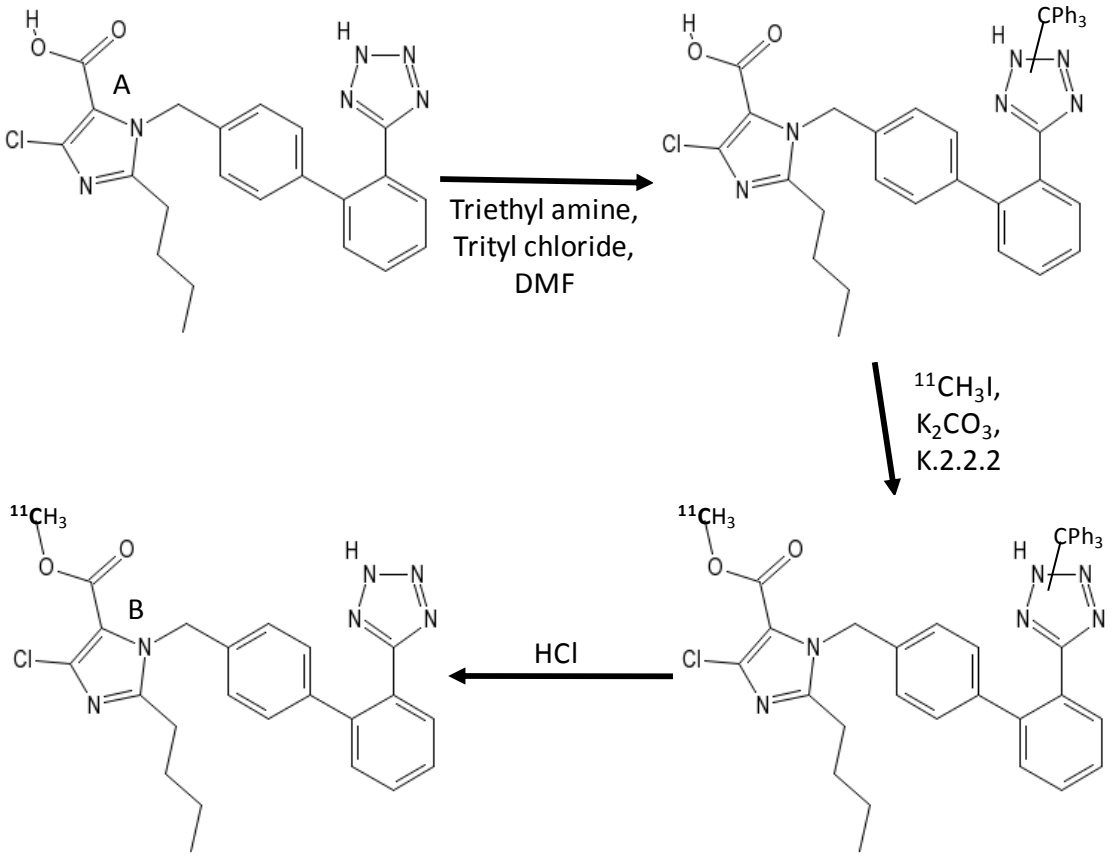

Figure 12 – Synthesis scheme of [^{11}C]Methyl-EXP3174 (B) starting from the parent compound EXP-3174 (A) (Hadizad et al. 2010).

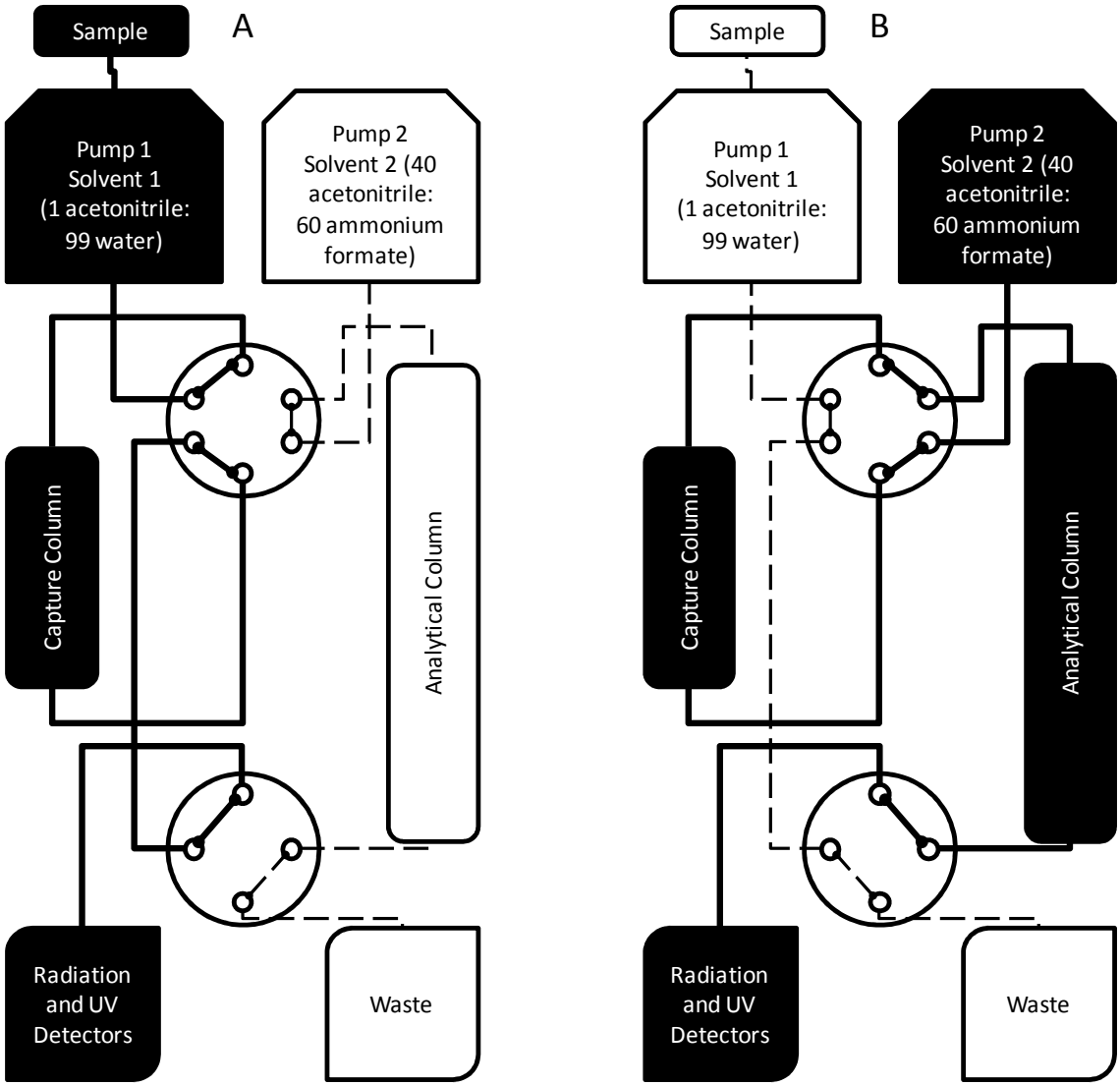

Figure 13 – Flow diagram of HPLC switch system used for metabolite analysis of rat plasma and tissues. In (A), sample is injected and is transferred with solvent 1 onto the capture column (capture column eluates are detected). In (B), both valves are switched and captured components are back-flushed using solvent 2 onto the analytical column (analytical column eluates are detected). Adapted from Hilton (Hilton et al. 2000).

5 RESULTS

5.1 MICROPET IMAGING

5.1.1 CONTROL SCANS

Control microPET scanning displayed highest uptake in the liver and kidneys (Figure 14). Early frames (0-60 seconds) showed signal in lungs and large vascular compartments, notably the vena cava, aorta and all four heart chambers. Initial spike in blood activity is observed with very quick washout and a fall in signal back to baseline at 15 minutes post-injection. Tracer largely accumulated uniformly and non-reversibly in the liver to reach a plateau in signal density at approximately 25 minutes. Accumulation was also observed in the kidneys, with slow uptake and highest signal at 3 minutes followed by very slow washout and fall to baseline at 35 minutes (Figure 15). Signal distribution is representative of kidney cortex and outer medulla. Good signal contrast between kidneys and whole blood is observed between 5 and 30 minutes post-injection (Figure 15). Best signal contrast is observed at 10 minutes, and this time point was selected for sacrifice in future biodistribution and metabolism studies. DV values generated using the Logan graphical analysis method for the kidneys are 1.63 ± 0.23 ml/g for the left kidney and 1.68 ± 0.22 ml/g for the right kidney (Figure 16).

5.1.2 TEST RE-TEST

Repeated scanning of the same rat showed good reliability and moderate to low variability. The mean difference between baseline and re-test scan was 0.11 ± 0.20 ml/g (7% of the mean DV) and was not significantly different from 0 (95% confidence interval: -0.01 to 0.22 ml/g). The SD (0.20 ml/g) represents 13.6% of the mean DV according to the Bland-Altman analysis (Figure 17) (Bland and Altman 1986).

5.1.3 INJECTED DOSE EFFECT

Uncorrected Logan DV values do not seem to be affected by injected activity (0.5-2.2 mCi, 18.5-81.4 MBq, R^2=0.0002, p=0.93) (Figure 18) or rat weight (200-450 g, R^2=0.02, p=0.34) (Figure 19). A significant slight downward trend in DV values is observed with increasing specific activity (100 to 2500 mCi/µmol, 3.7-92.5 GBq/µmol, R^2=0.16, p=0.008) (Figure 20), and a significant slight upward trend is observed with increasing injected mass (0.2-28.0 µg, R^2=0.25, p=0.001) (Figure 21) and injected dose (0.6-47 µg/kg, R^2=0.24, p=0.001) (Figure 22).

5.1.4 BINDING SPECIFICITY

[^{11}C]Methyl-Losartan microPET scanning with a blocking dose of Losartan or Candesartan displayed the highest uptake in the liver and very little uptake in the kidneys (Figure 23, Figure 24). Early frames (0-60 seconds) showed signal in the lungs and large vascular compartments, notably the vena cava, aorta and all four heart chambers. Initial spike in blood activity was observed with very quick washout and a fall in signal back to baseline at 15 minutes post-injection, similarly to control scans. In Losartan blocking scans, liver activity increased beyond peak blood activity at 3-5 min post-injection and washed out slowly starting at approximately 5 min (Figure 25). In Candesartan blocking scans, tracer largely accumulated uniformly in the liver to reach a plateau in signal density at approximately 15 minutes (Figure 26). Accumulation was not observed in the kidneys, and renal activity followed similar kinetics to what was observed in the blood (Figure 25, Figure 26).

Statistical tests show that DV values for Losartan blocking scans were significantly lower at 1.07 ± 0.07 ml/g for the left kidney (p=0.0008) and 1.09 ± 0.06 ml/g for the right kidney (p=0.007) when compared to baseline scans (1.75 ± 0.16 ml/g for the left kidney and 1.76 ± 0.25 ml/g for the right kidney). DV values for Candesartan blocking scans were also significantly lower at 0.95 ± 0.11 ml/g for the left kidney (p=0.039) and 1.10 ± 0.07 ml/g for the right kidney

(p=0.022) when compared to baseline scans (1.47 ± 0.19 ml/g for the left kidney and 1.57 ± 0.22 ml/g for the right kidney).

5.1.5 DISPLACEMENT STUDIES

Displacement studies were used to qualitatively confirm the specificity studies with [^{11}C]Methyl-Losartan microPET imaging. Early frames, pre-Losartan (20 mg/kg i.v.) bolus injection, looked identical to control scans. After the Losartan injection (either 10 min or 17 min post-tracer injection), the high activity in the liver began to decrease, as well as the activity in the kidneys. Interestingly, the activity in the blood increased during this interval (Figure 27, Figure 28). Towards the end of the scan, post-Losartan bolus, images looked very similar to blocking studies, indicating that [^{11}C]Methyl-Losartan is displaceable from the kidneys and liver by Losartan. No competition in the liver was observed in Candesartan blocking scans and therefore displacement studies were not performed with this drug.

5.1.6 INTRA-USER AND INTER-USER VARIABILITY

Repeated analysis of the same data by the same user displayed excellent correlation (R^2=0.9779), good repeatability and very low variability. The slope of the data was not significantly different from 1 (ideal correlation) (Figure 29) as was determined by the 95% confidence interval of the slope (0.996 to 1.024). The mean difference between analysis 1 and 2 was 0.01 ± 0.04 ml/g (1% of the mean DV) and was not significantly different from 0 (95% confidence interval: -0.01 to 0.04 ml/g). The SD (0.04 ml/g) represents 2.5% of the mean DV according to the Bland-Altman analysis (Figure 30) (Bland and Altman 1986).

Repeated analysis of the same data by a different user also showed moderate repeatability and low variability. The correlation coefficient (R^2) between the two sets of data was 0.8228 and the slope of the data was significantly different from 1 (ideal correlation) (Figure 31) as per the 95% confidence interval of the slope (0.910 to 0.969). The mean difference

between the results generated by user 1 and 2 was -0.09 ± 0.09 ml/g (5% of the mean DV) and was significantly different from 0 (95% confidence interval: -0.14 to -0.04 ml/g). The SD (0.09 ml/g) represents 5.9% of the mean DV according to the Bland-Altman analysis (Figure 32) (Bland and Altman 1986).

5.1.7 BLOOD AND PLASMA SAMPLING

The concentration of [^{11}C]Methyl-Losartan in plasma relative to whole blood is high from 0 to 60 min. The plasma to whole blood ratio is highest at the early time points (30 and 60 sec), approximately 0.97, and slowly decreases over time to approximately 0.70. The data was fitted to a downward logarithmic function with the formula: $y = (-0.061)\ln x + 0.965$, and agrees well with that model as is indicative of the high correlation coefficient, R^2=0.9497 (Figure 33).

5.1.8 [^{11}C]METHYL-EXP3174

[^{11}C]Methyl-EXP3174 scans displayed highest uptake in the liver and kidneys (Figure 34). Early frames (0-60 seconds) showed signal in lungs and large vascular compartments, notably the vena cava, aorta and all four heart chambers. Initial spike in blood activity is observed with very quick washout and a fall in signal back to baseline at 15 minutes post-injection. Tracer largely accumulated uniformly in the liver to reach a plateau after 20 minutes. Accumulation was also observed in the kidneys, with slow uptake and highest signal at 3 minutes followed by very slow washout and fall to baseline at 35 minutes (Figure 35). Compared to [^{11}C]Methyl-Losartan, the peak activity in the kidneys is lower, however good signal contrast between whole blood and kidneys is still observed between 5 and 30 minutes post-injection (Figure 35). DV values generated using the Logan graphical analysis method for the kidneys are 1.62 ml/g for the left kidney and 1.62 ml/g for the right kidney (n=2 scans, and thus no SD) (Figure 36).

5.2 BIODISTRIBUTION

5.2.1 CONTROL

Highest activity concentration at 10 minutes post injection was observed in the liver, kidney cortex and outer medulla; 44.6, 8.7 and 3.2 ratio to blood, respectively (Table 2, Figure 37). Tracer accumulation is consistent with signal distribution from microPET imaging results which show the highest signal in the liver and the kidney cortex.

5.2.2 COMPETITION

Blocking of AT_1 receptors with Losartan showed significant ($p<0.05$) uptake reduction in the liver, kidney cortex and outer medulla; 74.4%, 85.5% and 78.1% respectively. Blocking with Candesartan showed 75.8% and 72.2% reduction ($p<0.05$) in the kidney cortex and outer medulla, respectively, but no significant change in the liver (Table 2, Table 3, Figure 37). Blocking of the AT_2 receptor (PD-123,319), Mas receptor (A-779) and β-adrenergic receptor (Propranolol) showed no significant change in tracer uptake in any tissue (Table 2, Table 3, Figure 38). The statistical tests indicate significant increases in tracer uptake ($p<0.05$) with Losartan blockade in all brain regions studied. However, it is important to note that despite the statistical significance of these increases, these results may not be physiologically relevant due to the fact that in the control group (no blocking) the uptake ratio to blood in the heart is very small and less than 1 (0.1 ratio to blood) indicating lower activity concentration in the tissue relative to blood.

5.2.3 INJECTED DOSE EFFECT

A similar analysis to that performed in section 5.1.3 (Injected Dose Effect) using microPET was carried out with the biodistribution data to evaluate any effect due to injected activity, mass and dose on the ratio to blood values for the kidney cortex and outer medulla.

Only rats from the control group were used for this analysis. Although these data are limited, this examination indicates that there was no detectable effect on uptake ratio to blood across all injected activities (0.1-0.7 mCi, kidney cortex R^2=0.20 p=0.20, outer medulla R^2=0.05 p=0.55) (Figure 39), masses (0.3-4.3 μg, kidney cortex R^2=0.0001 p=0.98, outer medulla R^2=0.14 p=0.28) (Figure 40) and doses (1.2-16.6 μg/kg, kidney cortex R^2=0.003 p=0.88, outer medulla R^2=0.12 p=0.33) (Figure 41). These masses and doses are well within the limits of those used in microPET experiments.

5.3 AUTORADIOGRAPHY

Control group showed uptake in the kidney cortex, similarly to the results observed in the microPET and biodistribution studies. Blocking with Losartan and Candesartan showed a significant 59.0% and 24.3% decrease in tracer uptake, respectively. No significant blocking was observed with PD-123,319 or A-779 drug incubations (Figure 42, Figure 43). No blocking was observed with Propranolol, but as previously mentioned, Propranolol was excluded from statistical analysis for reasons discussed in section 6.2.3 (Statistical Test). This data indicates that [^{11}C]Methyl-Losartan binds specifically to the AT_1 receptor and is selective over the AT_2, Mas and β-adrenergic receptors.

5.4 METABOLITE ANALYSIS

5.4.1 CONTROLS

Injection of pure [^{11}C]Methyl-Losartan onto the HPLC system shows 99 ± 1.1 % retention of the tracer on the capture column as is demonstrated by the very low presentence of leach-trough (peak 1) (Figure 44, Figure 45). The retention time of [^{11}C]Methyl-Losartan (peak 4) after reversing the flow (post-switch) is approximately 7 min. Control plasma samples demonstrate 89.2 ± 3.3 % retention of [^{11}C]Methyl-Losartan (peak 4), while control kidney samples

demonstrate 94.7 ± 4.3 % retention on the capture column (Figure 46, Figure 47). The presence of leach-through in these samples is due to [^{11}C]Methyl-Losartan binding to proteins, which are not captured by the column. No other peaks were detected and it can therefore be concluded that the processing does not affect or degrade [^{11}C]Methyl-Losartan.

5.4.2 NORMAL AT 10 MIN

The plasma samples at 10 min revealed the presence of one (or more) hydrophilic metabolite(s) due to the higher proportion of leach-through (peak 1, 28.5 ± 9.3 %) compared to control. Curiously, there was a very minor peak at 3 min post-switch (peak 2), which was only present in 2 of the 4 samples studied. However this represented less than 1% of the overall activity detected and therefore cannot be decisively categorized as a major metabolite (Figure 48). In the kidney, the presence of the hydrophilic labeled metabolite(s) peak 1 (leach-through, 42.2 ± 13.2 %) is also demonstrated. There is also a major radioactive metabolite appearing at 3 min post-switch (peak 2) that represents 23.1 ± 2.5 % of the overall activity. [^{11}C]Methyl-Losartan represents 34.7 ± 13.9 % of the overall signal in the kidney at 10 min (Figure 49).

5.4.3 NORMAL AT 45 MIN

The plasma samples at 45 min were similar to the plasma samples at 10 min but with the leach-through peak being higher at 45 min (49.1 ± 26.8 %). However, the variability in this set of data was large, as is indicative of the SD representing approximately 50% of the mean value. The presence of peak 2 was not detected in these samples (Figure 50). In the kidney, the leach-through (peak 1) and the radioactive metabolite (peak 2) identified at 3 min post-switch increase over time to 52.7 ± 7.7 % and 33.7 ± 11.8 % of the overall activity, respectively. The [^{11}C]Methyl-Losartan proportion decreases over time and represents 13.5 ± 6.3 % of the overall signal at 45 min post-injection (Figure 51). Despite all the changes mentioned above, none were found to be statistically significant when compared to normal samples at 10 min.

5.4.4 LOSARTAN AND CANDESARTAN BLOCKING

Our *in vivo* microPET studies and *ex vivo* biodistribution studies indicate that introducing AT_1 receptor blockers such as Losartan and Candesartan significantly decreases signal concentration in the kidneys. The purpose of these metabolism experiments with AT_1 receptor blockers was to assess whether or not the remaining activity in the kidneys was due to non-specific binding of the metabolites. While interpreting the following results, it is important to consider that the overall activity in these samples is scaled down similarly to what is observed in biodistribution (approximately 75% reduction in tracer uptake on average).

Blocking with Losartan at 10 min showed a non-significant increase in the proportion of leach-through (peak 1) to 43.0 ± 5.2 % in the plasma samples. An increase in peak 2 to 6.6 ± 0.5 % and the appearance at 5 min post-switch of peak 3 which represents 3.9 ± 2.1 % of overall activity was observed and both are significantly different from samples of untreated rats at 10 min (Figure 52). In the kidney, no change was observed in the chromatograms (Figure 53). Blocking with Candesartan at 10 min did not show a significant change in any of the peak proportions when compared to samples of untreated rats 10 min, both in the plasma and kidney (Figure 54, Figure 55). Overall, these blocking studies would suggest that the observed metabolites behave similarly to [^{11}C]Methyl-Losartan with respect to AT_1 receptor binding in that they are displaceable by selective AT_1 receptor blockers. The entire dataset for all 4 groups is depicted in Table 4 and Figure 44.

5.4.5 TRACER-FREE KIDNEY AND METHYL-EXP3174

All kidney samples revealed 2 non-radioactive peaks at 2 and 4 min post-switch identified by the UV detector. A non-radioactive kidney sample was used to establish a baseline UV trace, and it was concluded that these peaks were inherent to the kidney samples and not introduced by any of the injections (Figure 56).

Finally, injection of the standard sample of authentic Methyl-EXP3174 onto the HPLC system revealed a retention time of approximately 12 min post-switch and does not correspond with any of the observed metabolites (Figure 57). It is therefore concluded that [^{11}C]Methyl-EXP3174 is not one of the labeled metabolites.

5.5 TABLES AND FIGURES

Table 2 – [^{11}C]Methyl-Losartan uptake at 10 min post-injection as measured by biodistribution studies (n=10 control, n=4 Losartan, n=4 Candesartan, n=8 PD-123,319, n=12 A-779, n=8 Propranolol). Data is expressed as a %ID/g ratio to blood ± SD. One way ANOVA and Bonferroni post-hoc were used for statistical analysis, *significantly different from control, $p<0.05$.

	Control	Losartan 20 mg/kg i.v. co-inj.	Candesartan 5 mg/kg i.v. co-inj.	PD-123,319 5 mg/kg i.v. 5 min prior	A-779 100 ug/kg i.v. 5 min prior	Propranolol 20 mg/kg i.p. 15 min prior
Right Atrium	0.80 ± 0.14	0.73 ± 0.12	0.69 ± 0.27	0.64 ± 0.22	0.86 ± 0.29	0.95 ± 0.36
Left Atrium	0.86 ± 0.11	0.78 ± 0.09	0.82 ± 0.31	0.65 ± 0.20	0.88 ± 0.32	0.90 ± 0.34
Right Ventricle	0.71 ± 0.12	0.64 ± 0.05	0.62 ± 0.13	0.57 ± 0.16	0.73 ± 0.20	0.79 ± 0.18
Left Ventricle	0.70 ± 0.12	0.65 ± 0.06	0.60 ± 0.13	0.54 ± 0.13	0.71 ± 0.18	0.78 ± 0.20
Septum	0.72 ± 0.12	0.65 ± 0.04	0.62 ± 0.16	0.55 ± 0.15	0.73 ± 0.19	0.78 ± 0.19
Aorta	0.81 ± 0.22	0.67 ± 0.09	0.59 ± 0.12	0.66 ± 0.18	0.90 ± 0.50	0.77 ± 0.18
Kidney Cortex	8.67 ± 2.79	1.26 ± 0.05*	1.90 ± 0.32*	6.32 ± 3.03	7.02 ± 2.76	13.14 ± 6.66
Outer Medulla	3.16 ± 1.22	0.77 ± 0.15*	0.88 ± 0.18*	2.40 ± 1.27	2.76 ± 1.35	5.41 ± 3.09
Inner Medulla	0.81 ± 0.31	0.65 ± 0.05	0.64 ± 0.20	0.55 ± 0.19	1.00 ± 0.39	0.80 ± 0.23
Adrenal Gland	0.58 ± 0.22	0.54 ± 0.17	0.42 ± 0.12	0.46 ± 0.12	0.59 ± 0.14	0.67 ± 0.32
Hypothalamus	0.11 ± 0.09	0.28 ± 0.02	0.06 ± 0.05	0.10 ± 0.09	0.10 ± 0.03	0.08 ± 0.02
Cerebellum	0.11 ± 0.04	0.26 ± 0.02	0.09 ± 0.03	0.08 ± 0.02	0.11 ± 0.04	0.09 ± 0.03
Brain Stem	0.10 ± 0.03	0.24 ± 0.01	0.09 ± 0.02	0.07 ± 0.02	0.09 ± 0.02	0.08 ± 0.02
Rest Brain	0.09 ± 0.03	0.26 ± 0.02	0.09 ± 0.03	0.07 ± 0.02	0.10 ± 0.03	0.08 ± 0.02
Lung	1.02 ± 0.23	0.85 ± 0.04	0.91 ± 0.27	0.96 ± 0.46	1.25 ± 0.41	1.33 ± 0.34
Liver	44.62 ± 14.86	11.43 ± 1.02*	31.08 ± 11.20	26.58 ± 12.81	49.51 ± 19.67	45.47 ± 16.35
Skeletal Muscle	0.43 ± 0.19	0.46 ± 0.02	0.28 ± 0.09	0.30 ± 0.13	0.47 ± 0.24	0.41 ± 0.12

Table 3 – [^{11}C]Methyl-Losartan percent change in uptake at 10 min post-injection as measured by biodistribution studies (n=10 control, n=4 Losartan, n=4 Candesartan, n=8 PD-123,319, n=12 A-779, n=8 Propranolol). With the exception of the control group (which is expressed as ratio to blood), the data is expressed as a percent change compared to control. One way ANOVA and Bonferroni post-hoc analyses were performed on ratio to blood values listed in Table 2, *significantly different from control, $p<0.05$.

		Percent change from control				
	Control (ratio to blood)	Losartan 20 mg/kg i.v. co-inj.	Candesartan 5 mg/kg i.v. co-inj.	PD-123,319 5 mg/kg i.v. 5 min prior	A-779 100 ug/kg i.v. 5 min prior	Propranolol 20 mg/kg i.p. 15 min prior
Right Atrium	0.80	-7.9%	-13.7%	-19.1%	7.9%	18.9%
Left Atrium	0.86	-9.1%	-4.6%	-24.2%	3.2%	5.0%
Right Ventricle	0.71	-10.9%	-13.7%	-19.7%	3.0%	10.9%
Left Ventricle	0.70	-7.7%	-13.9%	-22.4%	1.0%	11.5%
Septum	0.72	-10.4%	-14.2%	-23.6%	1.8%	8.7%
Aorta	0.81	-16.9%	-27.4%	-17.7%	11.2%	-5.2%
Kidney Cortex	8.67	-85.5% *	-78.1% *	-27.1%	-19.1%	51.5%
Outer Medulla	3.16	-75.8% *	-72.2% *	-24.2%	-12.7%	71.1%
Inner Medulla	0.81	-19.6%	-20.7%	-32.2%	24.1%	-0.4%
Adrenal Gland	0.58	-6.2%	-27.0%	-19.6%	2.4%	16.3%
Hypothalamus	0.11	160.9%	-39.8%	-3.1%	-6.5%	-25.0%
Cerebellum	0.11	134.5%	-17.6%	-27.7%	-2.0%	-19.2%
Brain Stem	0.10	136.9%	-16.1%	-29.3%	-9.0%	-24.1%
Rest Brain	0.09	177.9%	-9.3%	-28.9%	6.0%	-19.0%
Lung	1.02	-16.8%	-10.5%	-6.1%	23.0%	30.4%
Liver	44.62	-74.4% *	-30.3%	-40.4%	11.0%	1.9%
Skeletal Muscle	0.43	6.1%	-34.8%	-30.9%	7.9%	-4.2%

Table 4 – [^{11}C]Methyl-Losartan metabolite analysis for plasma and kidneys (n=4 normal at 10 min, n=3 blocked Losartan, n=3 blocked Candesartan, n=4 normal at 45 min). Samples were analyzed using HPLC system in line with a coincidence radiation detector. Peak area was quantified and expressed as a percentage of total area per sample. One way ANOVA and Bonferroni post-hoc were used for statistical analysis, *significantly different from normal at 10 min and normal at 45 min, $p<0.05$.

	Peak 1 (Leach-through)	Peak 2	Peak 3	Peak 4 (Methyl-Losartan)
		Plasma		
Normal at 10min	28.5% ± 9.3%	0.7%±0.8%	0.0%±0.0%	70.8% ± 9.9%
Blocked Losartan at 10min	43.0% ± 5.2%	6.6%±0.5%*	3.9%±2.1%*	46.4% ± 7.0%
Blocked Candesartan at 10min	23.0% ± 13.9%	0.3%±0.4%	0.1%±0.2%	76.6% ± 13.6%
Normal at 45min	49.1% ± 26.8%	0.0%±0.0%	0.0%±0.0%	50.9% ± 26.8%
		Kidney		
Normal at 10min	42.2% ± 13.2%	23.0%±2.5%	0.0%±0.0%	34.7% ± 13.9%
Blocked Losartan at 10min	47.3% ± 5.8%	22.9%±1.5%	0.0%±0.0%	29.7% ± 6.7%
Blocked Candesartan at 10min	37.9% ± 11.1%	14.6%±2.0%	0.0%±0.0%	47.6% ± 13.2%
Normal at 45min	52.7% ± 7.6%	33.7%±11.8%	0.0%±0.0%	13.5% ± 6.3%

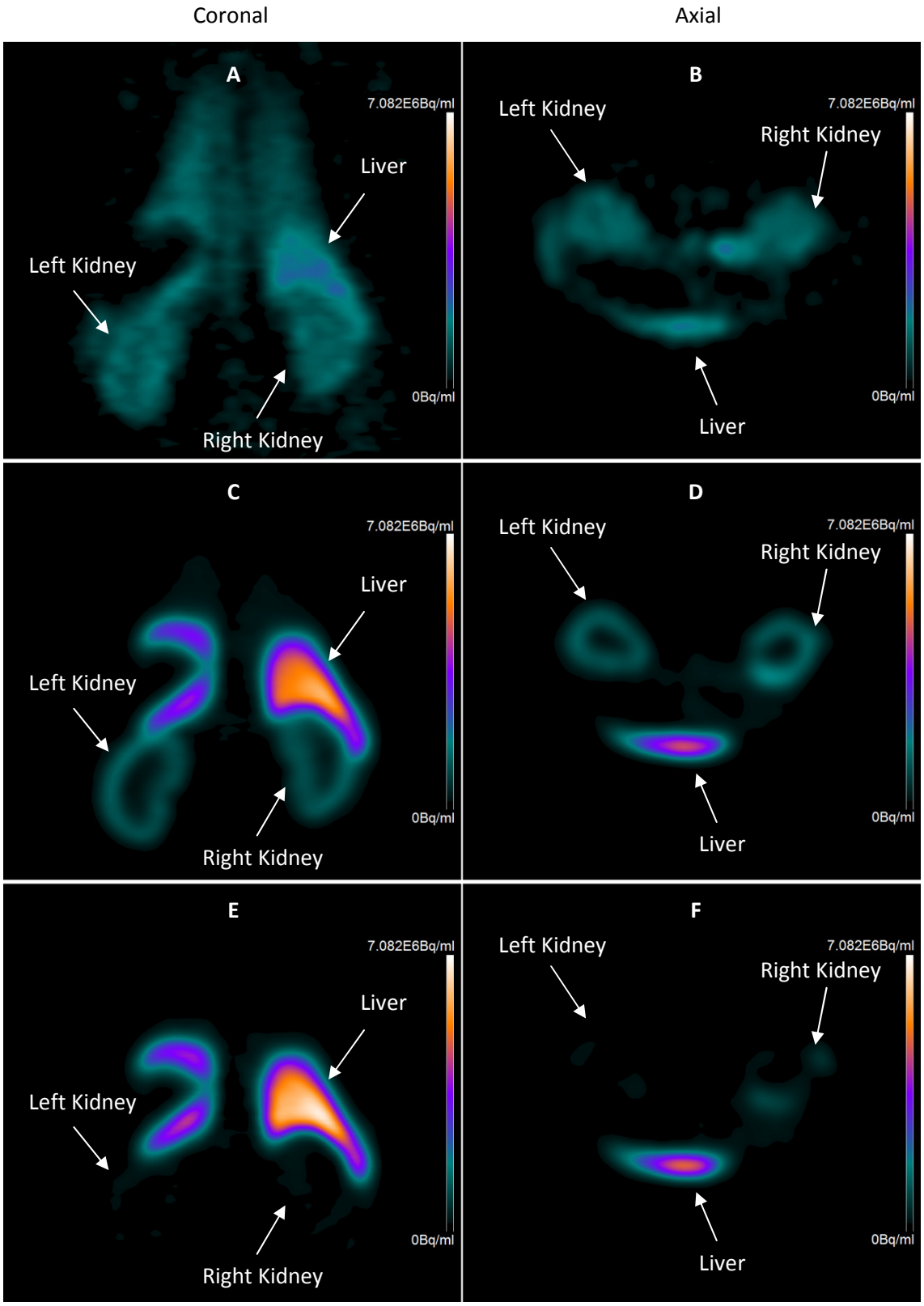

Figure 14 – Representative microPET images of [^{11}C]Methyl-Losartan control scans at 50-60 sec **(A,B)**, 5-10 min **(C,D)**, and 40-45 min **(E,F)** post-injection.

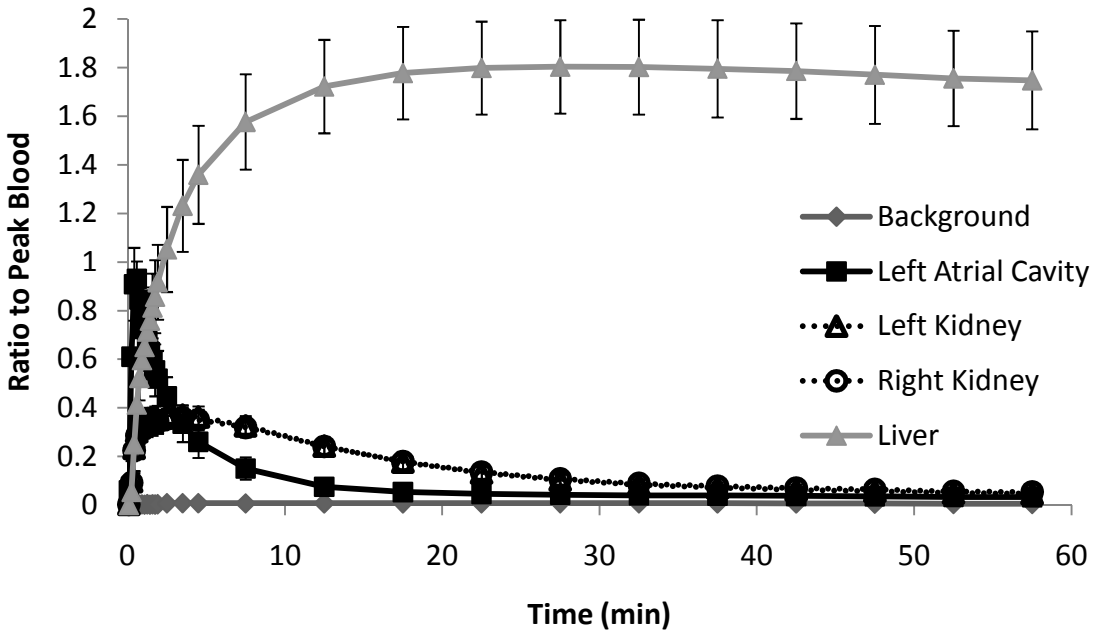

Figure 15 – Mean time activity curves of [^{11}C]Methyl-Losartan control microPET scans (n=20 scans). Data is expressed as mean ratio to peak blood activity ± SD.

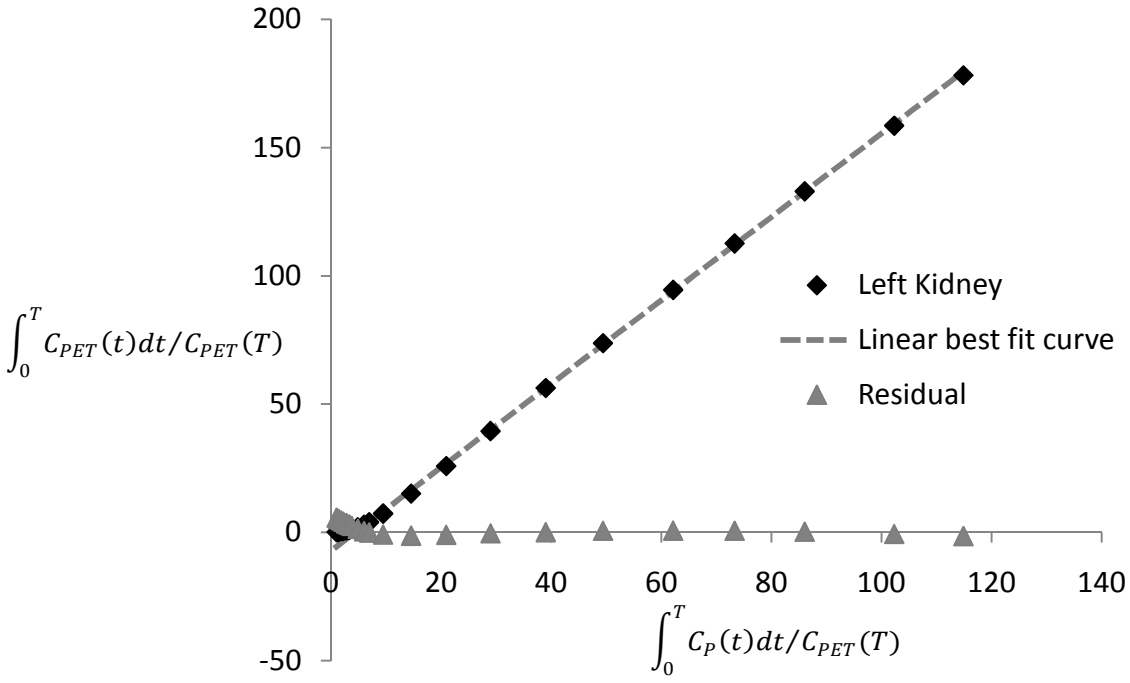

Figure 16 – Representative Logan plot of [^{11}C]Methyl-Losartan microPET scan. The x axis represents adjusted time whereas the y axis represents adjusted activity. A linear curve was fitted to the data. The slope of this curve represents the DV value.

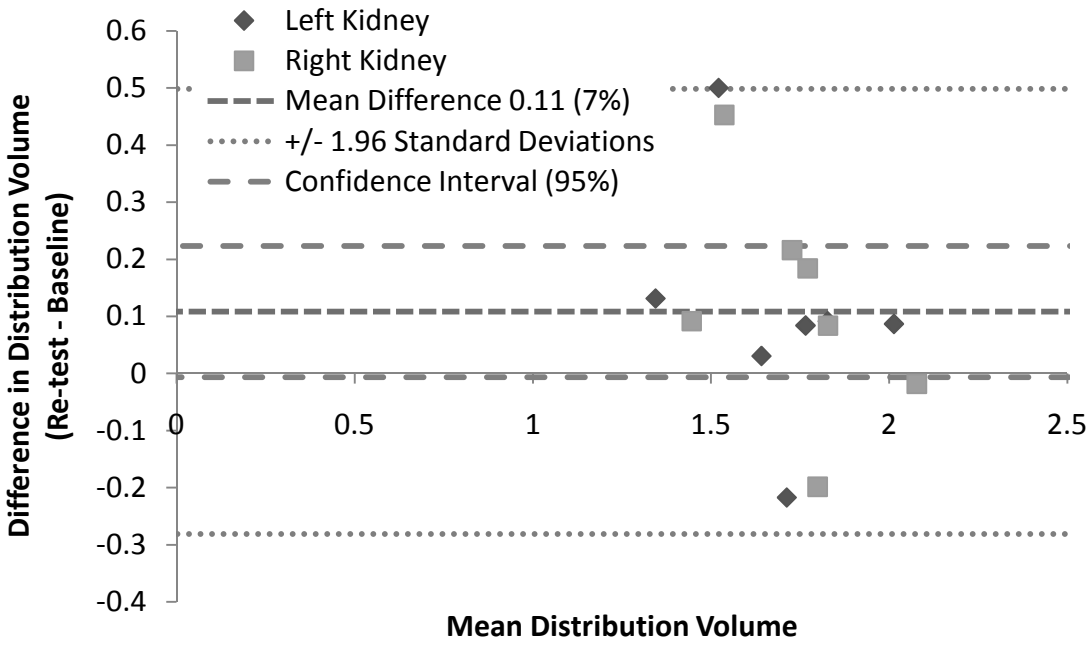

Figure 17 – Bland-Altman plot showing good test re-test DV reliability (n=7 scans). For each set of two scans, the generated DV values are subtracted from each other (always re-test scan - baseline scan) and plotted against the mean DV of both scans. "+/- 1.96 Standard Deviations" indicates the 95% confidence interval which is determined from the mean difference ± standard deviation of the differences.

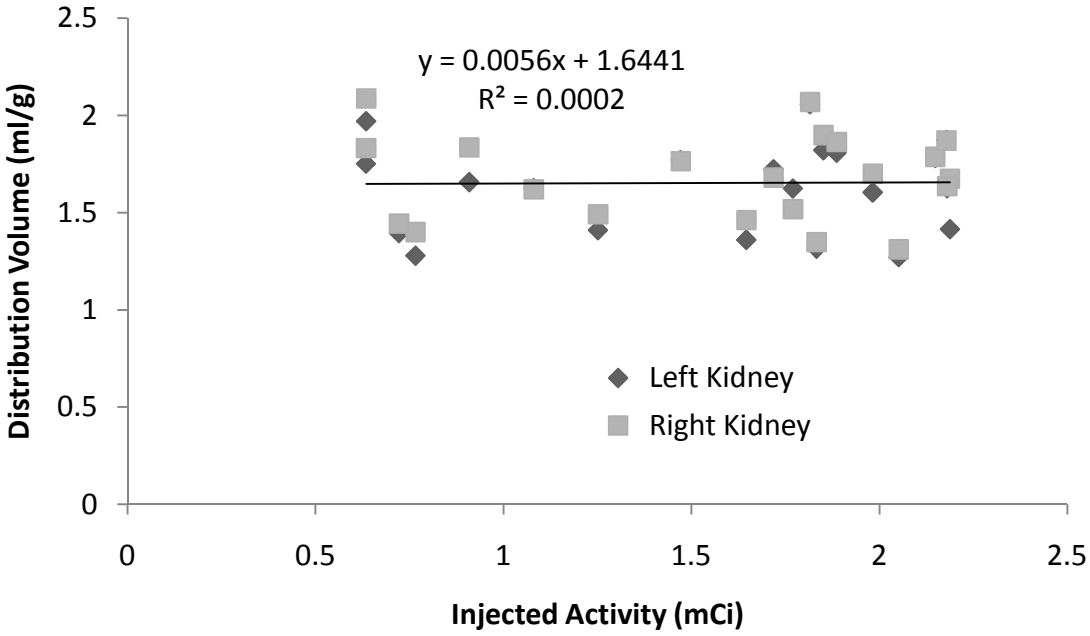

Figure 18 – Individual DV values for [^{11}C]Methyl-Losartan control microPET scans plotted as a function of injected activity for all control rats (n=21 scans). DVs show consistent values across injected activity range.

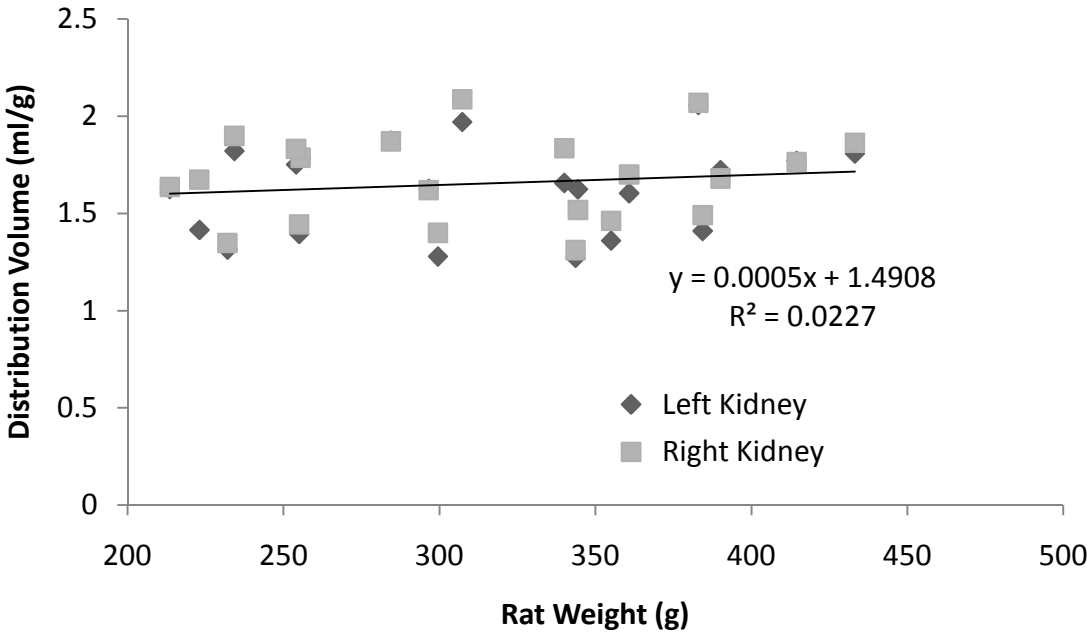

Figure 19 – Individual DV values for [^{11}C]Methyl-Losartan control microPET scans plotted as a function of rat weight for all control rats (n=21 scans). DVs show consistent values across rat weight range.

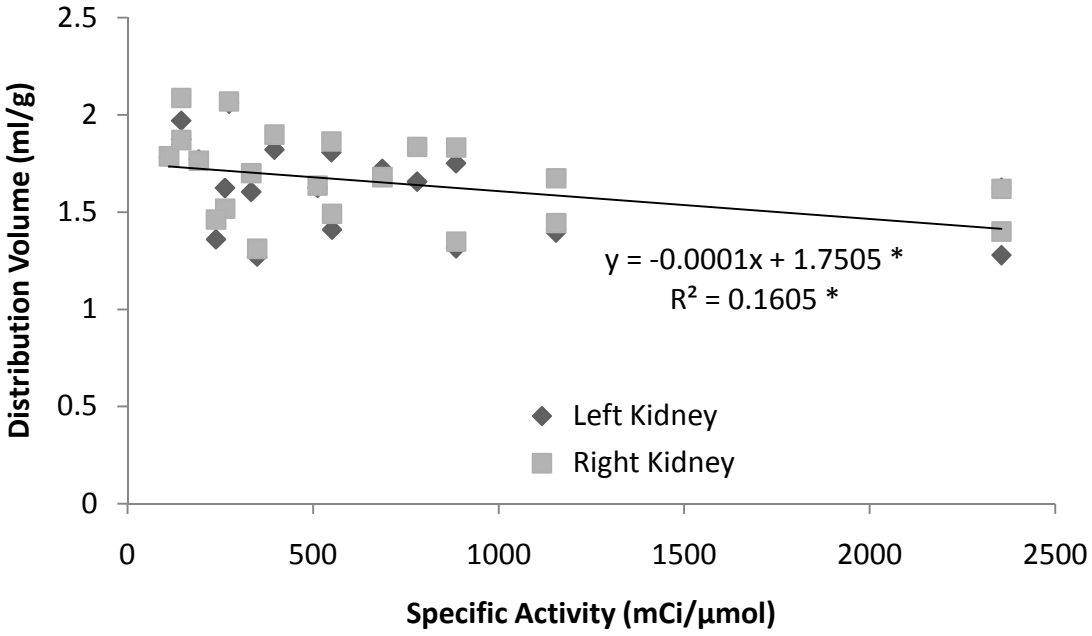

Figure 20 – Individual DV values for [^{11}C]Methyl-Losartan control microPET scans plotted as a function of specific activity for all control rats (n=21 scans). A significant slight downward trend in DV values is observed with increasing specific activity, *significantly different from 0, $p<0.05$.

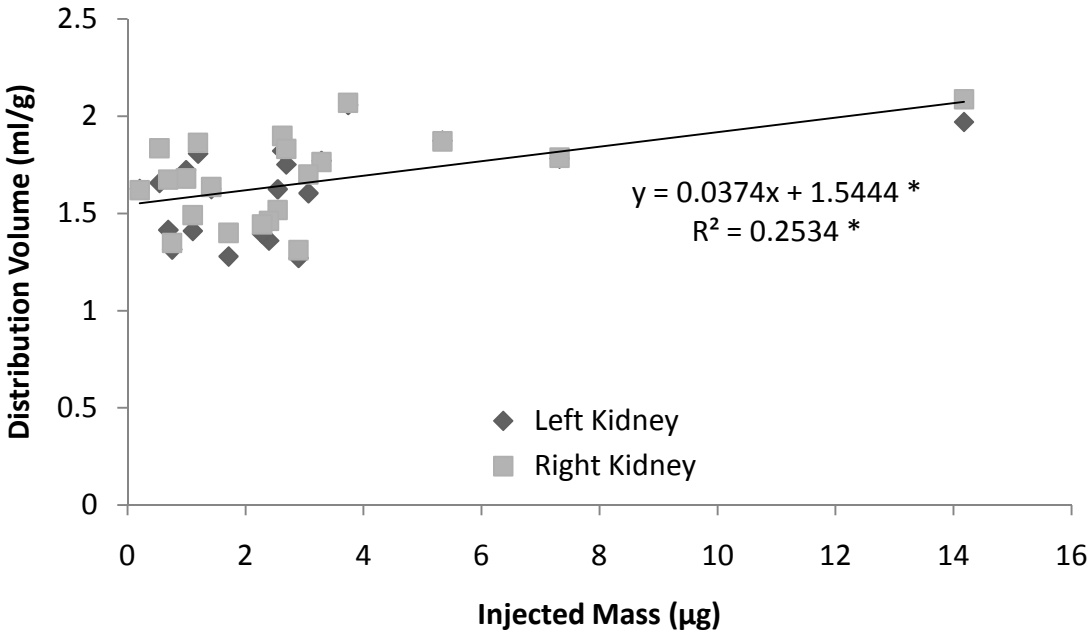

Figure 21 – Individual DV values for [^{11}C]Methyl-Losartan control microPET scans plotted as a function of injected mass for all control rats (n=21 scans). A significant slight upward trend in DV values is observed with increasing injected mass, *significantly different from 0, $p<0.05$.

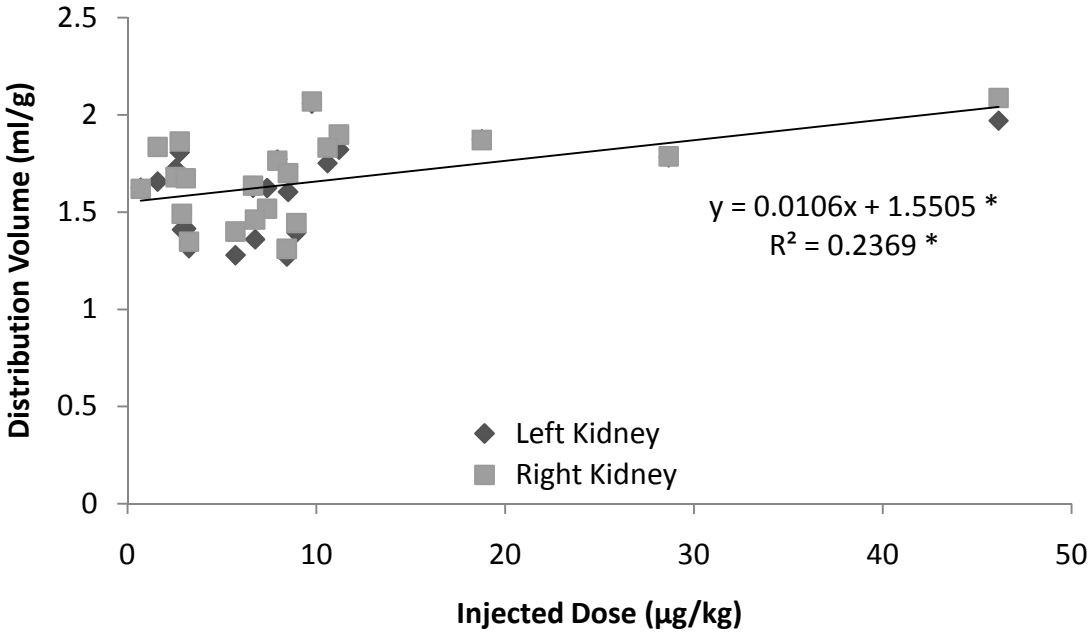

Figure 22 – Individual DV values for [^{11}C]Methyl-Losartan control microPET scans plotted as a function of injected dose for all control rats (n=21 scans). A significant slight upward trend in DV values is observed with increasing injected dose, *significantly different from 0, $p<0.05$.

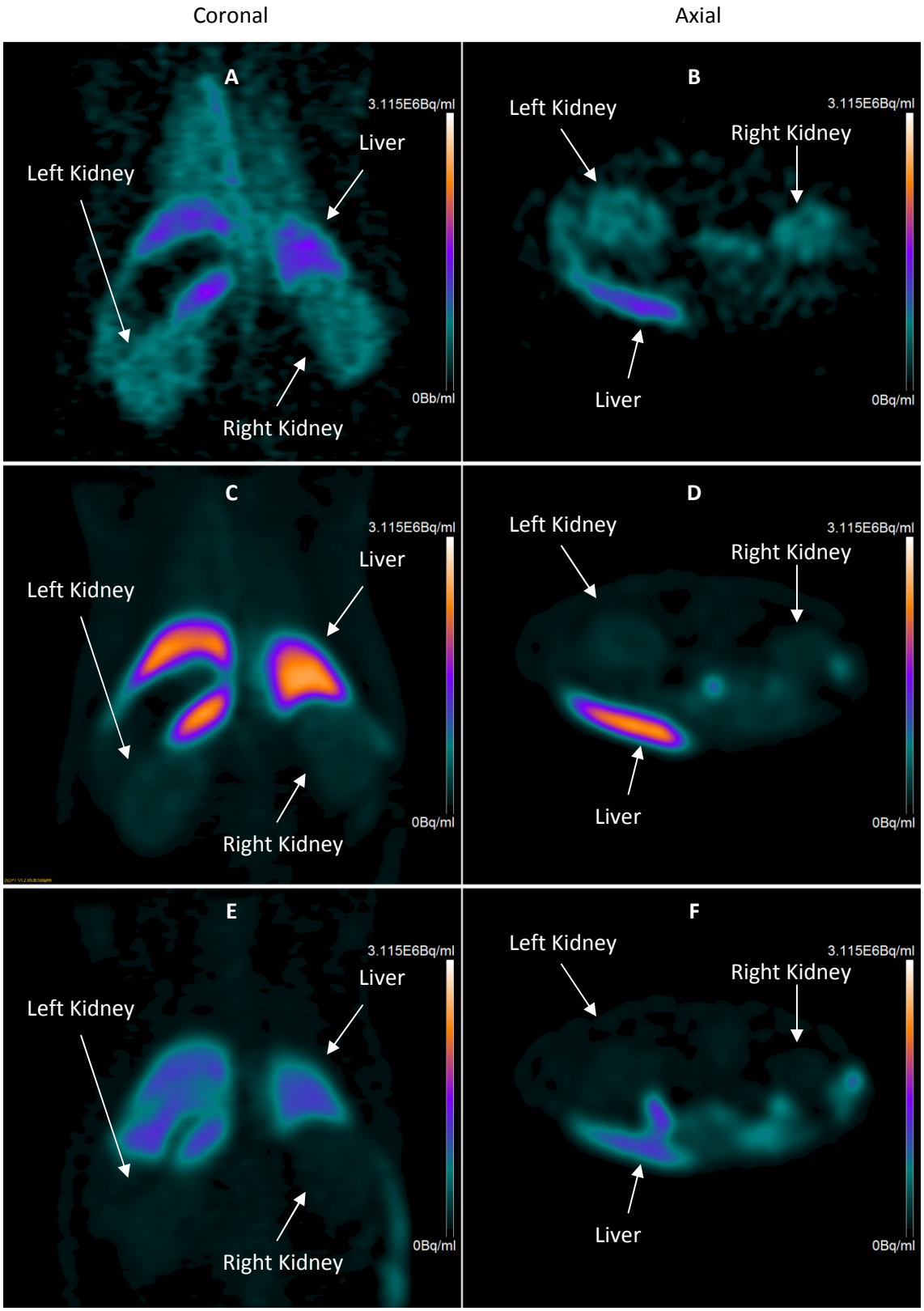

Figure 23 – Representative microPET images of [^{11}C]Methyl-Losartan blocking scan with Losartan (20 mg/kg i.v. co-injection) at 50-60 sec **(A,B)**, 5-10 min **(C,D)**, and 40-45 min **(E,F)** post-injection.

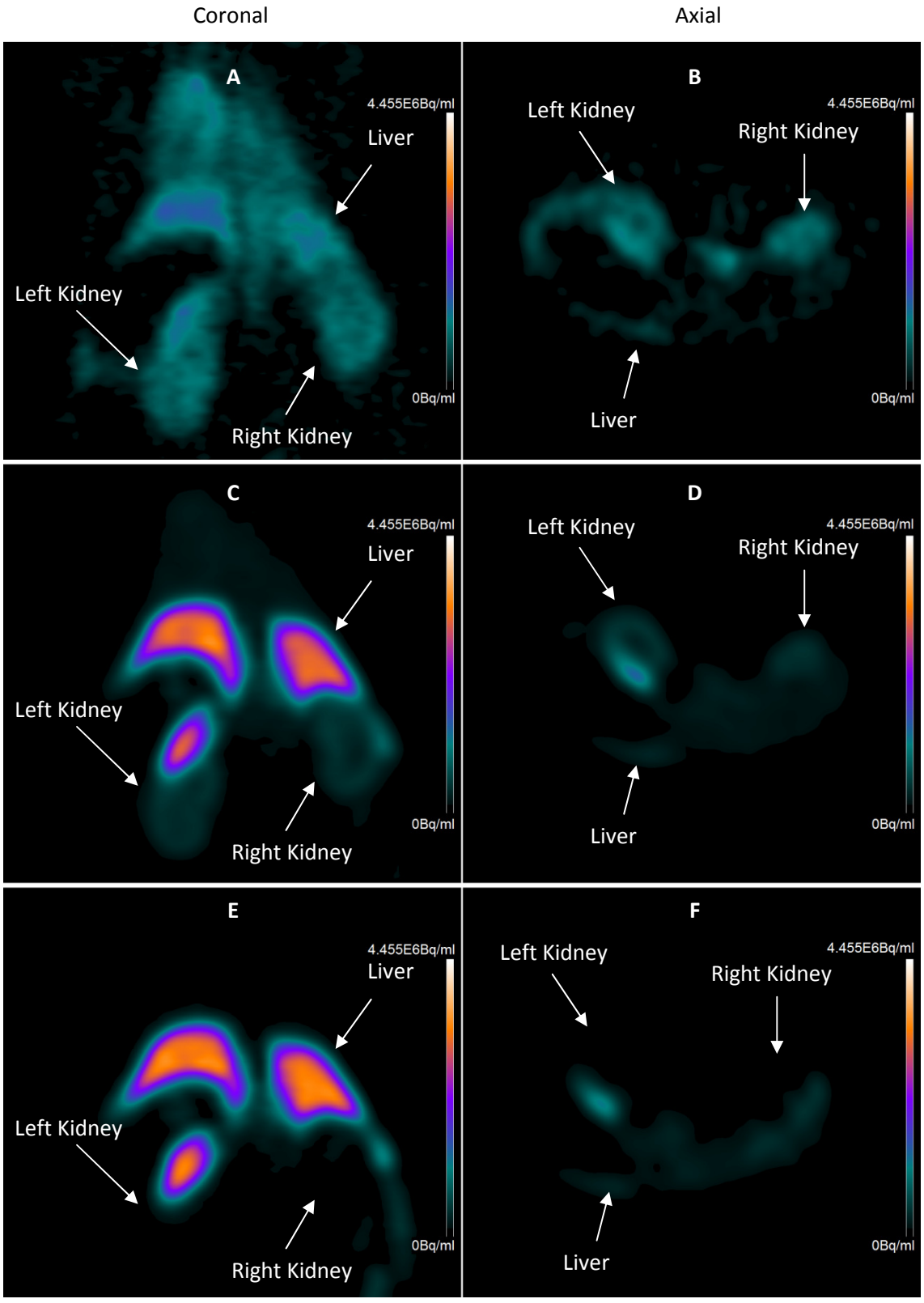

Figure 24 – Representative microPET images of [^{11}C]Methyl-Losartan blocking scan with Candesartan (5 mg/kg i.v. co-injection) at 50-60 sec **(A,B)**, 5-10 min **(C,D)**, and 40-45 min **(E,F)** post-injection.

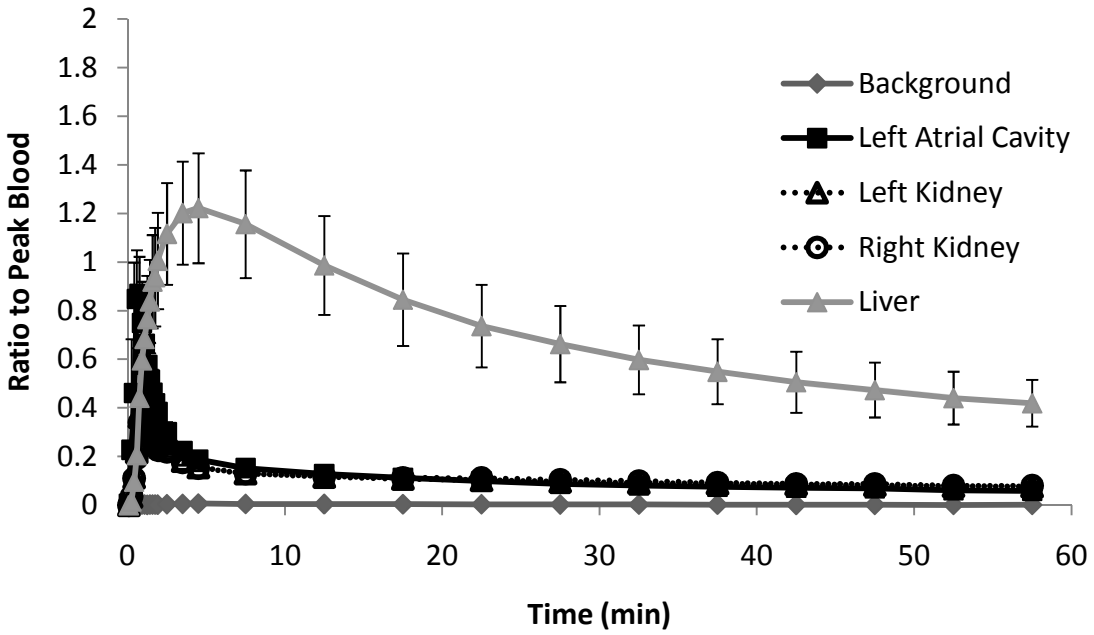

Figure 25 – Mean time activity curves of [^{11}C]Methyl-Losartan blocking microPET scans with Losartan (20 mg/kg i.v. co-injection) (n=4 scans). Data is expressed as mean ratio to peak blood activity ± SD.

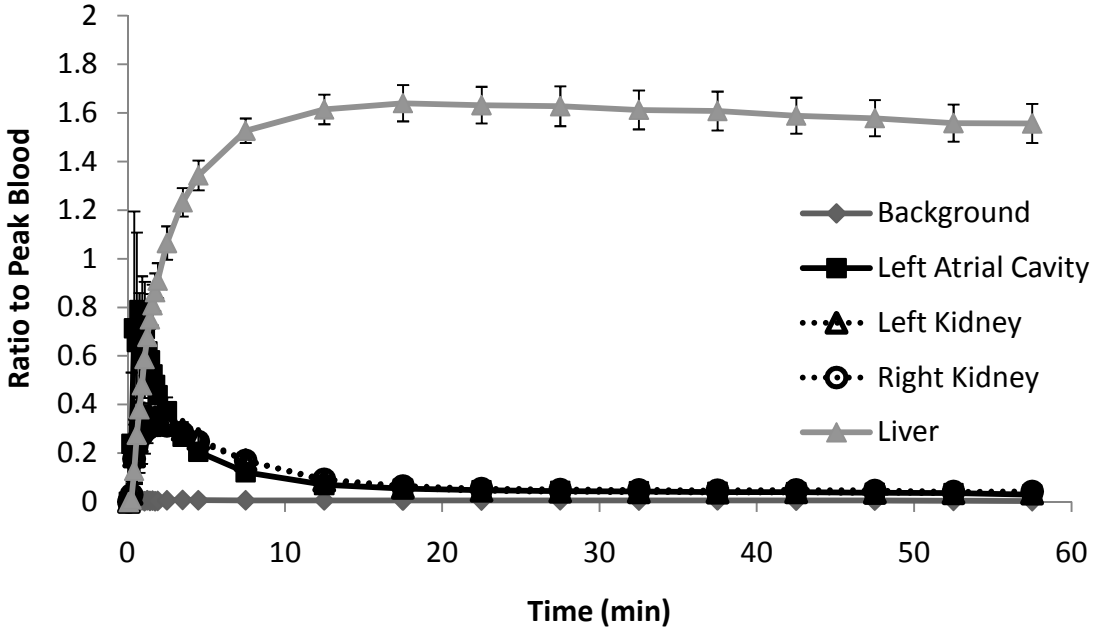

Figure 26 – Mean time activity curves of [^{11}C]Methyl-Losartan blocking microPET scans with Candesartan (5 mg/kg i.v. co-injection) (n=4 scans). Data is expressed as mean ratio to peak blood activity ± SD.

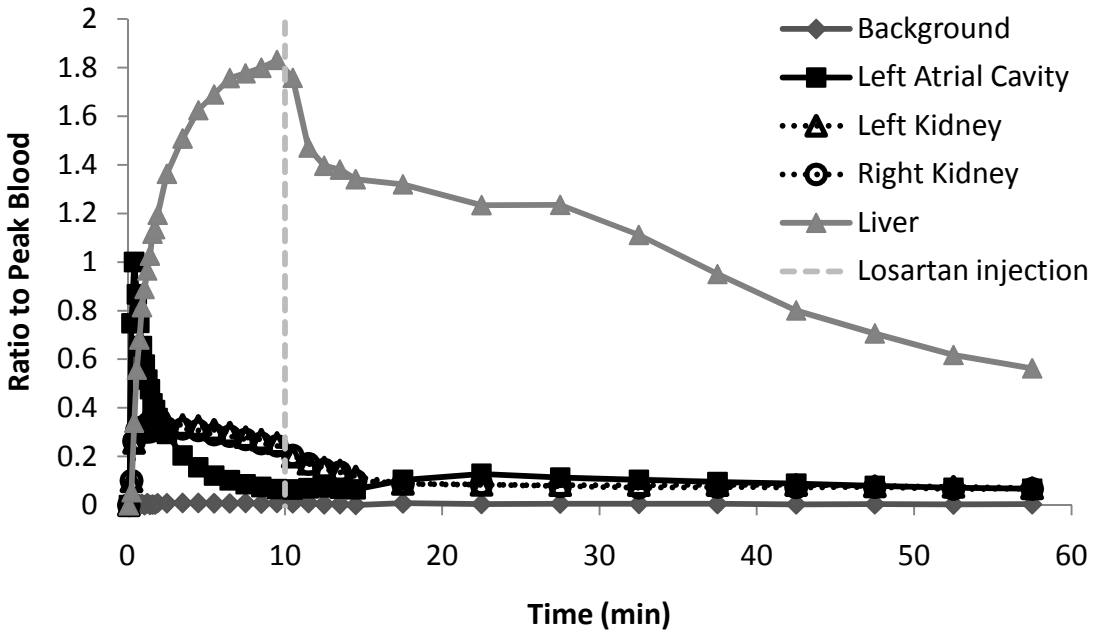

Figure 27 – Time activity curves of [^{11}C]Methyl-Losartan displacement microPET scan with Losartan (20 mg/kg i.v.) at 10 min post-injection (n=1 scan).

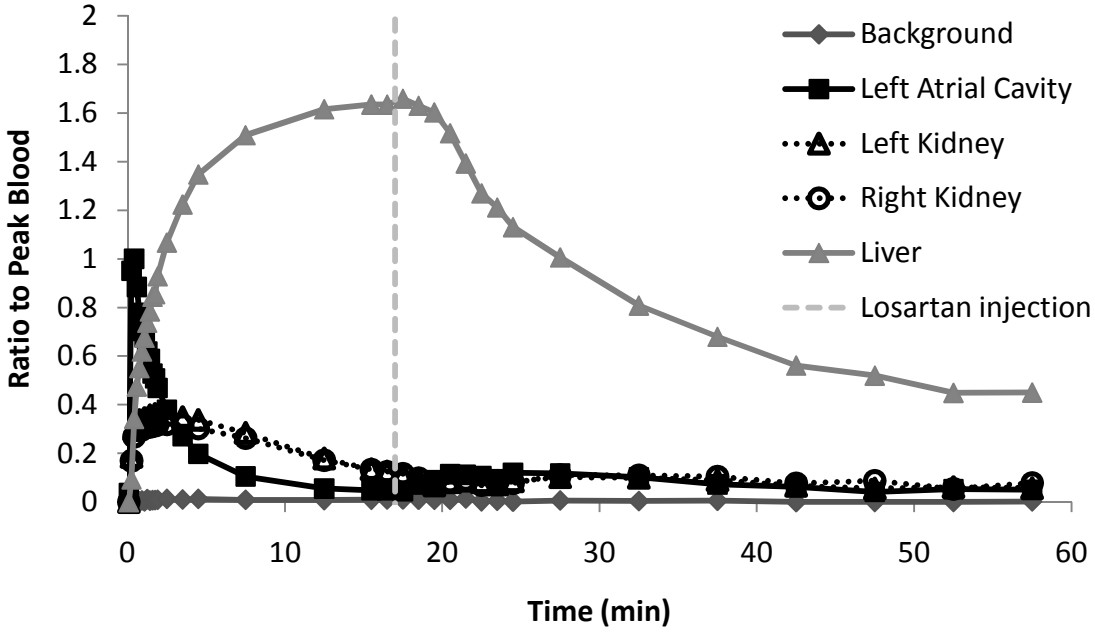

Figure 28 – Time activity curves of [^{11}C]Methyl-Losartan displacement microPET scan with Losartan (20 mg/kg i.v.) at 17 min post-injection (n=1 scan).

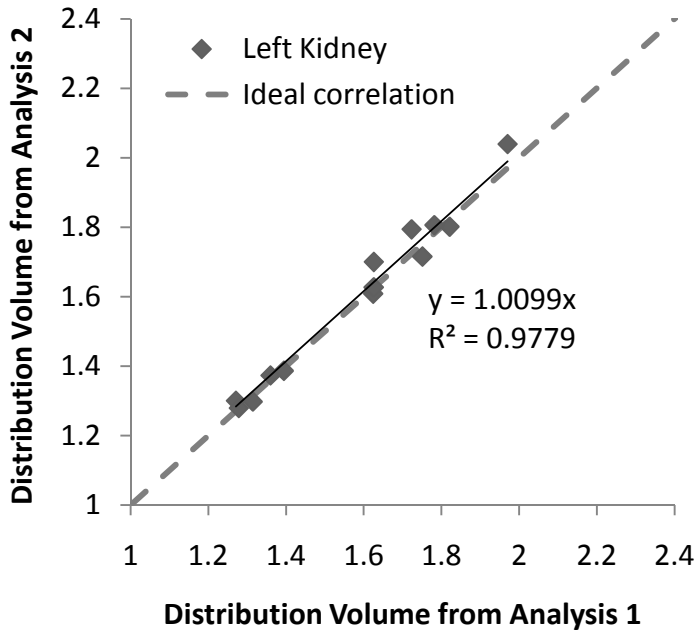

Figure 29 – Comparison plot showing correlation for intra-user DV analysis (n=13 scans). For each set of analyses, the generate DV values are plotted against each other and a best fit curve is generated.

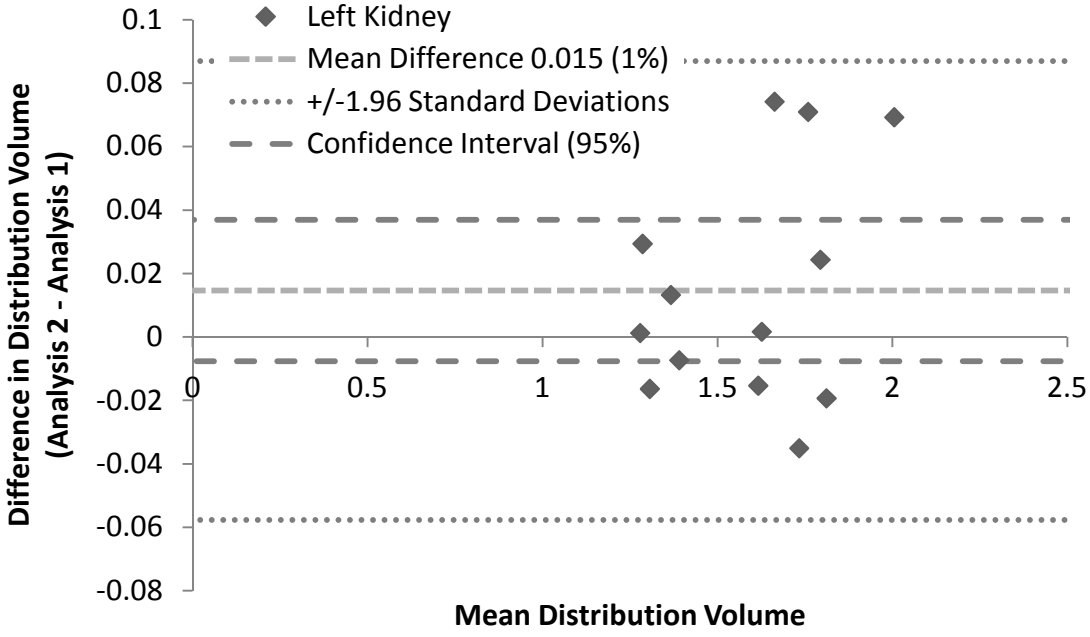

Figure 30 – Bland-Altman plot showing good intra-user DV analysis repeatability (n=13 scans). For each set of analyses, the generated DV values are subtracted from each other (always analysis 2 - analysis 1) and plotted against the mean DV of both analyses. "+/- 1.96 Standard Deviations" indicates the 95% confidence interval which is determined from the mean difference ± standard deviation of the differences.

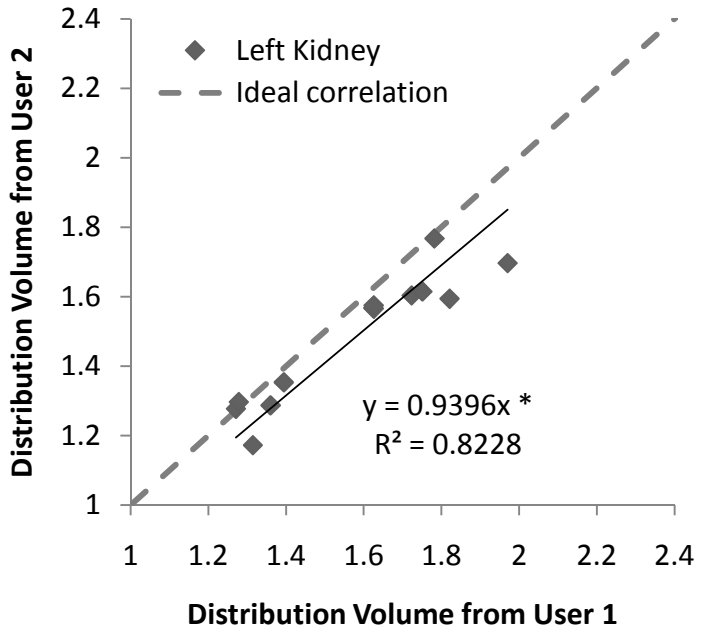

Figure 31 – Comparison plot showing correlation for inter-user DV analysis (n=13 scans). For each set of analyses, the generate DV values are plotted against each other and a best fit curve is generated, *significantly different from 1, p<0.05.

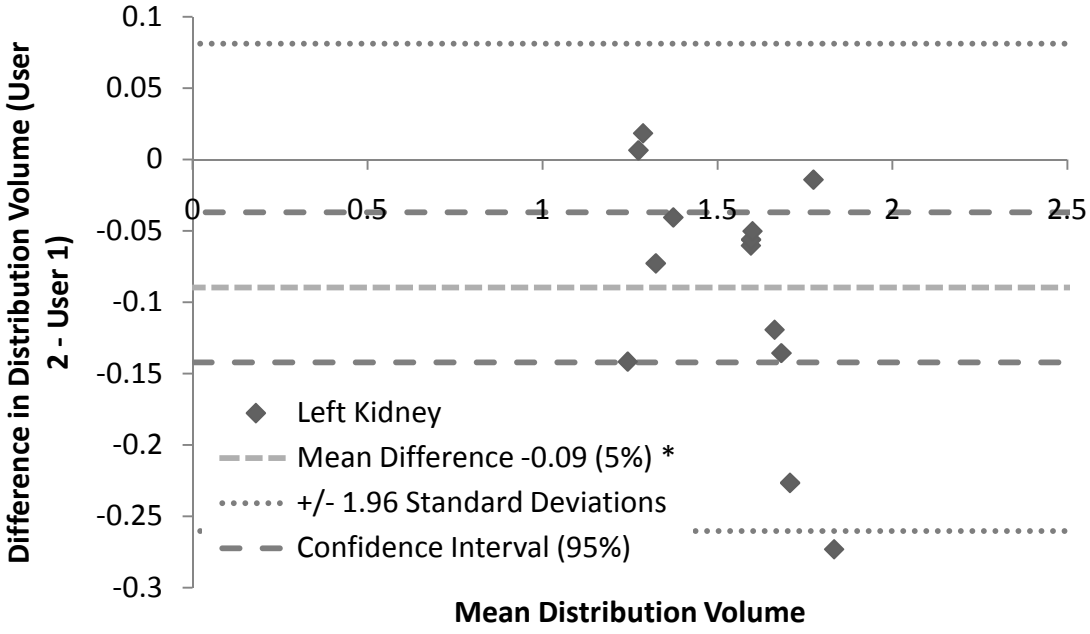

Figure 32 – Bland-Altman plot showing moderate inter-user DV analysis repeatability (n=13 scans). For each set of analyses, the generated DV values are subtracted from each other (always user 2 - user 1) and plotted against the mean DV of both analyses. "+/- 1.96 Standard Deviations" indicates the 95% confidence interval which is determined from the mean difference ± standard deviation of the differences, *significantly different from 0, p<0.05.

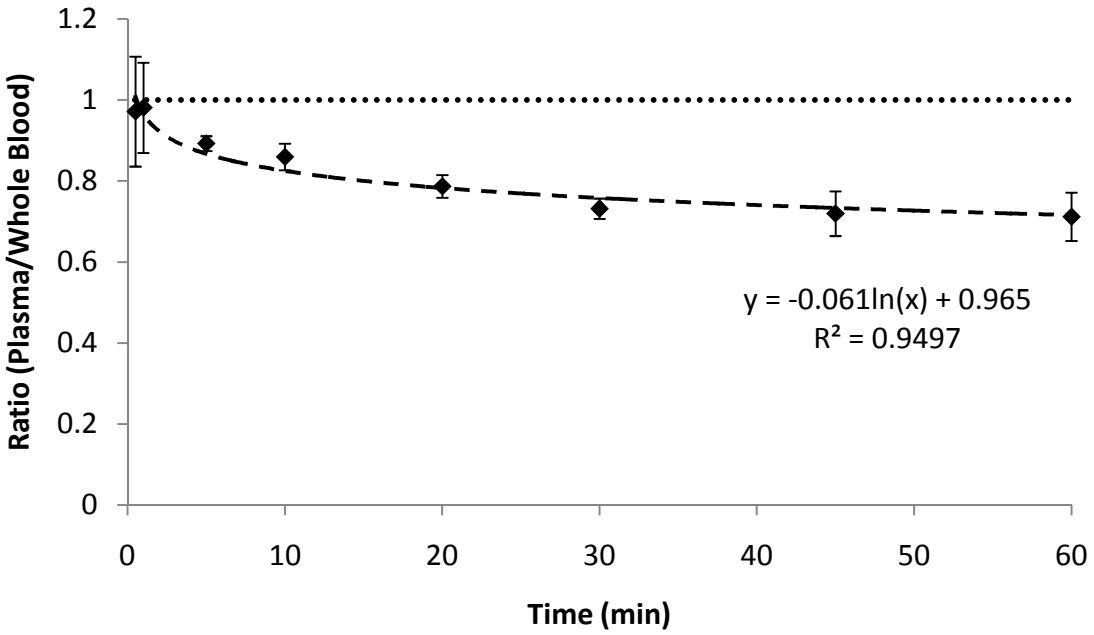

Figure 33 – Time activity curve of [^{11}C]Methyl-Losartan blood and plasma sampling (n=5 rats). The data is expressed as a ratio of [^{11}C]Methyl-Losartan concentration in the plasma over whole blood and was fitted to a downward logarithmic function defined by the formula.

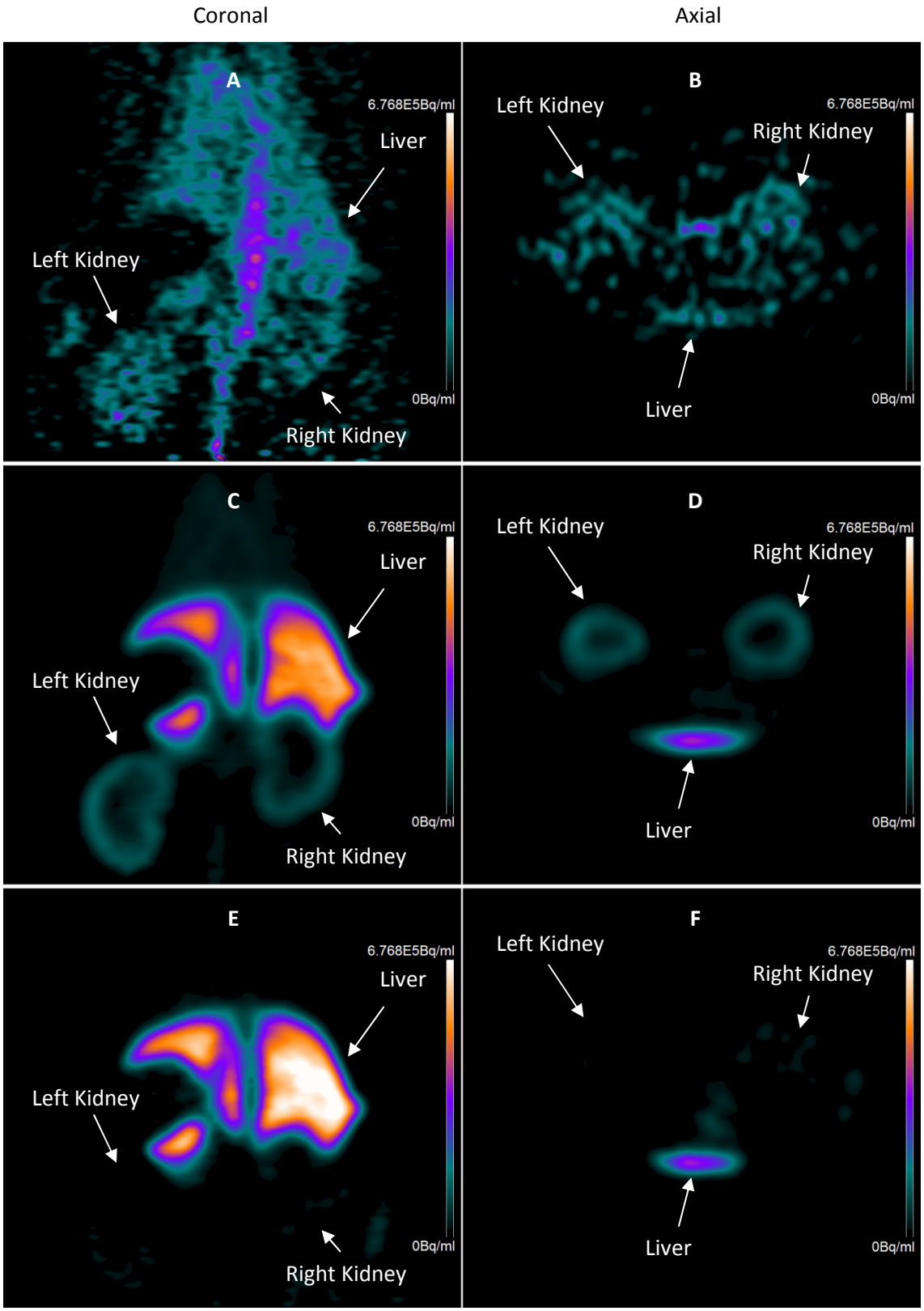

Figure 34 – Representative microPET images of [^{11}C]Methyl-EXP3174 control microPET scans at 50-60 sec **(A,B)**, 5-10 min **(C,D)**, and 40-45 min **(E,F)** post-injection.

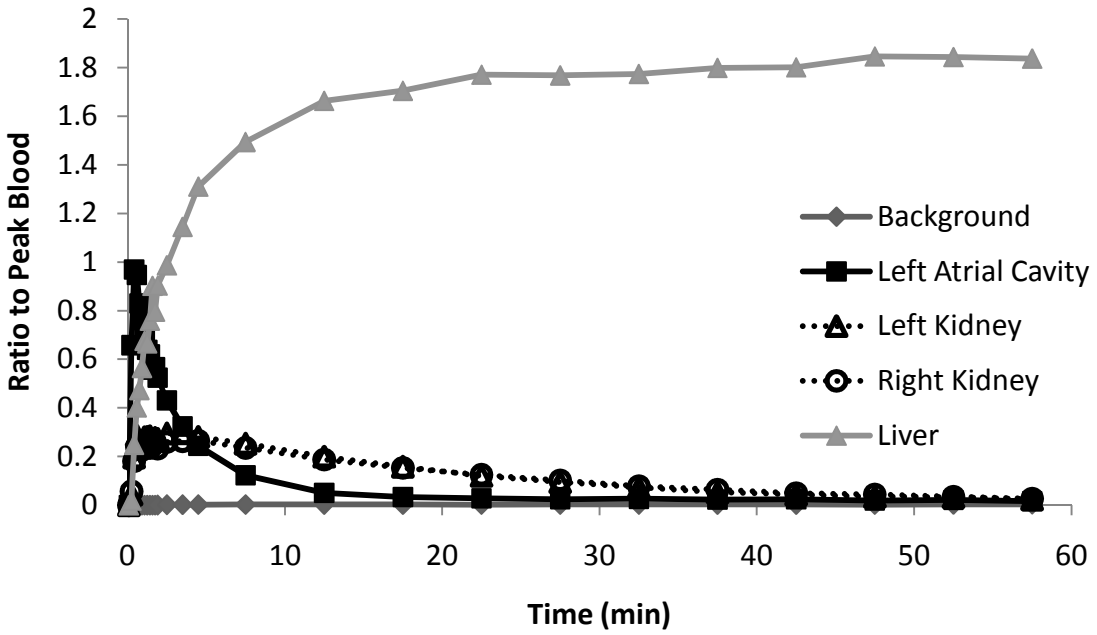

Figure 35 – Mean time activity curves of [^{11}C]Methyl-EXP3174 control microPET scans (n=2 scans). Data is expressed as mean ratio to peak blood activity.

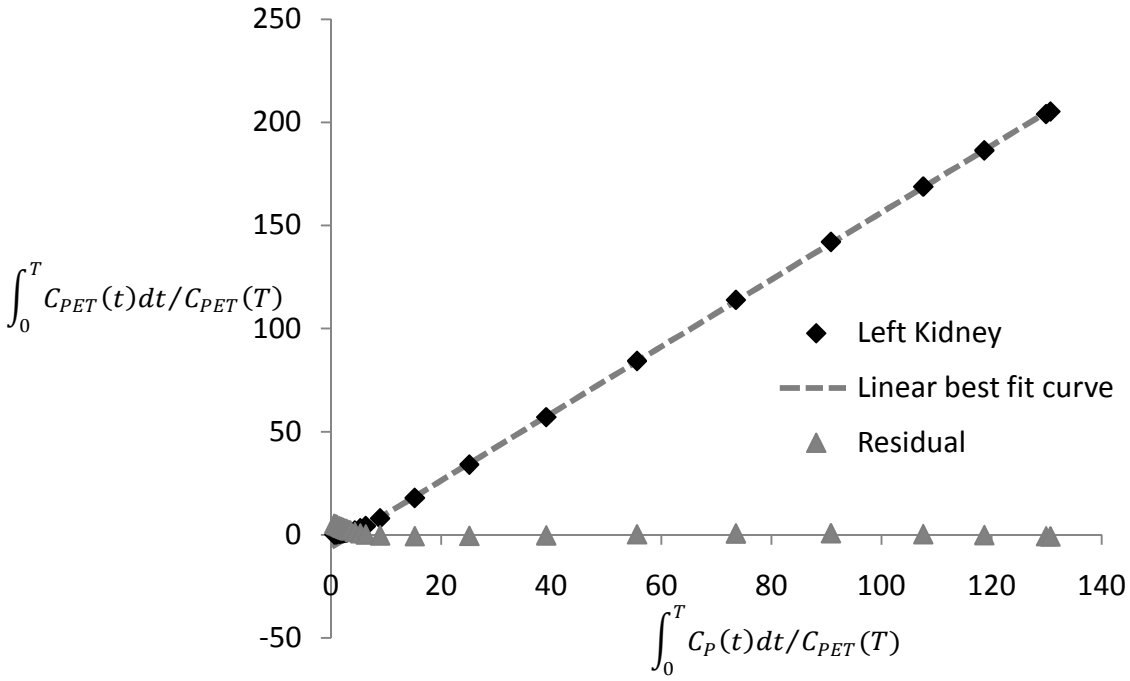

Figure 36 – Representative Logan plot of [^{11}C]Methyl-EXP3174 microPET scan. The x axis represents adjusted time whereas the y axis represents adjusted activity. A linear curve was fitted to the data. The slope of this curve represents the DV value.

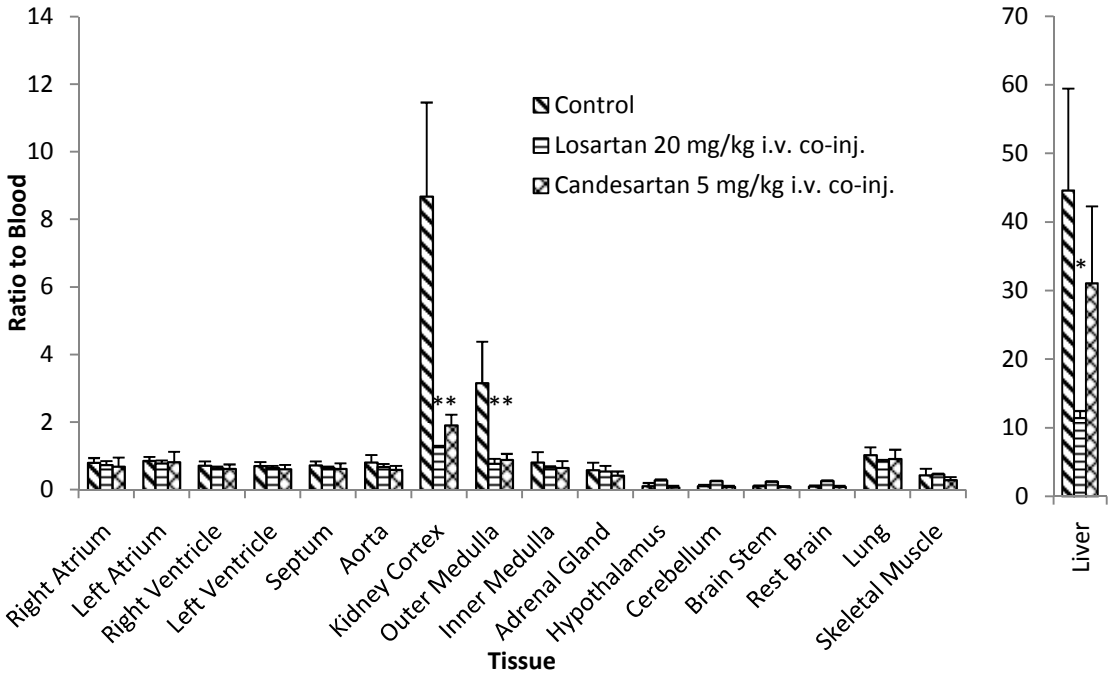

Figure 37 – [^{11}C]Methyl-Losartan uptake and specific binding at 10 min post-injection as assessed by biodistribution (n=10 control, n=4 Losartan, n=4 Candesartan). Results are expressed as %ID/g ratio to blood ± SD. One way ANOVA and Bonferroni post-hoc were used for statistical analysis, *significantly different from control, $p<0.05$.

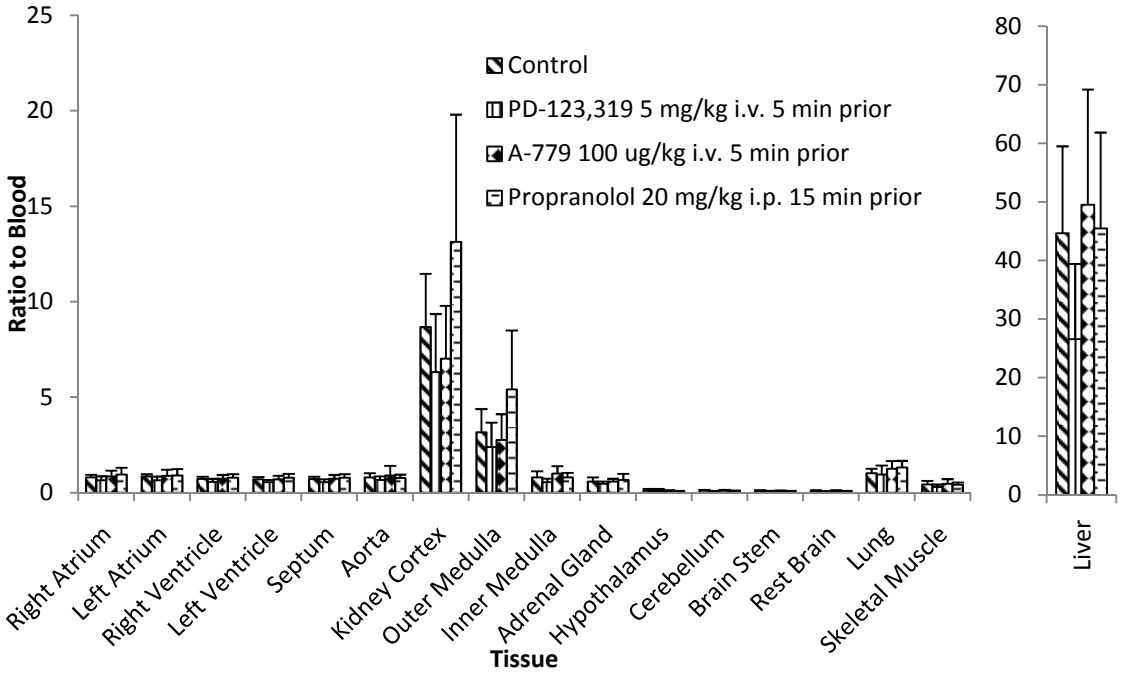

Figure 38 – [^{11}C]Methyl-Losartan uptake and selective binding at 10 min post-injection as assessed by biodistribution (n=10 control, n=8 PD-123,319, n=12 A-779, n=8 Propranolol). Results are expressed as %ID/g ratio to blood ± SD. One way ANOVA and Bonferroni post-hoc were used for statistical analysis, no significant changes were observed.

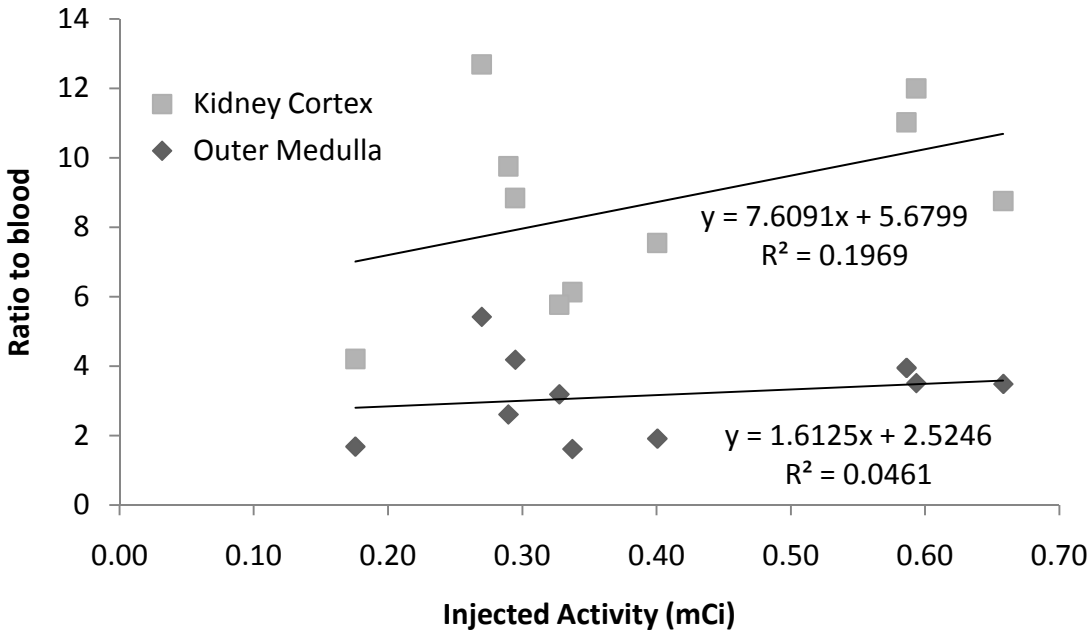

Figure 39 – [^{11}C]Methyl-Losartan uptake ratio to blood as a function of injected activity for all control rats in biodistribution studies (n=10 rats). Ratio to blood show consistent values across injected activity range.

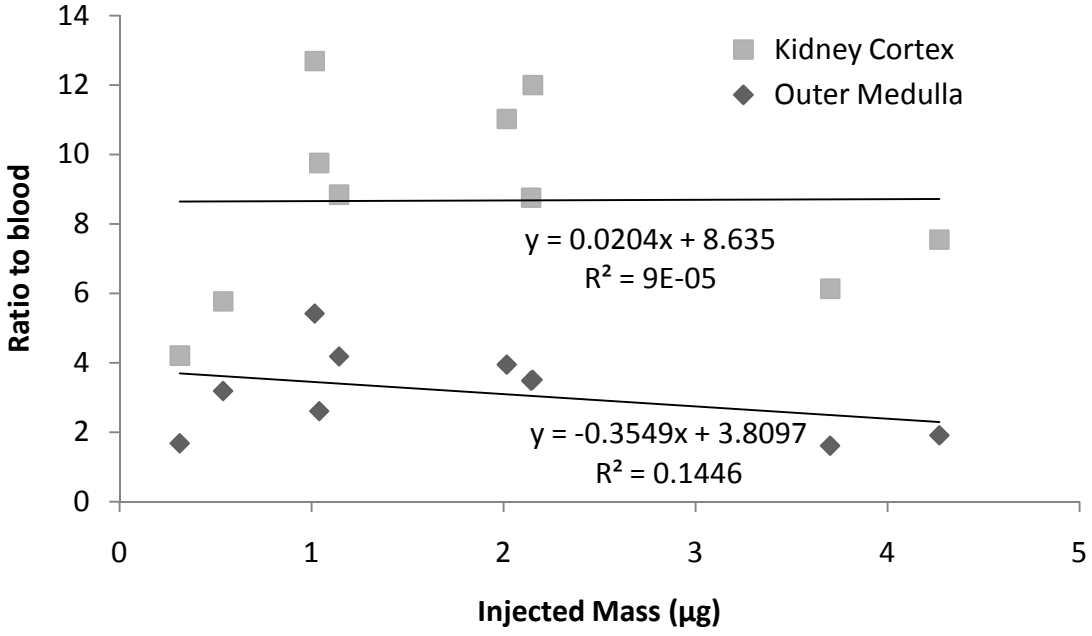

Figure 40 – [^{11}C]Methyl-Losartan uptake ratio to blood as a function of injected mass for all control rats in biodistribution studies (n=10 rats). Ratio to blood show consistent values across injected mass range.

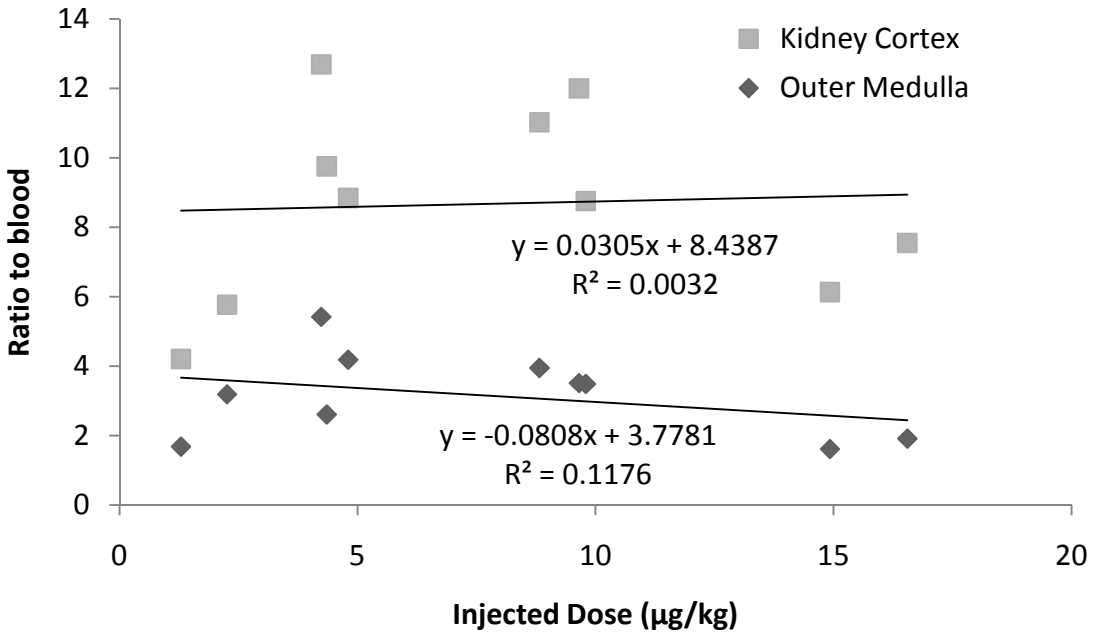

Figure 41 – [^{11}C]Methyl-Losartan uptake ratio to blood as a function of injected dose for all control rats in biodistribution studies (n=10 rats). Ratio to blood show consistent values across injected dose range.

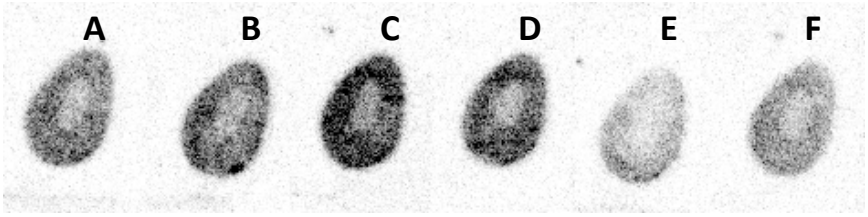

Figure 42 – Representative image of autoradiography with [^{11}C]Methyl-Losartan. (A) Control, (B) PD-123,319, (C) A-779, (D) Propranolol, (E) Losartan and (F) Candesartan.

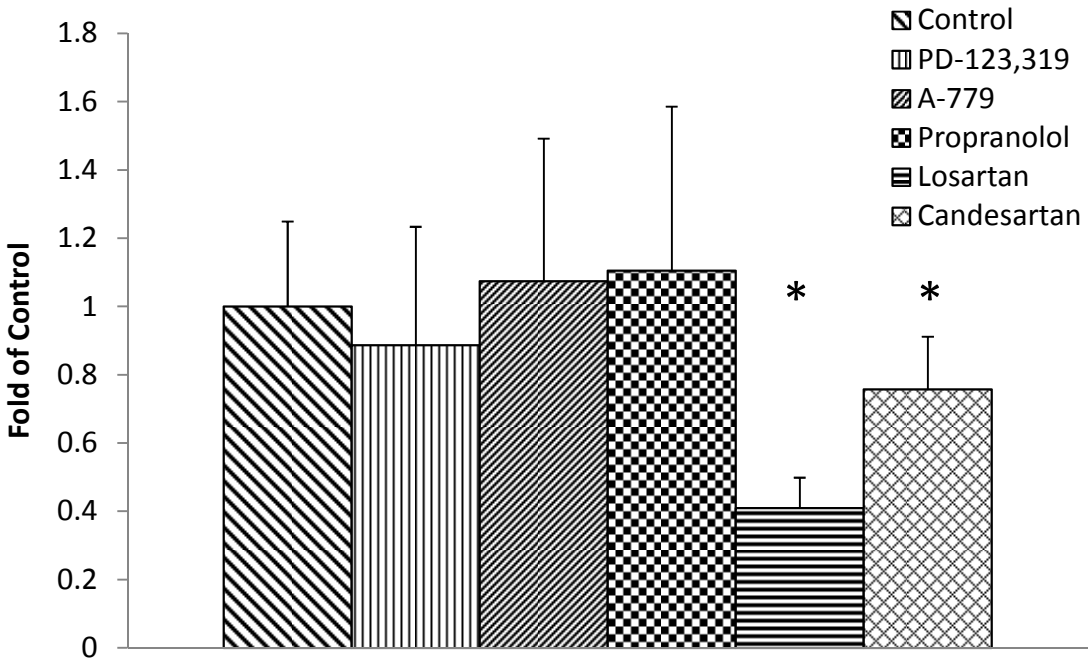

Figure 43 – [^{11}C]Methyl-Losartan specific and selective binding as evaluated by autoradiography (n=30 control, n=20 PD-123,319, n=21 A-779, n=22 Propranolol, n=30 Losartan, n=35 Candesartan kidney sections). Kidney sections were incubated in 5 nM [^{11}C]Methyl-Losartan with 10 nm PD-123,319 (AT_2 receptor blocker), A-779 (Mas receptor blocker), Propranolol (β receptor blocker), Losartan (AT_1 receptor blocker) or Candesartan (AT_1 receptor blocker) and radioactivy counted. Data is expressed a fold of control ± SD. One way ANOVA and Bonferroni post-hoc were used for statistical analysis, *significantly different from control, $p<0.05$.

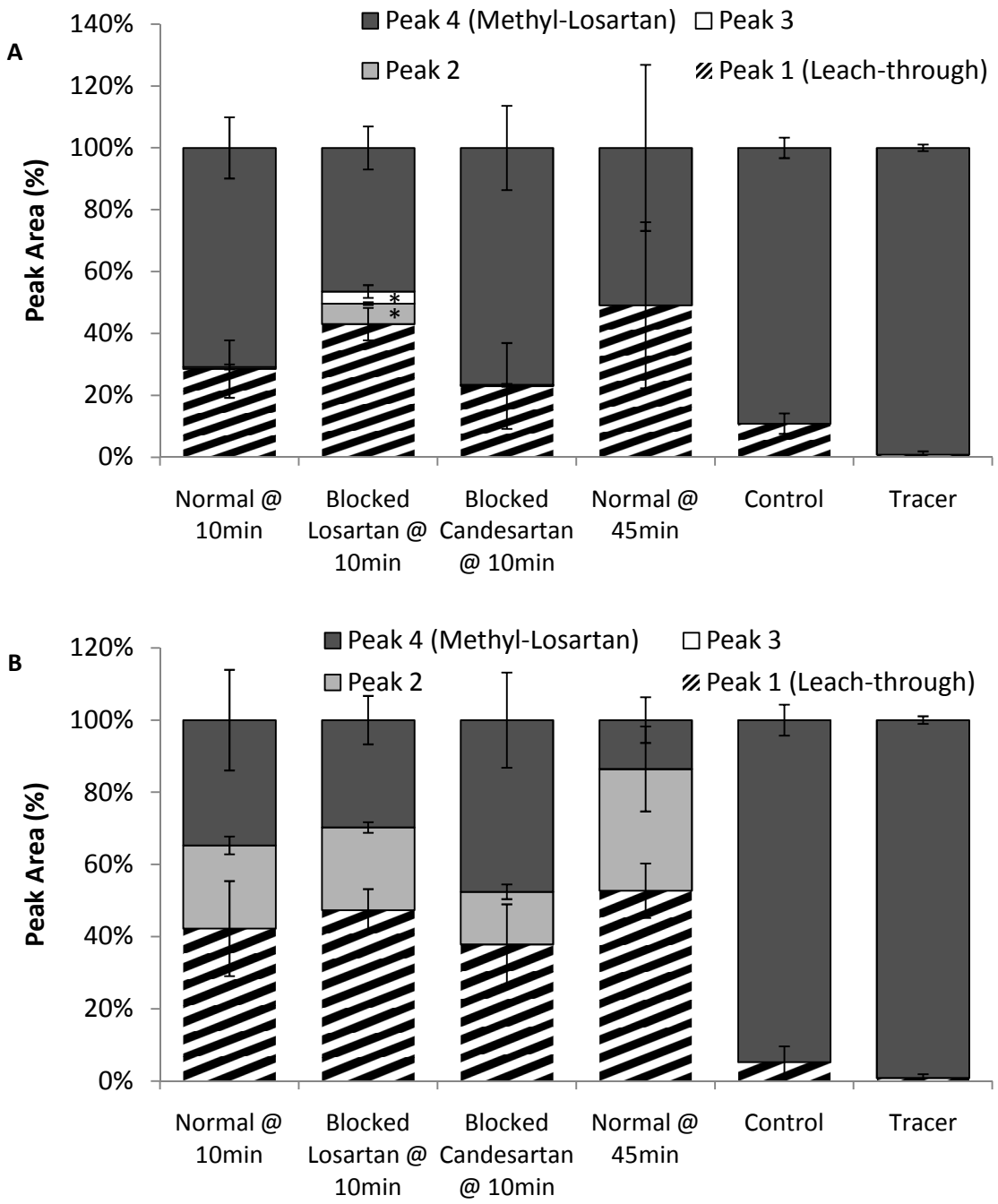

Figure 44 – [^{11}C]Methyl-Losartan metabolite analysis for plasma (A) and kidney (B) (n=4 normal at 10 min, n=3 blocked Losartan, n=3 blocked Candesartan, n=4 normal at 45 min, n=8 control plasma (A), n=9 control kidney (B), n=13 tracer). Peak area was quantified and expressed as a percentage of total area per sample. One way ANOVA and Bonferroni post-hoc were used for statistical analysis, * significantly different from normal at 10 min and normal at 45 min, $p<0.05$.

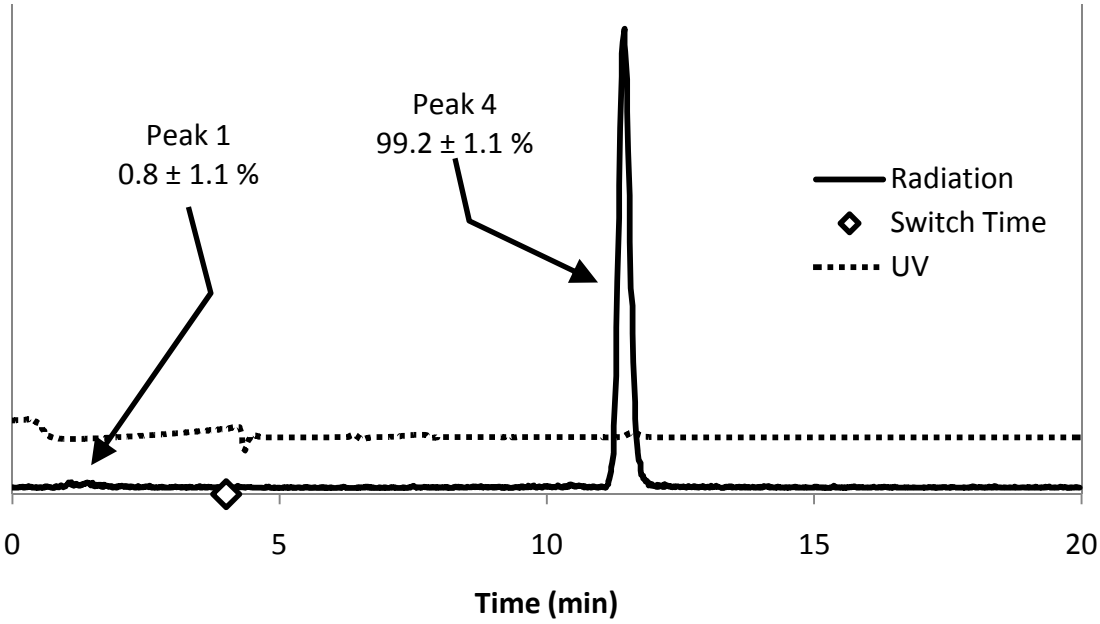

Figure 45 – Representative chromatogram of authentic [^{11}C]Methyl-Losartan injection onto the HPLC system (n=13 samples). Peak 1 represents leach-through, and peak 4 represents [^{11}C]Methyl-Losartan. The numbers indicate the mean area under the curve ± SD.

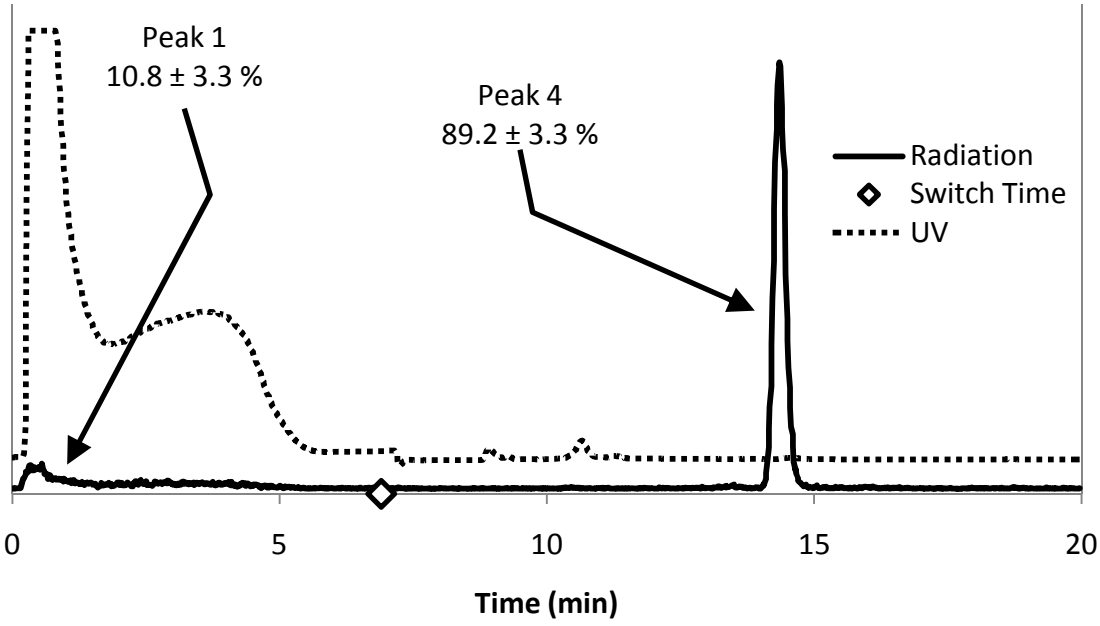

Figure 46 – Representative chromatogram of control plasma sample injection onto the HPLC system (n=8 samples). Peak 1 represents leach-through, and peak 4 represents [^{11}C]Methyl-Losartan. The numbers indicate the mean area under the curve ± SD.

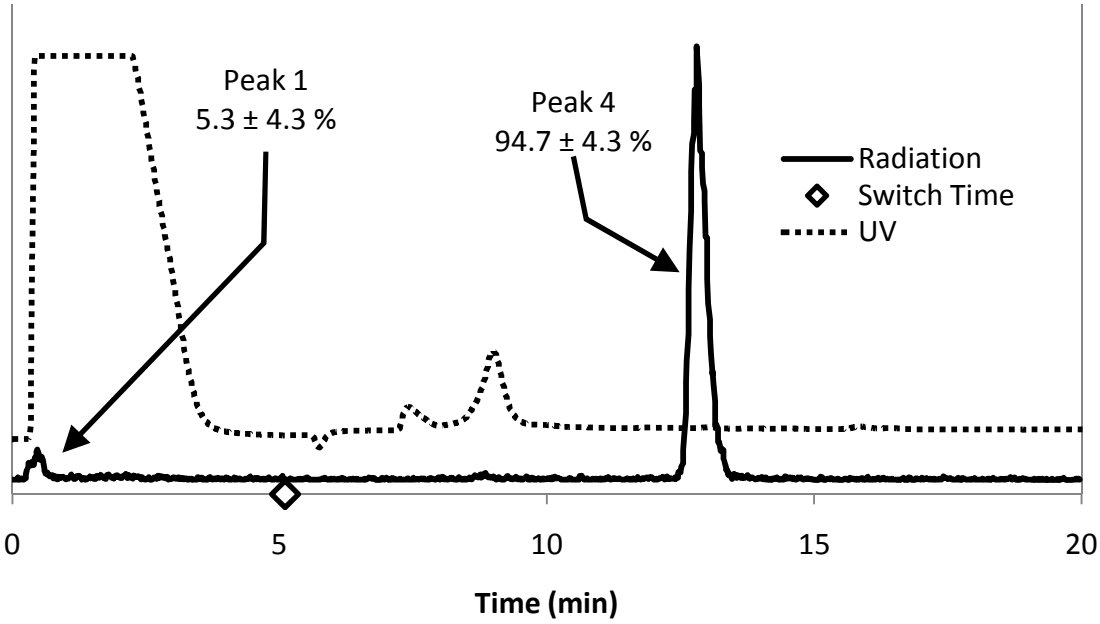

Figure 47 – Representative chromatogram of control kidney sample injection onto the HPLC system (n=9 samples). Peak 1 represents leach-through, and peak 4 represents [^{11}C]Methyl-Losartan. The numbers indicate the mean area under the curve ± SD.

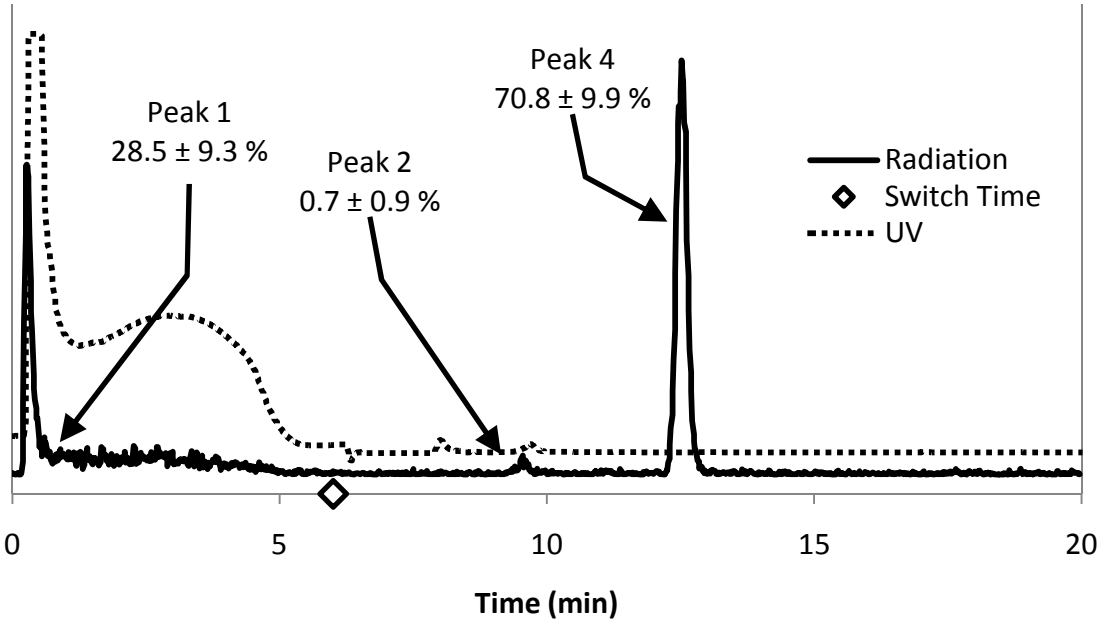

Figure 48 – Representative chromatogram of plasma sample at 10 min post-injection (n=4 samples). Peak 1 represents leach-through, peak 2 represents a metabolite, and peak 4 represents [^{11}C]Methyl-Losartan. The numbers indicate the mean area under the curve ± SD.

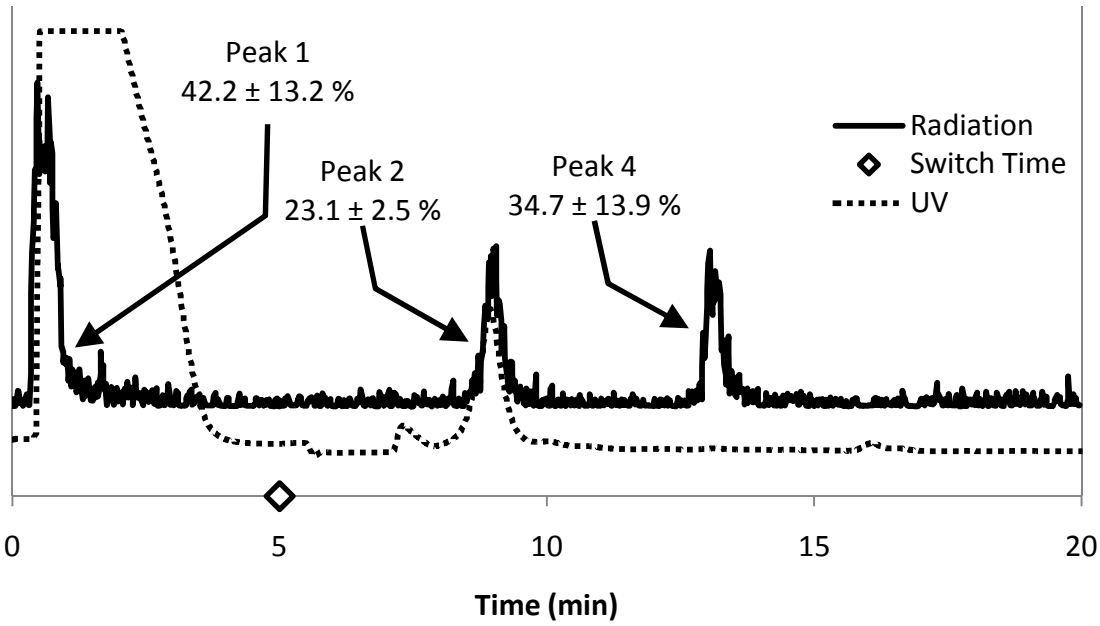

Figure 49 – Representative chromatogram of kidney sample at 10 min post-injection (n=4 samples). Peak 1 represents leach-through, peak 2 represents a metabolite, and peak 4 represents [^{11}C]Methyl-Losartan. The numbers indicate the mean area under the curve ± SD.

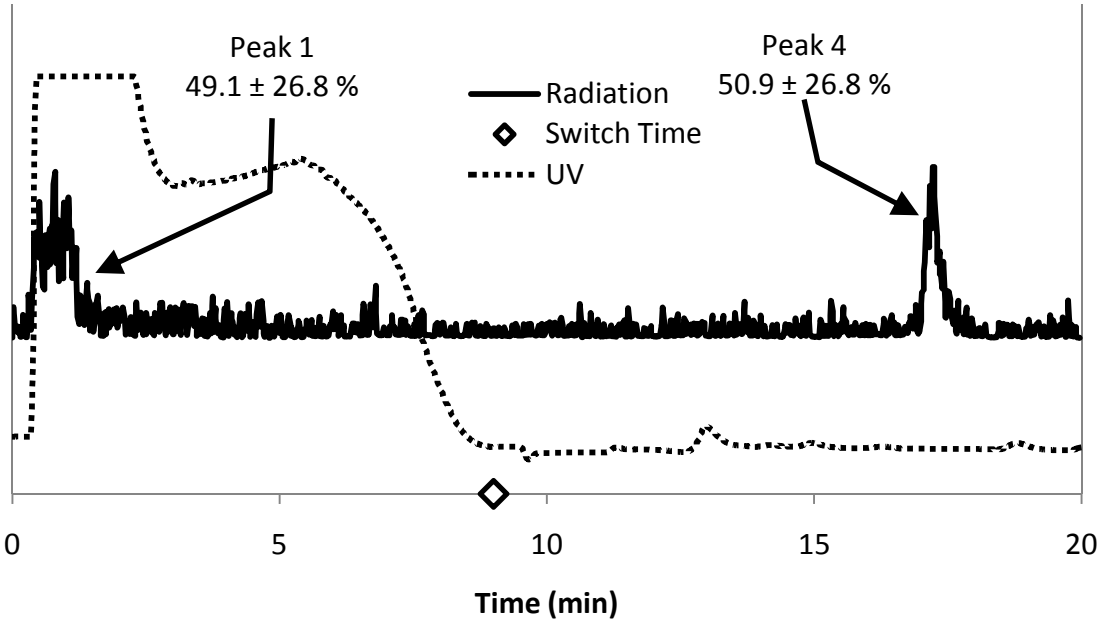

Figure 50 – Representative chromatogram of plasma sample at 45 min post-injection (n=4 samples). Peak 1 represents leach-through, and peak 4 represents [^{11}C]Methyl-Losartan. The numbers indicate the mean area under the curve ± SD.

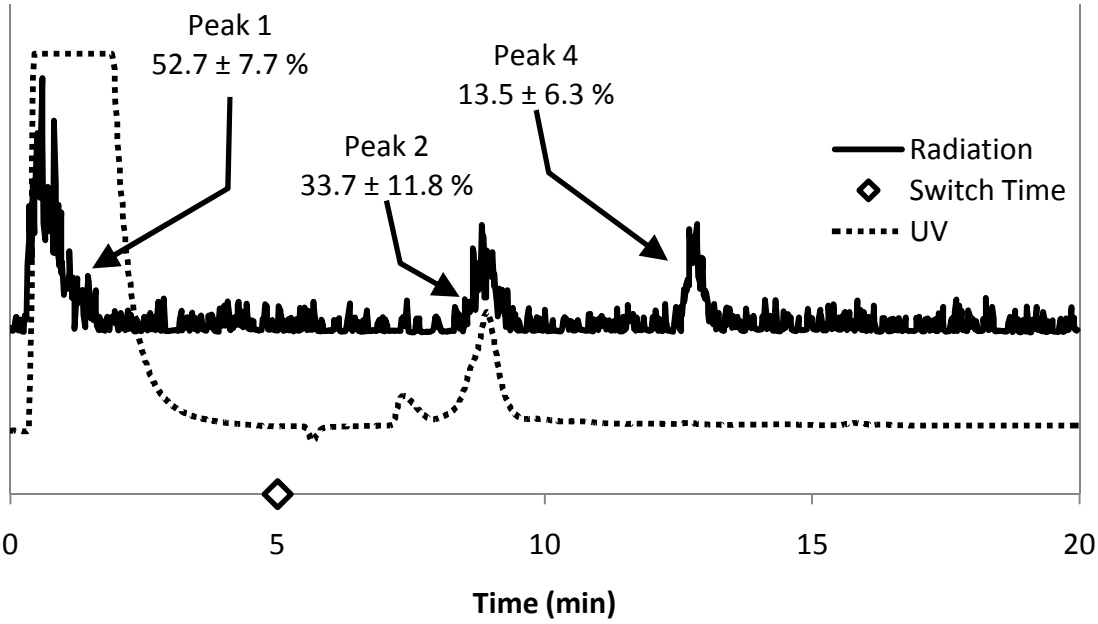

Figure 51 – Representative chromatogram of kidney sample at 45 min post-injection (n=4 samples). Peak 1 represents leach-through, peak 2 represents a metabolite, and peak 4 represents [^{11}C]Methyl-Losartan. The numbers indicate the mean area under the curve ± SD.

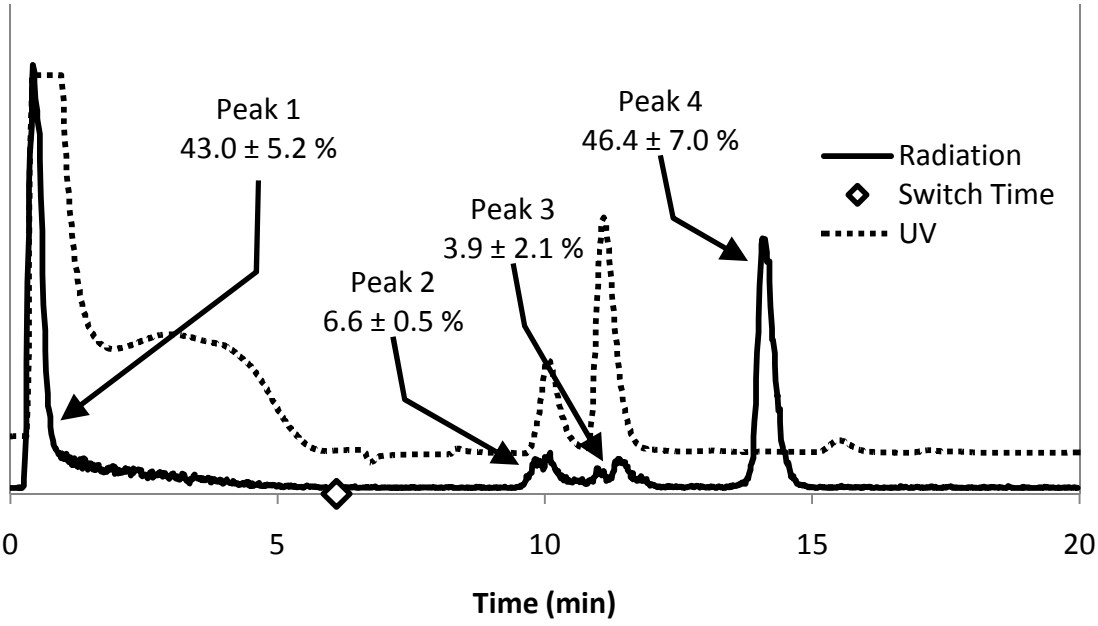

Figure 52 – Representative chromatogram of blocked plasma with Losartan at 10 min post-injection (n=3 samples). Peak 1 represents leach-through, peak 2 and peak 3 represent metabolites, and peak 4 represents [^{11}C]Methyl-Losartan. The numbers indicate the mean area under the curve ± SD.

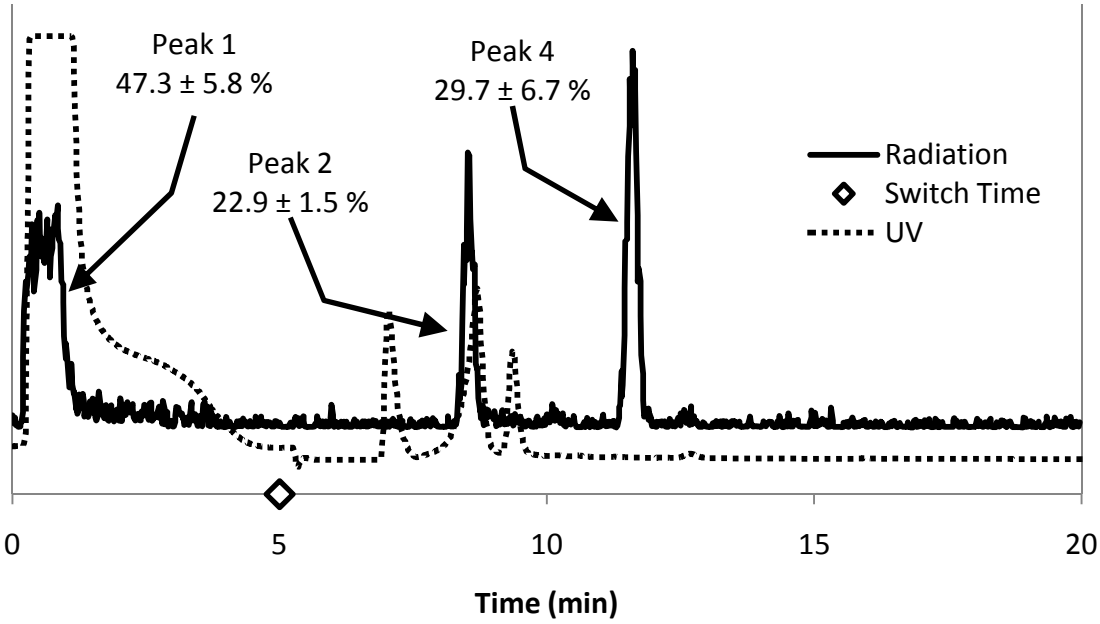

Figure 53 – Representative chromatogram of blocked kidney with Losartan at 10 min post-injection (n=3 samples). Peak 1 represents leach-through, peak 2 represents a metabolite, and peak 4 represents [^{11}C]Methyl-Losartan. The numbers indicate the mean area under the curve ± SD.

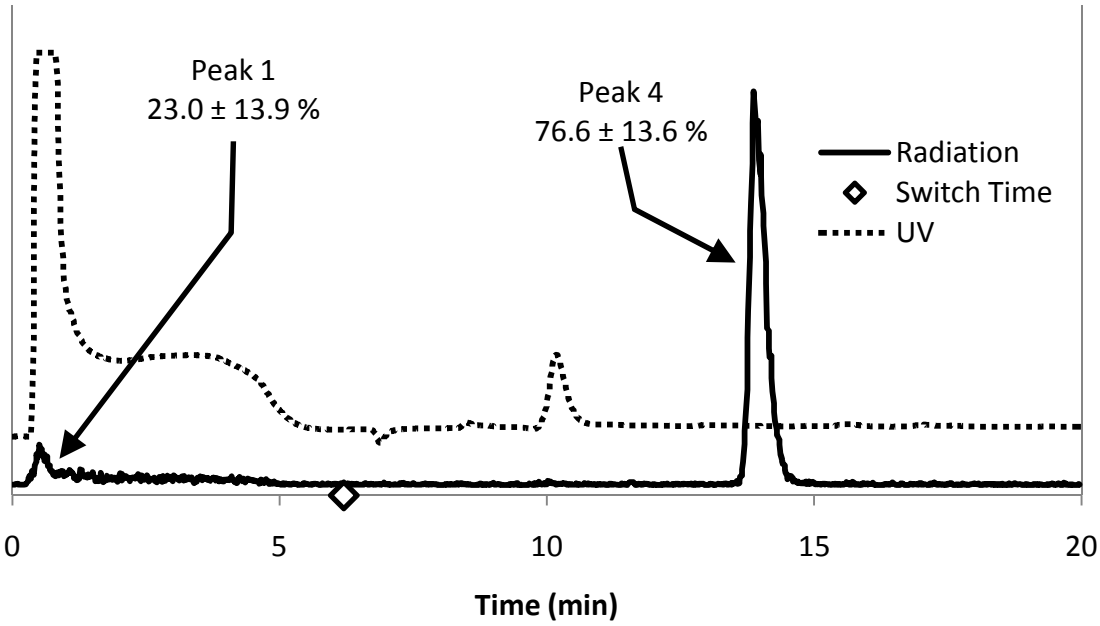

Figure 54 – Representative chromatogram of blocked plasma with Candesartan at 10 min post-injection (n=3 samples). Peak 1 represents leach-through, and peak 4 represents [^{11}C]Methyl-Losartan. The numbers indicate the mean area under the curve ± SD.

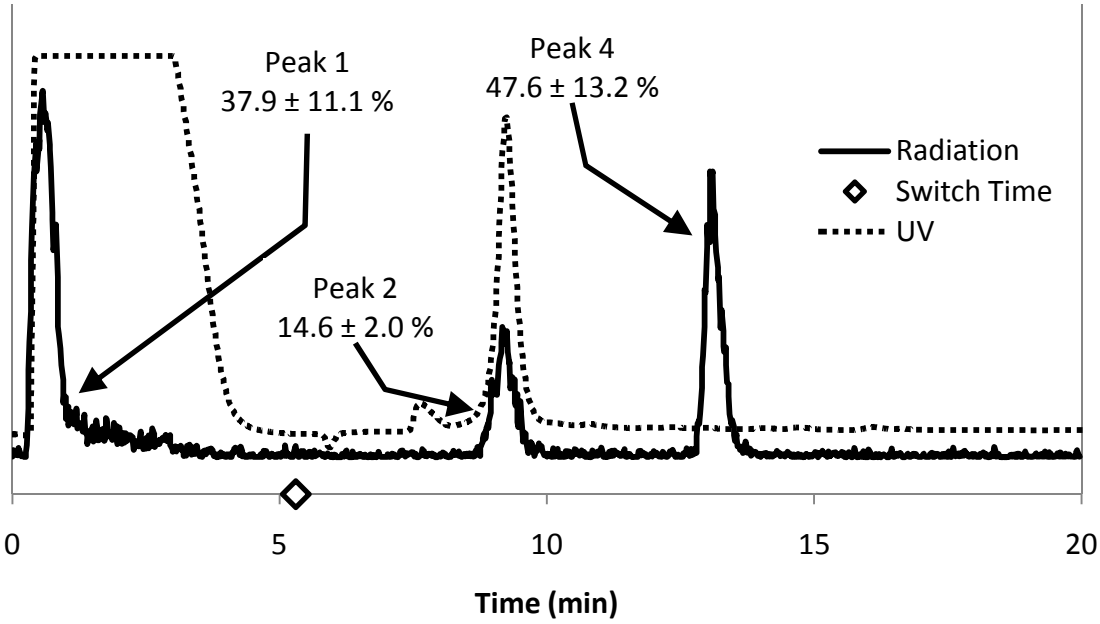

Figure 55 – Representative chromatogram of blocked kidney with Candesartan at 10 min post-injection (n=3 samples). Peak 1 represents leach-through, peak 2 represents a metabolite, and peak 4 represents [^{11}C]Methyl-Losartan. The numbers indicate the mean area under the curve ± SD.

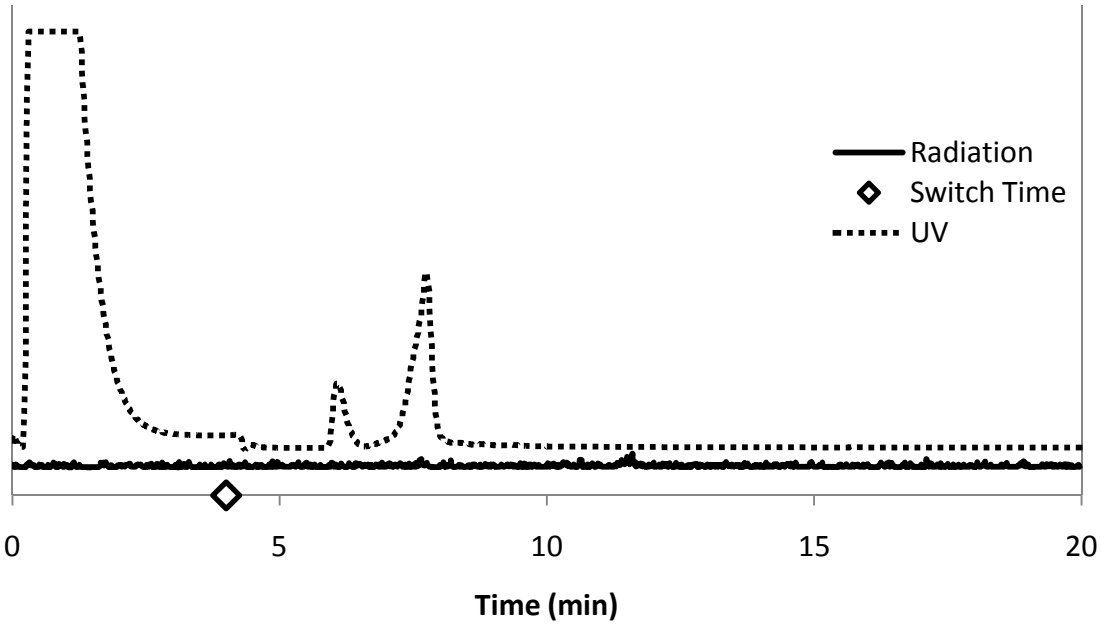

Figure 56 – Chromatogram of a non-radioactive kidney sample used to establish a baseline UV trace for all other kidney samples (n=1 sample).

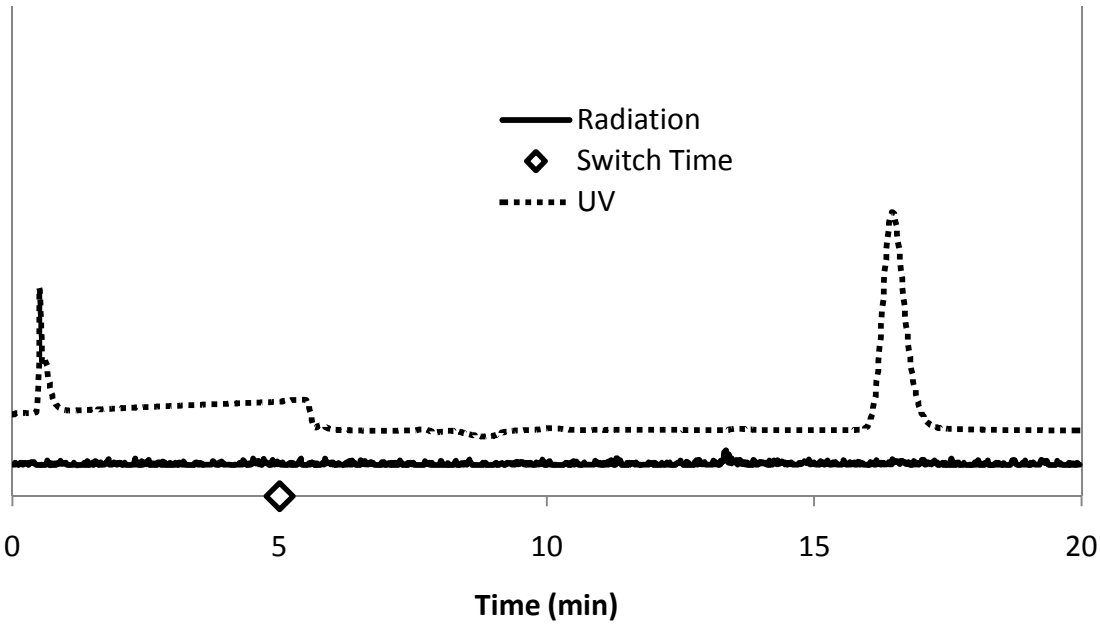

Figure 57 – Chromatogram authentic Methyl-EXP3174 standard injection onto the HPLC system used to determine the retention time of this compound (n=1 sample).

6 DISCUSSION

6.1 MICROPET IMAGING

6.1.1 CONTROL SCANS

MicroPET imaging studies reveal that [^{11}C]Methyl-Losartan is taken up in the kidneys and the liver. In the kidney, uptake is reversible as [^{11}C]Methyl-Losartan washes out over time and agrees with data available on Losartan binding suggesting it is a reversibly binding antagonist (Verheijen et al. 2004). The high intensity signal observed is consistent with the known distribution of AT_1 receptors in the kidney cortex and outer medulla (Allen et al. 2000). The tissue to blood contrast observed in the reconstructed images between 5 and 30 min post-injection indicates that signal in the kidney is not strictly due to blood flow and delivery of [^{11}C]Methyl-Losartan, but due to retention of the tracer in that organ. This contrast not only allows visualization of the renal cortex, it more importantly allows delineation of the organ for analysis and quantification purposes.

One limitation however in the delineation of the kidney is liver spillover. Spillover is a phenomenon that occurs in nuclear imaging, and in essence is due to the close proximity of high intensity signal in adjacent organs. This causes signal to "spill over" or blur into the delineated area and raise the apparent activity. For this reason, a specific standard operating procedure, outlined in section 8 (Appendix), was established to minimize spillover effect, and maintain consistency across the data.

In the liver, uptake is also observed, but its profile and kinetics differ greatly from what is observed in the kidney as accumulation and lack of washout are observed. Although AT_1 receptors are expressed in the liver (Murphy et al. 1991; Yu et al. 2010), it is highly likely that uptake is due to the clearance and elimination of [^{11}C]Methyl-Losartan from the blood via the hepatic metabolism machinery.

6.1.1.1 Lack of Uptake in the Heart

No uptake was observed in the heart with [^{11}C]Methyl-Losartan imaging on rats. It is important to note that in the rat heart, the AT_1 receptor density is very low and is approximately 30 to 400 fold lower than in the kidneys (Table 1) (Chang and Lotti 1991). This makes the heart an easily saturable system that can be largely affected by the injected dose of tracer. According to Hume, receptor occupancy must be below 5% to allow adequate quantification measurements (Hume et al. 1998). In practice, this places a constraint on the maximal amount of tracer dose that can be injected into the system. This is not to say that [^{11}C]Methyl-Losartan does not reach the myocardium and the AT_1 receptors in this tissue, however with the current injected doses of 0.6 to 47 μg/kg and specific activities of 100 to 2500 mCi/μmol, the activity concentration and count rate in the heart are too low to be detected. Alternatively, it could be theorized that by increasing the overall injected activity, myocardial uptake and detection might be possible. However two factors limit this option, the first being receptor occupancy as mentioned earlier and the second is the camera which becomes inefficient beyond a total activity of 2 mCi. It is expected therefore that with higher specific activity and lower dose injections, imaging of the AT_1 receptors in the heart may be possible with [^{11}C]Methyl-Losartan. We recently received a GE CPro module to produce ^{11}C-methane and ^{11}C-methyl-iodide in very high specific activity and will therefore be exploring this possibility in the future.

Thus far, only two groups have reported on myocardial imaging of the AT_1 receptor in the heart. Verjans and colleagues have shown that 3 weeks following MI, uptake of Tc-99m Losartan is observed in the infarct area whereas no uptake was observed in sham mice (Verjans et al. 2008). The Johns Hopkins group demonstrated that using [^{11}C]KR31173 PET imaging, uptake was observed in the infarct region of the myocardium at 1 to 3 weeks post-MI in rats (Fukushima et al. 2009; Higuchi et al. 2010). This same group also presented data on pigs which

somewhat confounded the results observed in small animals. In pigs, myocardial uptake and retention of [^{11}C]KR31173 was observed in all regions of the heart of normal animals. MI caused a decrease in signal intensity in the infarct area (Fukushima et al. 2010). These results would suggest that there is high inter-species variability in regards to either AT_1 receptor myocardial density, or tracer pharmacokinetic and binding properties.

6.1.1.2 Lack of Uptake in the Brain

The brain comprises one of the main tissues responsible for the regulation of blood pressure, sympathetic activity, drinking behavior, etc. via the RAS and thus is an important region of AT_1 receptor expression. Reports have demonstrated the presence of AT_1 receptors in the circumventricular organs (i.e. SFO, OVLT, ME, anterior pituitary, and area postrema of the hindbrain), median preoptic nucleus, PVN, AVPV, SCN, periventricular nuclei, and discrete regions of the lateral and dorsomedial hypothalamus of the brain, however no uptake was observed with [^{11}C]Methyl-Losartan. Losartan is not expected to cross the blood brain barrier to any great extent due to its hydrophilic nature. However, Zhang and colleagues have suggested that Losartan does cross the blood brain barrier and antagonize the AT_1 receptor centrally, though these experiments were performed at very high doses of drug (Zhang and Leenen 2001). One may hypothesize that by increasing the lipophilicity of Losartan (i.e. replacing the hydroxyl group by a methoxyl group as was done with [^{11}C]Methyl-Losartan), this will facilitate crossing the blood brain barrier and binding centrally to the AT_1 receptor. However, microPET imaging and biodistribution data suggests that this compound does not cross the blood brain barrier at current tracer doses of 0.6 to 47 μg/kg and specific activities of 100 to 2500 mCi/μmol.

To our knowledge, no studies have been published demonstrating uptake of AT_1 receptor radioligands in the brain.

6.1.2 TEST RE-TEST

Our test re-test studies indicate approximately 14% variability in the DV values obtained from repeated scans using different tracer formulations on the same rat. This is a very important consideration as it demonstrates good reliability of the results with [^{11}C]Methyl-Losartan microPET imaging. Experimentally, with disease models of altered AT_1 receptor expression, changes in receptor density should be accompanied with correlated changes in DV values. Using the left kidney DV values of all baseline scans (n=14), a power study was performed to estimate the sample size required to detect thresholds of changes based on the current observed variability in the data (Milton 1999). The results indicate that our current imaging and analysis protocol would allow the detection of a 15% change in DV values with a sample size of n=16, which is realistic and feasible. The detection of 10%, 20%, 30% and 40% changes in renal cortex AT_1 receptor expression would require sample sizes of n=30, n=10, n=6 and n<5, respectively. In clinical imaging of diseased patients, comparison to baseline scans is rarely available, and measurements are therefore compared to a mean of the population. Thus, it is preferable to have a population mean with as little variability as possible in order to detect changes.

6.1.3 INJECTED DOSE EFFECT

It has been established that DV values for the kidneys are not affected by injected activity or rat weight. Although a significant trend is observed with changing specific activity, injected mass and injected dose, this is driven by only a few data points (high specific activity, mass and dose) and is counter-intuitive to standard binding kinetics. With the available data, we do not consider these parameters to affect the DV values to any relevant extent and it is likely that due to the high density of AT_1 receptors in the kidneys, linear binding kinetics would be observed below 5% of maximal receptor occupancy. Moving forward, this removes

limitations in regards to these parameters for future studies involving renal imaging. As was mentioned previously, specific activity and injected dose are major considerations for cardiac imaging due to the very low AT_1 receptor density in the myocardium. However with the current data, no conclusions can be made about injected dose effects as no measurable uptake was observed with any of our scans.

6.1.4 BINDING SPECIFICITY

Using blocking doses of Losartan and Candesartan, a reduction in [^{11}C]Methyl-Losartan uptake in the kidneys was observed. Time activity plots suggest that activity in the kidney was similar to blood activity for the entire duration of the scan. This suggest that signal in the kidney is strictly due to blood flow and delivery of [^{11}C]Methyl-Losartan and not specific retention. This effect was observed similarly with Losartan and Candesartan suggesting that they are both capable of competing with [^{11}C]Methyl-Losartan for AT_1 receptor binding sites in the kidney. The DV values reported for the left and right kidney, for both blocking drugs, had a value of approximately 1 ml/g. In theory, a Logan DV value of 1 ml/g would mean that there is no contrast between the region of interest (ROI) and the blood. Generating a DV for blood, in the same manner as the kidneys, results in a DV value of 1 ml/g exactly. This further confirms that saturating doses of Losartan and Candesartan are able to effectively block tracer retention in the kidneys, and demonstrates that [^{11}C]Methyl-Losartan binds specifically to the AT_1 receptor *in vivo*.

In the liver, displaceable retention is observed only with Losartan and not with Candesartan. No absolute quantification measurements were calculated for the liver as the tracer kinetics do not follow any established model. Losartan co-injection likely causes partial washout of tracer from the liver due to the similarity in structure, whereas Candesartan was unable to cause blocking due to the dissimilarity in structure. This strongly suggests that the

effect is not due to AT_1 receptor binding, but to displacement from saturable non-specific binding sites and common metabolic pathways. However, this hypothesis remains to be tested and confirmed.

6.1.5 DISPLACEMENT STUDIES

Displacement studies with Losartan injections mid-scan (10 min and 17 min post-tracer injection) served as a qualitative assessment of binding specificity *in vivo*. These studies confirm that [^{11}C]Methyl-Losartan binds specifically to AT_1 receptors in the kidneys *in vivo*, and that binding is reversible. It is also interesting to note that a rise in blood activity was observed following Losartan bolus injection. Although the exact cause of this phenomenon is unknown, it is likely due to the displacement of tracer from the tissue compartments of the liver and kidneys to the blood compartment. Finally, displacement in the liver is observed, and as mentioned, is likely due to displacement from saturable non-specific binding sites and the common metabolic pathways of Losartan and [^{11}C]Methyl-Losartan.

6.1.6 INTRA-USER AND INTER-USER VARIABILITY

Results from the intra-user study suggest that data analysis techniques based on the developed standard operating procedure are very repeatable. With variability of less that 3% in the calculated DVs, this suggests high fidelity in ROI drawing. The inter-user study suggests that there is a very small yet significant difference between the analyses of both users. User #2 had a tendency to consistently under-estimate the DV, despite the fact that the data was well grouped around the mean DV. This can easily be corrected by following the analysis protocol outlined in section 8 (Appendix) more strictly. Despite this finding, it is suggested that the developed standard operating procedure be implemented as a tool for future studies in our center involving AT_1 receptor radioligands such as [^{11}C]Methyl-Losartan, [^{11}C]Methyl-EXP3174 , [^{11}C]Methyl-Candesartan and [^{11}C]TH4.

6.1.7 BLOOD AND PLASMA SAMPLING

To correct for the tracer concentration in plasma relative to whole blood, plasma sampling was performed over a 60 min time frame. This is necessary as the Logan DV model requires the plasma to serve as an input function instead of the blood, and this information is impossible to obtain from image analysis. The results from this study suggest a downward logarithmic function in the plasma to whole blood ratio of tracer concentration likely due to tracer extraction from the plasma into either tissue compartments or red blood cells, although this latter option is unlikely. As well, very high plasma protein binding is observed, above 70% until 60 min. This is to be expected as studies on Losartan suggest very high plasma protein binding upwards of 95% (Csajka et al. 1997).

For the purpose of this thesis, the plasma input function was not fitted to the data and Logan DV values should therefore be considered uncorrected. In practice, the analysis software considers the plasma input function to be equal (factor of 1) to the whole blood input function and is therefore able to calculate DV values. In theory, applying the plasma input function to the calculations should increase the DV values. For example, if we apply this function with a plasma factor of 0.8, this would indicate that only 80% of the signal is in the plasma (a factor of 1 indicates that all activity is in the plasma). Considering that the DV can be a ratio of activity in tissue over plasma at equilibrium, by decreasing the amount of available tracer for uptake, this increases the tissue to plasma ratio of activity, and consequently increases the DV value. Despite the limitation in the current dataset, applying the plasma input function correction will change all data points by the same factor and should therefore not change the interpretation of the results or any significant changes observed. Applying the plasma input function correction is beyond the scope of this thesis, and will be explored in the future.

6.1.8 [^{11}C]METHYL-EXP3174

EXP-3174 is a major downstream metabolite in Losartan and many of the effects of this drug are attributed to its conversion to EXP-3174, which has 10 times the affinity for the AT_1 receptor (Krovat and Langer 2003). By developing and utilizing a radiotracer based on a compound that is downstream in the metabolic cascade, it is likely that there will be fewer metabolites and therefore simpler kinetics. This alternative has yet to be explored in great depth. Preliminary results from [^{11}C]Methyl-EXP3174 microPET imaging studies suggest that this tracer follows similar kinetics to [^{11}C]Methyl-Losartan in rats. Understanding the kinetics of tracers and their labeled metabolites is an important step in generating the appropriate kinetic models for quantification in PET imaging. [^{11}C]Methyl-EXP3174 was hypothesized to be a likely labeled metabolite of [^{11}C]Methyl-Losartan, however metabolism studies have proven otherwise. [^{11}C]Methyl-EXP3174 may still be a promising agent for AT_1 receptor PET imaging studies and this compound will be studied in the future.

6.2 BIODISTRIBUTION

6.2.1 CONTROL

Biodistribution results indicate high signal concentration in the liver, kidney cortex and outer medulla, as is observed in microPET studies.

6.2.1.1 Lack of Uptake in Adrenal Glands

Our studies have not been able to demonstrate uptake of [^{11}C]Methyl-Losartan in the adrenal glands which is reported to have a high density of AT_1 receptors. In fact, Chang and colleagues have reported a higher AT_1 receptor density in the adrenal cortex when compared to the kidney cortex (Chang and Lotti 1991). Autoradiography studies performed on the adrenal gland using [^{125}I]Sar^{1},Ile^{8}-Ang II demonstrated that the majority of AT_1 receptors in the adrenal

gland are located in the small surface region of the cortex called the zona glomerulosa (Allen et al. 1999). This sub-section of the cortex represents approximately 5 to 10 % of the adrenal mass. In the biodistribution experiments described previously, the entire adrenal gland is excised, counted and weighed as a whole, whereas the kidneys are dissected into distinct layers. The radioactivity counts are then normalized the sample weight, and consequently uptake that occurs in the zona glomerulosa will be small relative to the entire organ. The %ID/g ratio to blood may not therefore reflect the true uptake of [^{11}C]Methyl-Losartan in the zona glomerulosa of the adrenal cortex. Thus, based this data, binding of [^{11}C]Methyl-Losartan to AT_1 receptors in the adrenal cortex cannot be excluded as a possibility.

This phenomenon was not discussed in the microPET imaging section because for imaging purposes, adrenal uptake was not measurable because the adrenal glands sit between the kidneys and liver. Due to the high activity concentration in the liver, spillover is a major factor affecting all adjacent tissues in imaging studies. For this reason, if uptake and high tracer concentration were present in the adrenal glands, their structure would be indistinguishable from that of the liver or kidneys. However, biodistribution studies are still necessary to measure true tissue uptake, despite their applicability to microPET quantification. As well, tissue dissection methods are much more accurate than microPET imaging in discerning uptake in nearby structures at a particular time point post-tracer injection.

In regards to other radioligands, Gibson and colleagues reported the uptake [^{125}I]Sar^{1},Ile^{8}-Ang II in rat adrenal glands using biodistribution studies, but suggested that this uptake was not specific to the AT_1 receptor (Gibson et al. 1994). As well, The Johns Hopkins group have reported uptake of [^{11}C]L-159,884 in the adrenal glands of dogs but not with any other species studied, including mice, rats, pigs or monkeys (Owonikoko et al. 2004). The same group also reported uptake of [^{11}C]KR31173 in mice adrenal glands which was displaceable by

specific AT_1 receptor antagonists (Mathews et al. 2004; Zober et al. 2006). Therefore it is likely that there are inter-tracer and inter-species differences and that our model may not be ideal for AT_1 receptor imaging in the adrenal gland.

6.2.2 COMPETITION

The *ex vivo* biodistribution data demonstrates that [^{11}C]Methyl-Losartan binds specifically to the AT_1 receptor as is evident by the 70% to 90% significant reductions in %ID/g ratio to blood in the kidney cortex and outer medulla with Losartan and Candesartan. In the liver, similarly to the microPET imaging results, Losartan and not Candesartan is able to block retention of [^{11}C]Methyl-Losartan at 10 min post-injection. As was mentioned previously, this is likely due to the similarity in structures and binding to saturable non-specific binding sites (see section 6.1.4 (Binding Specificity)).

The very low uptake in the brain regions in all studies is likely due to lack of blood-brain-barrier permeability. However, an interesting phenomenon occurs in the brain where blocking with Losartan significantly increases tracer uptake. This change is likely irrelevant as the control ratio to blood values for all brain regions are much less than 1 (a ratio to blood of 1 indicates identical concentrations in the tissue compared to blood) and therefore have a lower activity concentration than the circulating blood. As well, the variability in this group of data is very small, and might be subjected to Type I errors. A third possibility might be that due to the large reduction of tracer accumulation in the liver, the circulating levels of [^{11}C]Methyl-Losartan, and its metabolites are increased. These elevated levels of circulating tracer or its metabolites are therefore able to cross the blood brain barrier and accumulate in the brain causing an increase in retention.

Competition with saturating doses of all other drugs, i.e. PD-123,319 (AT_2 receptor antagonist), A-779 (Mas receptor antagonist) and Propranolol (β-adrenergic receptor

antagonist), show no significant decrease of [^{11}C]Methyl-Losartan retention in any of the tissues evaluated. Despite the low power of this study, the results indicate that [^{11}C]Methyl-Losartan binds selectively to the AT_1 receptor over the AT_2 receptor, Mas receptor and β-adrenergic receptor.

6.2.3 STATISTICAL TEST

For this study, an ANOVA was used to compare the means of multiple study groups to each other. At a fundamental level, one may consider the ANOVA to be similar to the generalized two sample t-test, except that it can handle more than 2 groups (Pagano and Gauvreau 2000). The first purpose of an ANOVA is to determine whether the means of the study groups are equal. If a difference is shown, in other words, if not all study group means are equal, a pairwise comparison between all groups can be performed to determine which means are significantly different from each other. This pairwise comparison is then Bonferroni corrected, to ensure that the overall probability of committing a Type I error (α error, false positive) when comparing the different groups is adequately controlled.

In our studies, we observed very high variability in the group of rats treated with Propranolol. Inclusion of this group in the general analysis would therefore increase the overall variability of the analysis, and subsequently increase the probability of Type II errors (Beta error, false negative) by reducing the power to detect differences between the other groups. Secondly, when evaluating the data, it is interesting to note that the mean uptake values with for the Propranolol group are higher than those of the control group when looking at the kidney cortex and outer medulla. Propranolol is suggested to increase peripheral vascular resistance and reduce cardiac output (Bakris 2009). However the mechanisms by which this affects [^{11}C]Methyl-Losartan uptake and/or washout are not established. It is possible that these, and other, pharmacodynamic effects are in part responsible for the increased uptake observed in

the kidneys. Finally, all the drugs used for specificity and selectivity testing were targeted at components of the RAS, with the exception of Propranolol. Losartan and Candesartan target the AT_1 receptor: main receptor responsible for the effects of the RAS (de Gasparo et al. 2000). PD-123,319 targets the AT_2 receptor, which also binds to Ang II and shares approximately 32% amino-acid sequence identity with a higher degree of similarity in the transmembrane region, making it the more likely target for non-specific binding (de Gasparo et al. 2000). A-779 is a blocker of the Mas receptor which binds to the degradation product of Ang II: Ang 1-7 (Bayorh et al. 2002). Propranolol was initially included in our studies because it targeted the unrelated g-protein coupled β-adrenergic receptors which are highly expressed in the myocardial tissue (Rockman et al. 2002), however no [^{11}C]Methyl-Losartan uptake was observed in the heart. Thus, for these reasons, the data from Propranolol group was excluded from the statistical tests used in the biodistribution study.

6.2.4 INJECTED DOSE EFFECT

When plotting the ratio to blood for the kidney cortex and outer medulla against all injected activities, masses and doses, no significant trends were observed. This confirms what was observed in the microPET imaging studies; suggesting that tracer uptake in the kidneys is not affected by overall tracer dose. This is likely due to high density of AT_1 receptors in the kidney and high saturation concentration in this organ.

6.3 AUTORADIOGRAPHY

In vitro autoradiography studies confirm the *in vivo* microPET imaging and *ex vivo* biodistribution specificity and selectivity results. The advantage of autoradiography studies is that the rat systemic factors can be bypassed and results are indicative of direct exposure of the tracer to the receptors. Therefore any pharmacokinetic or pharmacodynamic effects can be

ignored in this study. Using kidney sections, significant blocking was observed with only the specific AT_1 receptor antagonists Losartan and Candesartan. PD-123,319, A-779 and Propranolol had no effect on [^{11}C]Methyl-Losartan binding. This suggests further that [^{11}C]Methyl-Losartan binds specifically and selectively to the AT_1 receptor over the AT_2, Mas, and β-adrenergic receptors.

6.4 METABOLITE ANALYSIS

Metabolite analyses revealed the presence of 1 (or more) hydrophilic labeled metabolite(s) (peak 1, leach-though) in the plasma. In the kidney, the presence of 1 (or more) hydrophilic labeled metabolite(s) (peak 1, leach-though) and 1 hydrophobic labeled metabolite (peak 2) at 10 min post-injection have been identified. The absence of peak 2 in the plasma is interesting to note. This would suggest that this metabolite is either synthesized in the kidney, or synthesized elsewhere (i.e. in the liver) and transported to the kidney via the blood. This latter option would require that the metabolite be present in very low concentrations at any given point in the plasma and that it accumulates in the kidney over time.

The observations at 45 min show that the leach-through (peak 1) proportion increases while [^{11}C]Methyl-Losartan (peak 4) decreases over time in both plasma and kidney samples. This suggests that the hydrophilic metabolite(s) is(are) formed over time while the concentration of parent compound decreases. In the kidney, the reduction of the [^{11}C]Methyl-Losartan peak, and the increase of the hydrophobic metabolite (peak 2) also suggest a shift towards metabolites over time. If this metabolic transformation of [^{11}C]Methyl-Losartan into radiolabeled metabolites (peak 1 and peak 2) follows standard Michaelis-Menten kinetics over time ($v_0 = v_{max}[S]/K_M + [S]$, where v_0=current reaction rate, v_{max}=maximum reaction rate, $[S]$=substrate concentration, and K_M=inverse of enzyme affinity), a theoretical relationship between the tracer and its metabolites can be proposed as depicted in Figure 58.

There were no significant changes with Losartan blocking in the kidney samples and with Candesartan blocking in kidney and plasma samples. However, blocking with Losartan showed the significant appearance of 2 minor metabolites (peaks 2 and 3) in the plasma samples at 10 min. When considering the Losartan blocking data from the biodistribution and microPET studies, it is likely that these metabolites are displaced from the liver due to the high Losartan concentration. This would also suggest that these metabolites share common structure or metabolic pathways with Losartan in order to be displaced by this drug.

Studies have shown that Losartan is eliminated via hepatic pathways by cytochromes (Diez 2006), and given the similarity in structures between Losartan and Methyl-Losartan, it is possible that they would have similar pharmacokinetic profiles in the system. In contrary to hepatic excretion, radiotracers that are subject to renal elimination would be excreted from the blood in the glomerular capsule and would follow the nephron into the collecting ducts to be excreted in the urine. If that were the case, imaging studies would reveal activity in the kidney cortex, followed by the outer medulla, inner medulla, renal pelvis, ureters and bladder, respectively in that order. Initial imaging studies with [^{11}C]Methyl-Losartan were completed to 90 min, and in these scans, no activity was detected in the renal inner medulla or the bladder. Therefore we can conclude that [^{11}C]Methyl-Losartan is eliminated from the system via hepatic metabolism and not by the kidneys.

According to Stearns and colleagues, Losartan is transformed into seven different metabolites, and the relative abundance of these compounds differs between humans and rats. Rats primarily transform Losartan into EXP-3174 which was shown to exhibit 10 times the affinity of Losartan for the AT_1 receptor (Krovat and Langer 2003; Stearns et al. 1992). We originally hypothesized that the identity of peak 2 might be [^{11}C]Methyl-EXP3174. However, based on retention time of authentic methyl-EXP3174, this option was eliminated. The exact

identification of [^{11}C]Methyl-Losartan metabolites is not our primary objective and attempting to do so may prove very difficult. Additionally, with future work aimed at larger animals and humans, it is very likely that the metabolic profile could change. Therefore, for the purpose of this thesis, identification of tissue metabolites was not pursued further.

Another aspect to consider is despite the presence of metabolites in the plasma and kidney, microPET analysis reveals that tracer kinetics follow very closely the Logan DV model for reversibly binding radiotracers. The correlation coefficients when fitting the data to the Logan slope were above 0.98 for all scans. Additionally, blocking the AT_1 receptors with Losartan and Candesartan significantly, and almost completely, blocks [^{11}C]Methyl-Losartan uptake in the kidney. This suggests that these metabolites behave similarly to [^{11}C]Methyl-Losartan in regards to AT_1 receptor binding and minimally contribute to any non-specific binding. If we associate similar kinetic properties to [^{11}C]Methyl-Losartan and its metabolites, and fit the proposed metabolism model (Figure 58) to the time activity curves obtained in microPET imaging studies, this results in a theoretical time activity curve of [^{11}C]Methyl-Losartan and its metabolites in the kidney. The renal time activity curves obtained experimentally for the kidney would be broken down into two separate time activity curves (one for [^{11}C]Methyl-Losartan and one for its metabolites), which when summed together, result in the overall activity (Figure 59).

6.5 FIGURES

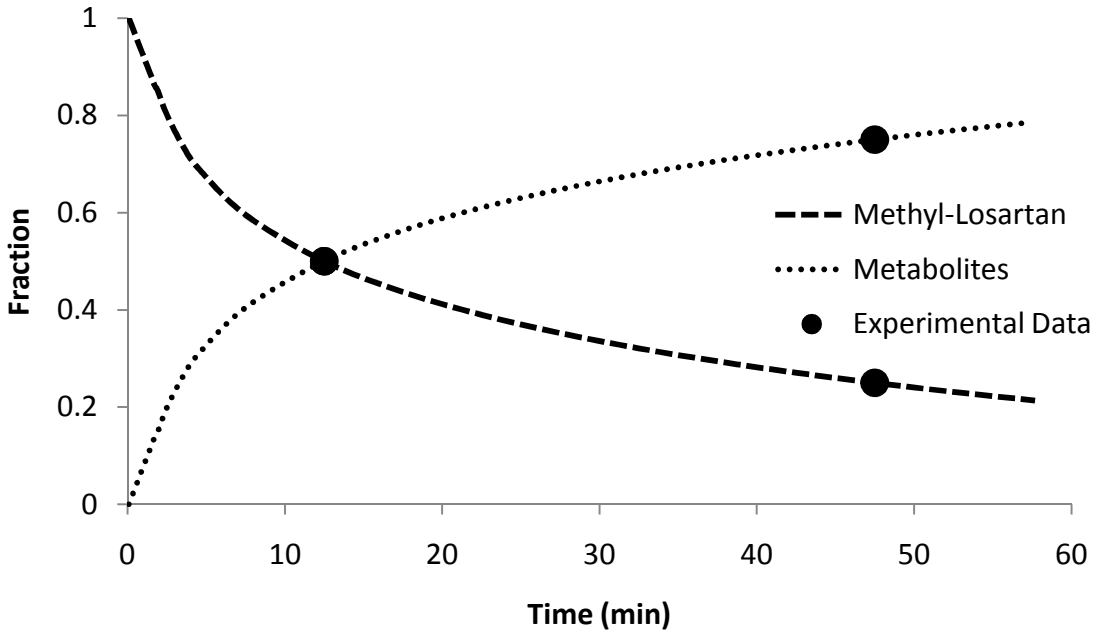

Figure 58 – Theoretical proposed change in relative proportion of [^{11}C]Methyl-Losartan in regards to its metabolites over time based on the currently available data.

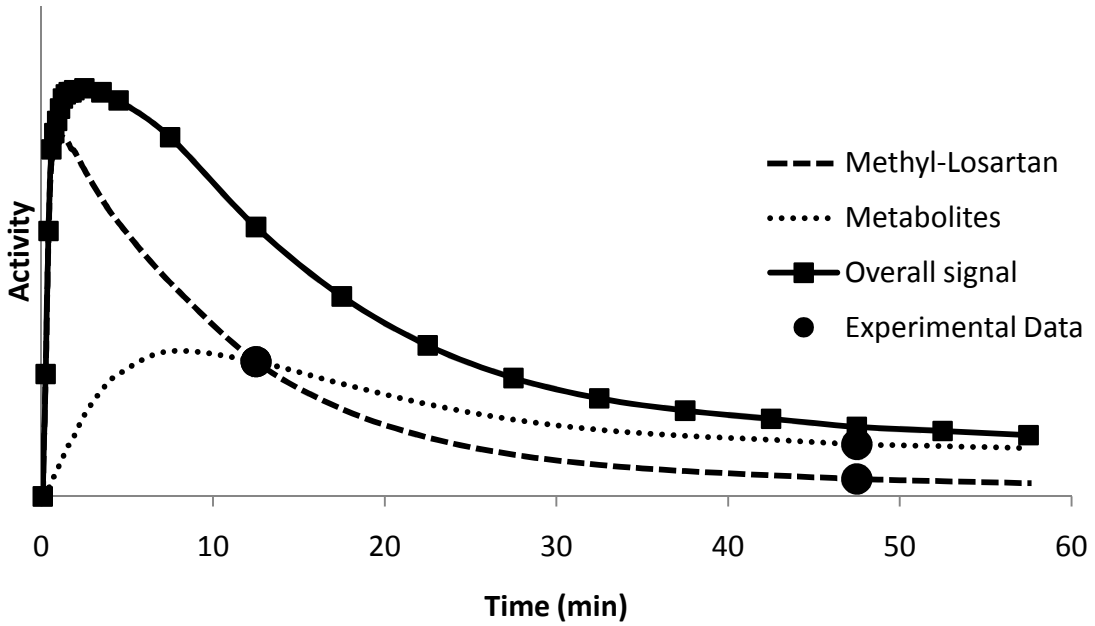

Figure 59 – Theoretical time activity curve of [^{11}C]Methyl-Losartan, its metabolites and the overall signal observed in microPET studies for the kidney. The experiment data is representative of the results obtained in metabolite analysis studies.

7 CONCLUSION

7.1 MAIN FINDINGS

In vivo microPET imaging reveals high uptake, good contrast and specific binding to AT_1 receptors in the rat kidney cortex. Repeated imaging studies show that our results are highly reliable, and that our image analysis techniques can be used to measure the tracer DV in the kidneys with high repeatability. Biodistribution studies confirm that uptake is similar to microPET values and that significant blocking is observed with Losartan and Candesartan, but not with any other drug treatment. Autoradiography studies show that [^{11}C]Methyl-Losartan binds to the renal cortex of the kidneys, localizing well with known AT_1R densities and blocking with Losartan and Candesartan significantly reduces this uptake. No blocking was observed with any other drug incubation. Collectively these results suggest that [^{11}C]Methyl-Losartan binds specifically to the renal AT_1 receptors, and that it is selective over the AT_2, Mas and β-adrenergic receptor. Metabolism studies reveal the presence of labeled hydrophilic metabolite(s) in the plasma and kidney and a hydrophobic metabolite in the kidney. Blocking with Losartan or Candesartan does not affect metabolite to tracer ratios, suggesting that these metabolites behave similarly to [^{11}C]Methyl-Losartan in regards to AT_1 receptor binding.

7.2 IMPACT AND FUTURE DIRECTIONS

Imaging the AT_1 receptor *in vivo* is an important development in the understanding of its role in normal physiology and many pathological conditions with altered AT_1 receptor expression, such as MI or diabetes. The advantage of using non-invasive nuclear imaging techniques such as PET is that they do not affect the system studied. Experimentally, this allows serial evaluation on animals to study the progression of disease without the need to sacrifice at every time point. This also allows the technology to be easily translated to clinical care.

Several groups are currently working to elucidate the changes occurring with the AT_1 receptor in a variety of diseases. However, only a handful of centers have attempted using nuclear imaging to study the AT_1 receptor *in vivo*. It is important to note that in general, access to radioisotopes and imaging equipment for experimental purposes is limited and expensive, and this applies to both PET and SPECT technologies. Thus far, only reports on animal imaging have been published, but clinical imaging is the ultimate purpose of our and other's work.

In the future, our goals will be to develop small animal models of disease to assess the abilities of [^{11}C]Methyl-Losartan to detect AT_1 receptor density changes *in vivo*. Current work is underway to evaluate the changes in AT_1 receptors in MI and 5/6 nephrectomy models, and the ability of [^{11}C]Methyl-Candesartan to detect these changes. Similar work is foreseen with [^{11}C]Methyl-Losartan and [^{11}C]Methyl-EXP3174 . Furthermore, eventually moving to larger animal models will allow for a closer representation of human disease and imaging. However, things such as camera efficiency, injected dose and blood input function need to be considered before advancing into humans. As well, extensive dosimetry studies will have to be performed before [^{11}C]Methyl-Losartan becomes a clinically viable tool. Despite these challenges, it is important to recognize that these characterization steps are necessary in order to develop useful radiotracers for clinical use in humans.

Ultimately, our aim is to develop a useful tool that allows non-invasive imaging of the AT_1 receptor in patients with disease. The goal is to establish [^{11}C]Methyl-Losartan as a clinically reliable tool in renal AT_1 receptor imaging. With that information, researchers will not only get a better understanding of disease, but may use that information to guide therapy and better patient outcome.

8 APPENDIX

DRAWING REGIONS OF INTEREST FOR [^{11}C]METHYL-LOSARTAN, [^{11}C]METHYL-EXP3174, [^{11}C]METHYL-CANDESARTAN AND [^{11}C]TH4 – STANDARD OPERATING PROCEDURE

Rawad E. Antoun, Kumiko C. Mackasey, Jennifer M. Renaud

Latest revision: August 25, 2010

Background

Animal Model

Normal male Sprague-Dawley rats weighing 200-500 g were used in all scans. Rats were injected with [^{11}C]Methyl-Losartan, intra-venously via the tail vein. To evaluate specificity of tracer, some rats were co-injected with blocking doses of selective AT_1 receptor antagonists Losartan (20 mg/kg, i.v.) or Candesartan (5 mg/kg, i.v.). These latter scans also serve as examples of situations where low renal uptake is observed.

Scanning

All animals were scanned using the Siemens Inveon Small Animal PET Scanner, which has as 12.7 cm axial FOV and a spatial resolution of ≤1.4 mm. Rats were anesthetized with 2% isoflurane for the entire duration of the scan, placed in the supine position, and camera was centered at the liver to include the heart and kidneys in the FOV.

Reconstruction

All data was collected and reconstructed using Siemens Inveon Acquisition Workplace software. Unless otherwise specified, for 60 min scans, data was reconstructed into a dynamic histogram with the following frame composition: 12 X 10 sec (frames 1-12), 3 X 60 sec (frames 13-15), 11 X 300 sec (frames 16-26). A 10 min transmission scan (Co-67) was always performed

either preceding or following the scan and used to apply attenuation correction and scatter correction.

Analysis Software

Siemens Inveon Research Workplace software was used to analyze all scans, i.e. drawings regions of interest (ROIs), obtaining time activity curves (TACs), and calculating Logan distribution volume (DV) values.

Aim

This standard operating protocol has been developed to establish a robust and repeatable method to draw renal ROIs independently of AT_1 receptor levels and tracer uptake in the kidneys.

Methods

Step 1 – Creating kidney ROIs

A. Under the color scale menu, select “20 step” color scale.
B. Sort through the frames and select frame 16 (5-10 min) as this is where the smoothest images and best tissue to background contrast are observed.
C. In the axial view, sort through the various slices of the image, and select one that is approximately in the mid-section of the left kidney. Use the axial and coronal views, along with crosshair to approximate the correct center.
D. Set the upper threshold of the color scale so that the highest intensity voxel in the kidney cortex be white (i.e. move the upper threshold down until you see a single white voxel, or as little white voxels as possible).
E. Set the lower threshold of the color scale so that the lowest intensity voxel in the kidney inner medulla be black (i.e. move the lower threshold up until you see a single black voxel, or as little black voxels as possible).

F. Under the “Create” tab, select the cube, and draw an ROI that will encompass the lower portion of the kidney. For the left kidney, limit the size of the box to the lower 2/3rd of the kidney, and for the right kidney, limit the box to the lower 3rd of the kidney to reduce any spillover effect from the liver.

G. Under the color scale menu, select “10 step” color scale.

H. Under the “Create” tab, select the thresholding option, and under “Container” select the previously created ROI.

I. Set the upper threshold so that all the high intensity voxels be included in the ROI (i.e. 100% of maximal intensity). While looking at the ROI on the image, set the lower threshold to stop at the interface between green and blue (i.e. stopping at 50% of maximal intensity). The lower threshold will be the main factor determining final shape and thickness of the ROI. The final kidney ROI should be 5-10 voxels thick and be continuous throughout the cortex.

J. Click “Create” to create the ROI.

K. Look through all the slices of your ROI. If necessary, edit your kidney ROI by erasing any areas that are too close to the liver that might be affected by spillover. To do this, under the “Edit” tab, select the eraser, and Right Kidney as your ROI.

Note 1: It is easier to create the ROI for the left kidney first as is it further from the liver and better defined in the image. When drawing the ROI for the right kidney, do not change the threshold limits set for the left kidney (step 1I). Both kidneys should be similar; therefore the ROIs should represent the same regions in both. The same applies if the right kidney ROI was done first.

Note 2: In certain cases, the bottom of the left kidney is cut off in the image. This is due to positioning the animal too low in the FOV. In this case, limit the lower edge of the cube (step 1F) to exclude to two bottom slices from the edge of the FOV.

Step 2 – Creating left atrial (LA) cavity ROI

A. Under the color scale menu, select "20 step" color scale.
B. Sort through frames 1 to 4 (0-10, 10-20, 20-30, 30-40 seconds respectively) and select the frame where the highest intensity in the heart cavity is observed.
C. In the axial view, sort through the various slices of the image, and select one that is approximately in the middle of the LA cavity. Use the axial and coronal views, along with crosshair to approximate the correct center.
D. Set the upper threshold of the color scale so that the highest intensity voxel in the LA cavity be white (i.e. move the upper threshold down until you see a single white voxel, or as little white voxels as possible).
E. Set the lower threshold of the color scale to 0% of maximal intensity.
F. Under the "Create" tab, select the sphere, and draw an ROI that will encompass the entire region of the LA.
G. Under the color scale menu, select "10 step" color scale.
H. Under the "Create" tab, select the thresholding option, and under "Container" select the previously created ROI.
I. Set the upper threshold so that all the high intensity voxels be included in the ROI (i.e. 100% of maximal intensity). While looking at the ROI on the image, set the lower threshold to stop at the interface between red and orange (i.e. stopping at 80% of maximal intensity). The lower threshold tab will be the main factor determining final

shape of the ROI. The final LA ROI should be fairly small and should represent the highest intensity voxels in that region.

J. Click “Create” to create the ROI.

K. Look through all the slices of your ROI. If necessary, edit your LA cavity ROI so that you are confident that it is entirely contained within the LA cavity space. Edit your LA ROI by erasing any areas that should not be included as part of the LA cavity. This includes any hot spots that might come from any of the other three heart chambers or the main arteries and veins feeding to the heart.

Step 3 – Creating background ROI

A. Use the same color scale, frame and section used for the LA cavity (step 2).

B. Under the create tab, select the “Paintbrush” option, and select “Sphere” and “20 pixels” for shape and size respectively.

C. Select an area to the side of the animal away from the body (be careful for the arms) and create ROI.

Step 4 – Creating liver ROI

A. Use the same color scale, frame and section used for the kidneys (step 1).

B. Under the “Create” tab, select the “Paintbrush” option, and select “Sphere” and “20 pixels” for shape and size respectively.

C. Select an area towards the anterior face of the liver, away from any darker spots and create ROI.

D. Under the edit tab, select the “Paintbrush” option, and select “Sphere” and “20 pixels” for shape and size respectively, and the liver as your ROI.

E. Edit your liver ROI by creating two extra areas (towards the posterior) in the right and left lobes of the liver. The final ROI should include three unconnected spots that represent the overall liver distribution.

Note: Tracer and signal distribution should be uniform throughout the liver. With the exception of the interlobular space occupied by the various circulatory systems, selecting any area should yield similar results.

Step 5 – Saving ROIs

A. Under the "Save" tab, you can save your created ROIs for future use and analysis.

B. Be sure to fill in the description in the save process as this will be your only way to differentiate between the various sets of ROIs from different scans.

Step 6 – Obtaining TACs

A. Select "Kinetic Analysis" and highlight your five ROIs.

B. Select the "Save" tab and save your TACs as CSV files (to note, this will only save the highlighted ROIs).

Step 7 – Generating Logan DV values

A. Select "Kinetic Analysis" and highlight the two kidney ROIs.

B. Select the "Model" tab under which you can select the "Logan" model and the LA cavity as the whole blood curve.

C. Click on the "Advanced" button, set start time to 20 min frame 19 (20-25 min) and end time to 55 min frame 26 (55-60 min).

D. Click "Apply" and "OK".

E. Click "Fit" to obtain the Logan plot for the kidneys and to generate the DV values.

F. Select the kidney of interest and click on "Output".

G. An information box will appear. "VD (ml/g)" is the DV value in question.

H. To save the DV values, click on “Save All Outputs”.

Low Renal Uptake Scans

When very low uptake in the kidney is observed (i.e. scan with blocking doses of Losartan), it is very difficult to draw an ROI as per the detailed instructions above. In this scenario, a baseline control scan should be performed 1-2 weeks beforehand and analyzed as described above.

A. Using the import ROI function, import the renal ROIs from the baseline scan into the current image.
B. As the kidneys will not be visible in later time frames (i.e. frame 16, 5-10 min), use the early frames when the kidney is delineated by early blood flow (i.e. frames 1 to 12, 0-120 sec) as a reference.
C. Use the positioning tools to reposition and rotate these ROIs so that they match with current position of the kidneys.
D. As blocking does not affect background counts, blood activity, or early hepatic uptake, proceed as described above to draw the background, LA cavity and liver ROIs.

9 REFERENCES

Allen AM, Yamada H, and Mendelsohn FA. 1990. In vitro autoradiographic localization of binding to angiotensin receptors in the rat heart. Int J Cardiol 28(1):25-33.

Allen AM, Zhuo J, and Mendelsohn FA. 1999. Localization of angiotensin AT1 and AT2 receptors. J Am Soc Nephrol 10 Suppl 11:S23-29.

Allen AM, Zhuo J, and Mendelsohn FA. 2000. Localization and function of angiotensin AT1 receptors. Am J Hypertens 13(1 Pt 2):31S-38S.

Asano K, Dutcher DL, Port JD, Minobe WA, Tremmel KD, Roden RL, Bohlmeyer TJ, Bush EW, Jenkin MJ, Abraham WT et al. . 1997. Selective downregulation of the angiotensin II AT1-receptor subtype in failing human ventricular myocardium. Circulation 95(5):1193-1200.

Baker KM, Chernin MI, Schreiber T, Sanghi S, Haiderzaidi S, Booz GW, Dostal DE, and Kumar R. 2004. Evidence of a novel intracrine mechanism in angiotensin II-induced cardiac hypertrophy. Regul Pept 120(1-3):5-13.

Bakris G. 2009. An in-depth analysis of vasodilation in the management of hypertension: focus on adrenergic blockade. J Cardiovasc Pharmacol 53(5):379-387.

Bayorh MA, Eatman D, Walton M, Socci RR, Thierry-Palmer M, and Emmett N. 2002. 1A-779 attenuates angiotensin-(1-7) depressor response in salt-induced hypertensive rats. Peptides 23(1):57-64.

Bergsma DJ, Ellis C, Kumar C, Nuthulaganti P, Kersten H, Elshourbagy N, Griffin E, Stadel JM, and Aiyar N. 1992. Cloning and characterization of a human angiotensin II type 1 receptor. Biochem Biophys Res Commun 183(3):989-995.

Birkenhager WH, and de Leeuw PW. 1999. Non-peptide angiotensin type 1 receptor antagonists in the treatment of hypertension. J Hypertens 17(7):873-881.

Bland JM, and Altman DG. 1986. Statistical methods for assessing agreement between two methods of clinical measurement. Lancet 1(8476):307-310.

Bonnardeaux A, Davies E, Jeunemaitre X, Fery I, Charru A, Clauser E, Tiret L, Cambien F, Corvol P, and Soubrier F. 1994. Angiotensin II type 1 receptor gene polymorphisms in human essential hypertension. Hypertension 24(1):63-69.

Brenner BM, Cooper ME, de Zeeuw D, Keane WF, Mitch WE, Parving HH, Remuzzi G, Snapinn SM, Zhang Z, and Shahinfar S. 2001. Effects of losartan on renal and cardiovascular

outcomes in patients with type 2 diabetes and nephropathy. N Engl J Med 345(12):861-869.

Brown L, Wall D, Marchant C, and Sernia C. 1997. Tissue-specific changes in angiotensin II receptors in streptozotocin-diabetic rats. J Endocrinol 154(2):355-362.

Cappelli A, Nannicini C, Gallelli A, Giuliani G, Valenti S, Mohr GP, Anzini M, Mennuni L, Ferrari F, Caselli G et al. . 2008. Design, synthesis, and biological evaluation of AT1 angiotensin II receptor antagonists based on the pyrazolo[3,4-b]pyridine and related heteroaromatic bicyclic systems. J Med Chem 51(7):2137-2146.

Carini DJ, Duncia JV, Aldrich PE, Chiu AT, Johnson AL, Pierce ME, Price WA, Santella JB, 3rd, Wells GJ, Wexler RR et al. . 1991. Nonpeptide angiotensin II receptor antagonists: the discovery of a series of N-(biphenylylmethyl)imidazoles as potent, orally active antihypertensives. J Med Chem 34(8):2525-2547.

Carretero OA, and Oparil S. 2000. Essential hypertension. Part I: definition and etiology. Circulation 101(3):329-335.

Chang RS, and Lotti VJ. 1991. Angiotensin receptor subtypes in rat, rabbit and monkey tissues: relative distribution and species dependency. Life Sci 49(20):1485-1490.

Cohn JN. 2000. Rationale for angiotensin II receptor blocker therapy in chronic heart failure. J Renin Angiotensin Aldosterone Syst 1(2 Suppl):S38-40.

Csajka C, Buclin T, Brunner HR, and Biollaz J. 1997. Pharmacokinetic-pharmacodynamic profile of angiotensin II receptor antagonists. Clin Pharmacokinet 32(1):1-29.

Curnow KM, Pascoe L, and White PC. 1992. Genetic analysis of the human type-1 angiotensin II receptor. Mol Endocrinol 6(7):1113-1118.

Dahlof B, Devereux RB, Kjeldsen SE, Julius S, Beevers G, de Faire U, Fyhrquist F, Ibsen H, Kristiansson K, Lederballe-Pedersen O et al. . 2002. Cardiovascular morbidity and mortality in the Losartan Intervention For Endpoint reduction in hypertension study (LIFE): a randomised trial against atenolol. Lancet 359(9311):995-1003.

de Gasparo M, Catt KJ, Inagami T, Wright JW, and Unger T. 2000. International union of pharmacology. XXIII. The angiotensin II receptors. Pharmacol Rev 52(3):415-472.

De Mello WC. 2006. On the pathophysiological implications of an intracellular renin receptor. Circ Res 99(12):1285-1286.

Diez J. 2006. Review of the molecular pharmacology of Losartan and its possible relevance to stroke prevention in patients with hypertension. Clin Ther 28(6):832-848.

Dilauro M, and Burns KD. 2009. Angiotensin-(1-7) and its effects in the kidney. ScientificWorldJournal 9:522-535.

Dorn GW, 2nd. 2009. Novel pharmacotherapies to abrogate postinfarction ventricular remodeling. Nat Rev Cardiol 6(4):283-291.

Douglas J, and Catt KJ. 1976. Regulation of angiotensin II receptors in the rat adrenal cortex by dietary electrolytes. J Clin Invest 58(4):834-843.

Du Y, Yao A, Guo D, Inagami T, and Wang DH. 1995. Differential regulation of angiotensin II receptor subtypes in rat kidney by low dietary sodium. Hypertension 25(4 Pt 2):872-877.

Ferrario CM, and Iyer SN. 1998. Angiotensin-(1-7): a bioactive fragment of the renin-angiotensin system. Regul Pept 78(1-3):13-18.

Fukushima K, Higuchi T, DiPaula A, Schuleri H, Hilton J, Mathews WB, Dannals RF, Szabo Z, Lardo AC, and Bengel FM. 2010. Myocardial angiotensin II subtype 1 receptor (AT1R) imaging using PET-CT with 11C-KR31173 - A translational effort in the porcine model. Abstract. J Nucl Med 51(2 Supplement):12P.

Fukushima K, Xia J, Lautamaki R, Fox J, Mathews WB, Szabo Z, and Bengel F. 2009. Assessment of regional myocardial angiotensin II receptor upregulation after myocardial infarction by PET. Abstract. Journal of Nuclear Medicine.

Furuta H, Guo DF, and Inagami T. 1992. Molecular cloning and sequencing of the gene encoding human angiotensin II type 1 receptor. Biochem Biophys Res Commun 183(1):8-13.

Fyhrquist F, and Saijonmaa O. 2008. Renin-angiotensin system revisited. J Intern Med 264(3):224-236.

Germano G, and Berman DS, editors. 2006. Clinical Gated Cadiac SPECT. Second Edition: Blackwell Futura.

Gibson RE, Beauchamp HT, Fioravanti C, Brenner N, and Burns HD. 1994. Receptor binding radiotracers for the angiotensin II receptor: radioiodinated [Sar1, Ile8]Angiotensin II. Nucl Med Biol 21(4):593-600.

Goldfarb DA, Diz DI, Tubbs RR, Ferrario CM, and Novick AC. 1994. Angiotensin II receptor subtypes in the human renal cortex and renal cell carcinoma. J Urol 151(1):208-213.

Greene M, Thackeray JT, Kenk M, Thorn SL, Bevilacqua L, Harper ME, Beanlands RS, and Dasilva JN. 2009. Reduced in vivo phosphodiesterase-4 response to acute noradrenaline challenge in diet-induced obese rats. Can J Physiol Pharmacol 87(3):196-202.

Hadizad T, Collins J, Beanlands RS, and Dasilva JN. 2010. Radiosynthesis of [11C]methyl-EXP3174, a potential imaging agent for angiotensin AT1 receptors. Abstract. World Molecular Imaging Congress, Sep 8-11, Kyoto, Japan.

Hadizad T, Kirkpatrick SA, Mason S, Burns K, Beanlands RS, and Dasilva JN. 2009a. Novel O-[(11)C]methylated derivatives of candesartan as angiotensin II AT(1) receptor imaging ligands: radiosynthesis and ex vivo evaluation in rats. Bioorg Med Chem 17(23):7971-7977.

Hadizad T, Mason S, Collins J, Kirkpatrick S, Beanlands RS, and Dasilva JN. 2009b. Radiosynthesis of [11C]methyl-losartan, a potential imaging agent for angiotensin AT1 receptors. Abstract. Journal of labelled compounds and radiopharmaceuticals 52(S1):S426.

Haller H, Lindschau C, Erdmann B, Quass P, and Luft FC. 1996. Effects of intracellular angiotensin II in vascular smooth muscle cells. Circ Res 79(4):765-772.

Hamill TG, Burns HD, Dannals RF, Mathews WB, Musachio JL, Ravert HT, and Naylor EM. 1996. Development of [^{11}C]L-159,884: A Radiolabelled, Nonpeptide Angiotensin II Antagonist that is Useful for Angiotensin II, AT_1 Receptor Imaging. Appl Radiat Isot 47(2):221-218.

Hanif K, Bid HK, and Konwar R. 2010. Reinventing the ACE inhibitors: some old and new implications of ACE inhibition. Hypertens Res 33(1):11-21.

Harada K, Sugaya T, Murakami K, Yazaki Y, and Komuro I. 1999. Angiotensin II type 1A receptor knockout mice display less left ventricular remodeling and improved survival after myocardial infarction. Circulation 100(20):2093-2099.

Haywood GA, Gullestad L, Katsuya T, Hutchinson HG, Pratt RE, Horiuchi M, and Fowler MB. 1997. AT1 and AT2 angiotensin receptor gene expression in human heart failure. Circulation 95(5):1201-1206.

Higuchi T, Fukushima K, Xia J, Lautamaki R, Fox J, Mathews WB, Szabo Z, and Bengel FM. 2010. Use of the AT1R ligand C-11 KR31173 for monitoring of the myocardial effect of drugs inhibiting the renin-angiotensin system after myocardial infarction. Abstract. J Nucl Med 51(2 Supplement):74P.

Hilton J, Yokoi F, Dannals RF, Ravert HT, Szabo Z, and Wong DF. 2000. Column-switching HPLC for the analysis of plasma in PET imaging studies. Nucl Med Biol 27(6):627-630.

Hume SP, Gunn RN, and Jones T. 1998. Pharmacological constraints associated with positron emission tomographic scanning of small laboratory animals. Eur J Nucl Med 25(2):173-176.

Hume SP, and Myers R. 2002. Dedicated small animal scanners: a new tool for drug development? Curr Pharm Des 8(16):1497-1511.

Ito M, Oliverio MI, Mannon PJ, Best CF, Maeda N, Smithies O, and Coffman TM. 1995. Regulation of blood pressure by the type 1A angiotensin II receptor gene. Proc Natl Acad Sci U S A 92(8):3521-3525.

Iwai N, and Inagami T. 1992. Regulation of the expression of the rat angiotensin II receptor mRNA. Biochem Biophys Res Commun 182(3):1094-1099.

Karnik SS, Gogonea C, Patil S, Saad Y, and Takezako T. 2003. Activation of G-protein-coupled receptors: a common molecular mechanism. Trends Endocrinol Metab 14(9):431-437.

Kaschina E, and Unger T. 2003. Angiotensin AT1/AT2 receptors: regulation, signalling and function. Blood Press 12(2):70-88.

Kenk M, Greene M, Thackeray J, deKemp RA, Lortie M, Thorn S, Beanlands RS, and DaSilva JN. 2007. In vivo selective binding of (R)-[11C]rolipram to phosphodiesterase-4 provides the basis for studying intracellular cAMP signaling in the myocardium and other peripheral tissues. Nucl Med Biol 34(1):71-77.

Kenk M, Thackeray JT, Thorn SL, Dhami K, Chow BJ, Ascah KJ, DaSilva JN, and Beanlands RS. 2010. Alterations of pre- and postsynaptic noradrenergic signaling in a rat model of adriamycin-induced cardiotoxicity. J Nucl Cardiol 17(2):254-263.

Kim SE, Scheffel U, Szabo Z, Burns HD, Gibson RE, Ravert HT, Mathews WB, Hamill TG, and Dannals RF. 1996. In vivo labeling of angiotensin II receptors with a carbon-11-labeled selective nonpeptide antagonist. J Nucl Med 37(2):307-311.

Klein R, Renaud JM, Ziadi MC, Thorn SL, Adler A, Beanlands RS, and deKemp RA. 2010. Intra- and inter-operator repeatability of myocardial blood flow and myocardial flow reserve measurements using rubidium-82 pet and a highly automated analysis program. J Nucl Cardiol 17(4):600-616.

Krovat EM, and Langer T. 2003. Non-peptide angiotensin II receptor antagonists: chemical feature based pharmacophore identification. J Med Chem 46(5):716-726.

Lewis EJ, Hunsicker LG, Bain RP, and Rohde RD. 1993. The effect of angiotensin-converting-enzyme inhibition on diabetic nephropathy. The Collaborative Study Group. N Engl J Med 329(20):1456-1462.

Lewis EJ, Hunsicker LG, Clarke WR, Berl T, Pohl MA, Lewis JB, Ritz E, Atkins RC, Rohde R, and Raz I. 2001. Renoprotective effect of the angiotensin-receptor antagonist irbesartan in patients with nephropathy due to type 2 diabetes. N Engl J Med 345(12):851-860.

Llorens-Cortes C, Greenberg B, Huang H, and Corvol P. 1994. Tissular expression and regulation of type 1 angiotensin II receptor subtypes by quantitative reverse transcriptase-polymerase chain reaction analysis. Hypertension 24(5):538-548.

Logan J, Fowler JS, Volkow ND, Wolf AP, Dewey SL, Schlyer DJ, MacGregor RR, Hitzemann R, Bendriem B, Gatley SJ et al. . 1990. Graphical analysis of reversible radioligand binding from time-activity measurements applied to [N-11C-methyl]-(-)-cocaine PET studies in human subjects. J Cereb Blood Flow Metab 10(5):740-747.

Lourenco CM, Kenk M, Beanlands RS, and DaSilva JN. 2006. Increasing synaptic noradrenaline, serotonin and histamine enhances in vivo binding of phosphodiesterase-4 inhibitor (R)-[11C]rolipram in rat brain, lung and heart. Life Sci 79(4):356-364.

Mathews WB, Burns HD, Dannals RF, Ravert HT, and Naylor EM. 1995. Carbon-11 Labeling of a Potent, Nonpeptide, AT1-Selective Angiotensin-II Receptor Antagonist: MK-996. Journal of Labelled Compounds and Radiopharmaceuticals 36:729-737.

Mathews WB, Yoo SE, Lee SH, Scheffel U, Rauseo PA, Zober TG, Gocco G, Sandberg K, Ravert HT, Dannals RF et al. . 2004. A novel radioligand for imaging the AT1 angiotensin receptor with PET. Nucl Med Biol 31(5):571-574.

Matsoukas JM, Hondrelis J, Keramida M, Mavromoustakos T, Makriyannis A, Yamdagni R, Wu Q, and Moore GJ. 1994. Role of the NH2-terminal domain of angiotensin II (ANG II) and [Sar1]angiotensin II on conformation and activity. NMR evidence for aromatic ring clustering and peptide backbone folding compared with [des-1,2,3]angiotensin II. J Biol Chem 269(7):5303-5312.

McAlpine HM, Morton JJ, Leckie B, Rumley A, Gillen G, and Dargie HJ. 1988. Neuroendocrine activation after acute myocardial infarction. Br Heart J 60(2):117-124.

Meggs LG, Coupet J, Huang H, Cheng W, Li P, Capasso JM, Homcy CJ, and Anversa P. 1993. Regulation of angiotensin II receptors on ventricular myocytes after myocardial infarction in rats. Circ Res 72(6):1149-1162.

Mento PF, Pica ME, Hilepo J, Chang J, Hirsch L, and Wilkes BM. 1998. Increased expression of glomerular AT1 receptors in rats with myocardial infarction. Am J Physiol 275(4 Pt 2):H1247-1253.

Milton JS. 1999. Statistical Methods in the Biological and Health Sciences. Third Edition: McGraw-Hill.

Murphy TJ, Alexander RW, Griendling KK, Runge MS, and Bernstein KE. 1991. Isolation of a cDNA encoding the vascular type-1 angiotensin II receptor. Nature 351(6323):233-236.

Naruse M, Tanabe A, Sato A, Takagi S, Tsuchiya K, Imaki T, and Takano K. 2002. Aldosterone breakthrough during angiotensin II receptor antagonist therapy in stroke-prone spontaneously hypertensive rats. Hypertension 40(1):28-33.

Neves SR, Ram PT, and Iyengar R. 2002. G protein pathways. Science 296(5573):1636-1639.

Nikiforovich GV, Kao JL, Plucinska K, Zhang WJ, and Marshall GR. 1994. Conformational analysis of two cyclic analogs of angiotensin: implications for the biologically active conformation. Biochemistry 33(12):3591-3598.

Nikiforovich GV, and Marshall GR. 1993. Three-dimensional recognition requirements for angiotensin agonists: a novel solution for an old problem. Biochem Biophys Res Commun 195(1):222-228.

Nishiyama A, Yoshizumi M, Rahman M, Kobori H, Seth DM, Miyatake A, Zhang GX, Yao L, Hitomi H, Shokoji T et al. . 2004. Effects of AT1 receptor blockade on renal injury and mitogen-activated protein activity in Dahl salt-sensitive rats. Kidney Int 65(3):972-981.

O'Donnell JM. 1993. Antidepressant-like effects of rolipram and other inhibitors of cyclic adenosine monophosphate phosphodiesterase on behavior maintained by differential reinforcement of low response rate. J Pharmacol Exp Ther 264(3):1168-1178.

Owonikoko TK, Fabucci ME, Brown PR, Nisar N, Hilton J, Mathews WB, Ravert HT, Rauseo P, Sandberg K, Dannals RF et al. . 2004. In vivo investigation of estrogen regulation of adrenal and renal angiotensin (AT1) receptor expression by PET. J Nucl Med 45(1):94-100.

Ozdemir S, Tandogan B, Ulusu NN, and Turan B. 2009. Angiotensin II receptor blockage prevents diabetes-induced oxidative damage in rat heart. Folia Biol (Praha) 55(1):11-16.

Pagano M, and Gauvreau K. 2000. Principles of Biostatistics: Brooks/Cole.

Paul M, Poyan Mehr A, and Kreutz R. 2006. Physiology of local renin-angiotensin systems. Physiol Rev 86(3):747-803.

Pierson ME, and Freer RJ. 1992. Analysis of the active conformation of angiotensin II: a comparison of AII and non-peptide AII antagonists. Abstract. Pept Res 5(2):102-105.

Pitt B, Poole-Wilson PA, Segal R, Martinez FA, Dickstein K, Camm AJ, Konstam MA, Riegger G, Klinger GH, Neaton J et al. . 2000. Effect of losartan compared with captopril on mortality in patients with symptomatic heart failure: randomised trial--the Losartan Heart Failure Survival Study ELITE II. Lancet 355(9215):1582-1587.

Pitt B, Segal R, Martinez FA, Meurers G, Cowley AJ, Thomas I, Deedwania PC, Ney DE, Snavely DB, and Chang PI. 1997. Randomised trial of losartan versus captopril in patients over 65 with heart failure (Evaluation of Losartan in the Elderly Study, ELITE). Lancet 349(9054):747-752.

Ramasubbu K, Mann DL, and Deswal A. 2007. Anti-angiotensin therapy: new perspectives. Cardiol Clin 25(4):573-580; vi-vii.

Ravid M, Lang R, Rachmani R, and Lishner M. 1996. Long-term renoprotective effect of angiotensin-converting enzyme inhibition in non-insulin-dependent diabetes mellitus. A 7-year follow-up study. Arch Intern Med 156(3):286-289.

Re RN, and Cook JL. 2006. The intracrine hypothesis: an update. Regul Pept 133(1-3):1-9.

Regitz-Zagrosek V, Fielitz J, Dreysse R, Hildebrandt AG, and Fleck E. 1997. Angiotensin receptor type 1 mRNA in human right ventricular endomyocardial biopsies: downregulation in heart failure. Cardiovasc Res 35(1):99-105.

Reiss K, Capasso JM, Huang HE, Meggs LG, Li P, and Anversa P. 1993. ANG II receptors, c-myc, and c-jun in myocytes after myocardial infarction and ventricular failure. Am J Physiol 264(3 Pt 2):H760-769.

Reuter H, Adam C, Gronke S, Zobel C, Frank KF, Muller-Ehmsen J, Brabender J, and Schwinger RH. 2006. The increased angiotensin II (type 1) receptor density in myocardium of type 2 diabetic patients is prevented by blockade of the renin-angiotensin system. Diabetologia 49(12):3067-3074.

Rockman HA, Koch WJ, and Lefkowitz RJ. 2002. Seven-transmembrane-spanning receptors and heart function. Nature 415(6868):206-212.

Santos RA, Simoes e Silva AC, Maric C, Silva DM, Machado RP, de Buhr I, Heringer-Walther S, Pinheiro SV, Lopes MT, Bader M et al. . 2003. Angiotensin-(1-7) is an endogenous ligand for the G protein-coupled receptor Mas. Proc Natl Acad Sci U S A 100(14):8258-8263.

Schieffer B, Wirger A, Meybrunn M, Seitz S, Holtz J, Riede UN, and Drexler H. 1994. Comparative effects of chronic angiotensin-converting enzyme inhibition and angiotensin II type 1

receptor blockade on cardiac remodeling after myocardial infarction in the rat. Circulation 89(5):2273-2282.

Sechi LA, Griffin CA, and Schambelan M. 1994. The cardiac renin-angiotensin system in STZ-induced diabetes. Diabetes 43(10):1180-1184.

Stearns RA, Miller RR, Doss GA, Chakravarty PK, Rosegay A, Gatto GJ, and Chiu SH. 1992. The metabolism of DuP 753, a nonpeptide angiotensin II receptor antagonist, by rat, monkey, and human liver slices. Drug Metab Dispos 20(2):281-287.

Sumida Y, Umemura S, Kobayashi S, Kihara M, Tamura K, Ishigami T, Ochiai H, Chiba E, Nyui N, and Ishii M. 1998. Angiotensin II receptors in cardiac left ventricles of Dahl rats. Clin Exp Pharmacol Physiol 25(3-4):252-256.

Sun CK, Chang LT, Sheu JJ, Wang CY, Youssef AA, Wu CJ, Chua S, and Yip HK. 2007. Losartan preserves integrity of cardiac gap junctions and PGC-1 alpha gene expression and prevents cellular apoptosis in remote area of left ventricular myocardium following acute myocardial infarction. Int Heart J 48(4):533-546.

Szabo Z, Kao PF, Burns HD, Gibson RE, Hamill TG, Ravert HT, Kim SE, Mathews WB, Musachio JL, Scheffel U et al. . 1998. Investigation of angiotensin II/AT1 receptors with carbon-11-L-159,884: a selective AT1 antagonist. J Nucl Med 39(7):1209-1213.

Szabo Z, Speth RC, Brown PR, Kerenyi L, Kao PF, Mathews WB, Ravert HT, Hilton J, Rauseo P, Dannals RF et al. . 2001. Use of positron emission tomography to study AT1 receptor regulation in vivo. J Am Soc Nephrol 12(7):1350-1358.

Tan F, Morris PW, Skidgel RA, and Erdos EG. 1993. Sequencing and cloning of human prolylcarboxypeptidase (angiotensinase C). Similarity to both serine carboxypeptidase and prolylendopeptidase families. J Biol Chem 268(22):16631-16638.

Tan J, Wang H, and Leenen FH. 2004. Increases in brain and cardiac AT1 receptor and ACE densities after myocardial infarct in rats. Am J Physiol Heart Circ Physiol 286(5):H1665-1671.

Thackeray JT, Beanlands RS, and Dasilva JN. 2007. Presence of specific 11C-meta-Hydroxyephedrine retention in heart, lung, pancreas, and brown adipose tissue. J Nucl Med 48(10):1733-1740.

Tzakos AG, Gerothanassis IP, and Troganis AN. 2004. On the structural basis of the hypertensive properties of angiotensin II: a solved mystery or a controversial issue? Curr Top Med Chem 4(4):431-444.

Urata H, Nishimura H, and Ganten D. 1996. Chymase-dependent angiotensin II forming systems in humans. Am J Hypertens 9(3):277-284.

van Geel PP, Pinto YM, Buikema H, and van Gilst WH. 1998. Is the A1166C polymorphism of the angiotensin II type 1 receptor involved in cardiovascular disease? Abstract. Eur Heart J 19(Suppl G).

van Kats JP, Duncker DJ, Haitsma DB, Schuijt MP, Niebuur R, Stubenitsky R, Boomsma F, Schalekamp MA, Verdouw PD, and Danser AH. 2000. Angiotensin-converting enzyme inhibition and angiotensin II type 1 receptor blockade prevent cardiac remodeling in pigs after myocardial infarction: role of tissue angiotensin II. Circulation 102(13):1556-1563.

Vaziri ND, Bai Y, Ni Z, Quiroz Y, Pandian R, and Rodriguez-Iturbe B. 2007. Intra-renal angiotensin II/AT1 receptor, oxidative stress, inflammation, and progressive injury in renal mass reduction. J Pharmacol Exp Ther 323(1):85-93.

Verheijen I, Vanderheyden PM, De Backer JP, and Vauquelin G. 2004. AT1 receptor antagonists. Curr Med Chem Cardiovasc Hematol Agents 2(1):69-77.

Verjans JW, Lovhaug D, Narula N, Petrov AD, Indrevoll B, Bjurgert E, Krasieva TB, Petersen LB, Kindberg GM, Solbakken M et al. . 2008. Noninvasive imaging of angiotensin receptors after myocardial infarction. JACC Cardiovasc Imaging 1(3):354-362.

Wagenaar LJ, Voors AA, Buikema H, and van Gilst WH. 2002. Angiotensin receptors in the cardiovascular system. Can J Cardiol 18(12):1331-1339.

Wagner J, Gehlen F, Ciechanowicz A, and Ritz E. 1999. Angiotensin II receptor type 1 gene expression in human glomerulonephritis and diabetes mellitus. J Am Soc Nephrol 10(3):545-551.

Wahl RL, editor. 2002. Principles and Practices of Positron Emission Tomography: Lippincott Williams & Wilkins.

Wang DH, Du Y, Zhao H, Granger JP, Speth RC, and Dipette DJ. 1997a. Regulation of angiotensin type 1 receptor and its gene expression: role in renal growth. J Am Soc Nephrol 8(2):193-198.

Wang DH, Yao A, Zhao H, and DiPette DJ. 1997b. Distinct mechanisms of modulation of angiotensin II type I receptor gene expression in heart and aorta. Hypertension 29(5):1104-1108.

Wang JM, Veerasingham SJ, Tan J, and Leenen FH. 2003. Effects of high salt intake on brain AT1 receptor densities in Dahl rats. Am J Physiol Heart Circ Physiol 285(5):H1949-1955.

Wright JW, Krebs LT, Stobb JW, and Harding JW. 1995. The angiotensin IV system: functional implications. Front Neuroendocrinol 16(1):23-52.

Xia J, Seckin E, Xiang Y, Vranesic M, Mathews WB, Hong K, Bluemke DA, Lerman LO, and Szabo Z. 2008. Positron-emission tomography imaging of the angiotensin II subtype 1 receptor in swine renal artery stenosis. Hypertension 51(2):466-473.

Yang H, Lu D, and Raizada MK. 1997. Angiotensin II-induced phosphorylation of the AT1 receptor from rat brain neurons. Hypertension 30(3 Pt 1):351-357.

Yu L, Zheng M, Wang W, Rozanski GJ, Zucker IH, and Gao L. 2010. Developmental changes in AT1 and AT2 receptor-protein expression in rats. J Renin Angiotensin Aldosterone Syst.

Zhang J, and Leenen FH. 2001. Peripheral administration of AT1 receptor blockers and pressor responses to central angiotensin II and sodium. Can J Physiol Pharmacol 79(10):861-867.

Zober TG, Mathews WB, Seckin E, Yoo SE, Hilton J, Xia J, Sandberg K, Ravert HT, Dannals RF, and Szabo Z. 2006. PET Imaging of the AT1 receptor with [11C]KR31173. Nucl Med Biol 33(1):5-13.